PREPARATION AND CHARACTERIZATION OF CARBON-SUPPORTED POLYANILINE-PALLADIUM COMPOSITE ELECTRODES

A Dissertation
Presented to
The Academic Faculty

by

Erin L. Gawron

In Partial Fulfillment
of the Requirements for the Degree
Doctor of Philosophy in the
School of Chemistry and Biochemistry

Georgia Institute of Technology
December 2017

PREPARATION AND CHARACTERIZATION OF CARBON-SUPPORTED POLYANILINE-PALLADIUM COMPOSITE ELECTRODES

Approved by:

Dr. Jiří Janata, Advisor
School of Chemistry and Biochemistry
Georgia Institute of Technology

Dr. Paul Russo
School of Materials Science and Engineering
Georgia Institute of Technology

Dr. Facundo Fernandez
School of Chemistry and Biochemistry
Georgia Institute of Technology

Dr. Jennifer Steeb
Global Security Sciences Division
Argonne National Laboratory

Dr. Joseph Sadighi
School of Chemistry and Biochemistry
Georgia Institute of Technology

Date Approved: October 12, 2017

To all the little girls who want to grow up to be scientists; may they all know they are capable and worthy of pursuing their dreams.

ACKNOWLEDGEMENTS

There are many people I would like to thank that helped me along the way during these five-and-a-half years at the Georgia Institute of Technology. It was not easy for me to pursue my dream of working on my Ph.D. because that meant giving up a career as a high-school teacher after ten years in the classroom. I would like to thank my co-workers and students at Heritage High School for encouraging me to make the difficult decision to leave, all in the pursuit of higher knowledge.

The most important to thank are Professor Art Janata and Dr. Mira Josowicz for their sacrifices for me in order to push me to 'think like a Ph.D.' In 2012, Georgia Tech Chemistry had an unusually large incoming class. There were too many analytical students and not enough professors with openings. Art and Mira were kind enough to push back retirement and take two of us students as their final students. In 2017, I am the LAST student that the Janata group will graduate. Art and Mira have treated me like family and have truly lived up to their motto of educating the "whole student" by offering advice and encouragement, especially when troubles arose in my own family. They have taken me into their home and kept me fed with plenty of coffee and chocolate to last a lifetime. I will truly miss our daily science talks over coffee. I know I learned more from those discussions than from anywhere or anything else. I also have to thank my "secondary" advisor Steve Hira. His guidance and mentorship have proved invaluable at many times, especially while keeping me calm during lab by offering advice. Thank you to Alex Jonke for his guidance in continuing this project.

I need to thank the people on campus that kept me sane through this entire process. I have to thank Allison Harbottle and Malvina Kowalik for being great companions in the lab and letting me vent when I needed it, and always being game to go get free things all over campus. I would also like to thank Brandon Sharp for being my restaurant-going buddy, never judging my snide remarks, sharing videos and memes to make me laugh, sharing songs to help me get in the work groove, and supplying me with all the couponing goodies I could need. I would also like to thank Johanna Smeekens and Hailey Bureau for being a support during coffee breaks and lunches and for seeing me through my dilemmas of the heart. Thanks go out to Charles Wang, Mac Thompson and Tomas Krizek for their laughter and support in the lab. I need to give a special thank you to my bud, Caroline Hoyt. She has kept me absolutely sane with the many lunch dates (Jimmy John's anyone?), coffee excursions, daily texts and "writing parties" as we have held each other up during this entire process.

Thank you to my parents, Julia Gawron and Greg Gawron, my step-mom Doreen Gawron, and my brother Greg Gawron. All four have provided support and encouragement and made sure I had everything I needed. A special thanks goes to my uncle, Bill Ruzinsky, for showing me how much fun science, especially chemistry, can be. He fostered my scientific curiosity from the time I was 3 years old. I also have to thank my best friend from Rose-Hulman, Jared Tatum, for being an inspiration and encouraging me to work toward this. I would also like to thank the residents of Adair Estate for allowing me to serve as their concierge and providing me with a great place to live surrounded by great people.

I would also like to thank the members of my committee for taking the time out of their busy days to help me think through my research, evaluate my work, and check that I

had what I needed to succeed. There are so many people at Georgia Tech to thank that had a part of my success, but I especially appreciate Dr. J. Cameron Tyson and Dr. Kenyetta Johnson for listening to my woes, helping me work through situations and making sure my program was a smooth one. I also appreciate and thank Dr. Carrie Shepler, Dr. Christy O'Mahoney, Dr. Ken Brown and Dr. Leigh Bottomley. Being a teaching assistant with and for these folks has left me with a better appreciation for a career in higher education, and their mentorship has given me the confidence to continue to pursue teaching as a career path.

Finally, my immediate family. My girls Hagia and Clara have been just what I've needed to come home to everyday. Their wagging tails and excited kisses each and every day have reminded me of unconditional love. Their cuddles on the couch have also kept my stress low and my blood pressure down. I love both of those furry little girls with all my heart. And last, but absolutely not least, I have to thank my rock, my love, my boyfriend Alexander Hyla. I met him when I first got to campus, got to know him very well through curling and other social events, and lo-and-behold four years later we ended up dating. Fast forward another year and we are getting ready to move to another country together. I can't even begin to describe what he has done for me, especially during this last stretch. He makes sure I am taken care of every step of the way, from housework, to food, to curling bonspiels, to classic rock concerts --he is there. He is always there. He always has a hug ready, or finishes my sentences, and he always knows what I need. I love him dearly and couldn't imagine life without him now, he has made me happier than I ever could have been.

TABLE OF CONTENTS

LIST OF TABLES

LIST OF FIGURES

LIST OF SYMBOLS AND ABBREVIATIONS

AU·L/mol	absorbance units * liters/moles
BE	binding energy
cm	centimeter
cm^{-1}	wavenumber (Raman shift)
C/PANI	carbon supported polyaniline
C/PANI-Pd	carbon supported polyaniline with inserted palladium
C/Pt	carbon with deposited platinum
CV	cyclic voltammetry/voltammogram
ESA	electrochemical surface area
EB	emeraldine base
ES	emeraldine salt
eV	electron volt
g/cm^3	grams per centimeter cubed
HPLC	high performance liquid chromatography
LEB	leucoemeraldine base
LES	leucoemeraldine salt
LSV	linear sweep voltammogram
M	Molarity
mC/cm^2	millicoulombs per centimeter squared
mL	milliliters
mm	millimeters
mM	millimolar

mV/s	millivolts per second
μL	microliters
μm	micrometers
μΩm	microohms meters
nm	nanometers
OCP	open cell potential
PANI	polyaniline
PANI(ES)	emeraldine salt form of polyaniline
PANI(PN)	pernigraniline form of polyaniline
PNB	pernigraniline base
PNS	pernigraniline salt
RuHex	hexaminеruthenium (II) chloride/hexaaminеruthenium (III) chloride
s	second
SEM/FE-SEM	secondary electron microscopy/field effect-secondary electron microscopy
V	volts
XPS	X-ray photoelectron spectroscopy

SUMMARY

Polyaniline is an electronically conducting polymer whose redox state can be precisely controlled. The nitrogen groups in the polymer are weak bases, which can be protonated and because of the redox and acid –base properties, it can be used as a matrix for insertion of various metal complexes. Our preparation uses the conducting form of PANI with precisely controlled potentials and solution conditions in order to insert Pd into the polymer matrix. The goals of this thesis were to identify which carbon substrate provides the best support for the deposition of PANI, to find which Pd species in aqueous acidic solution results in the most favorable interactions with the polymer, and to elucidate the nature of these interactions in a controlled and systematic way, in order to create C/PANI-Pd composite materials.

This thesis is divided into eight chapters. The first chapter discusses the chemistry and behavior of polyaniline, the speciation and reduction of palladium (II) chlorocomplexes, and polyaniline as a support matrix for Pd metal. The second chapter outlines the experimental methods used and describes the palladium insertion cycle. This cycle takes advantage of the affinity of chloropalladate anion for the nitrogen-containing groups of the polyaniline and the control over the oxidation state of the polymer. The optimization of the palladium insertion process is discussed in chapter three. Various parameters such as pH, holding potentials, reduction sweep, and conditioning are explored with characterization through Raman spectroscopy and X-ray photoelectron spectroscopy (XPS).

Chapters four and five outline the characterization of the carbon electrode support material. In chapter 4, two carbon substrates are compared and characterized through XPS, Raman spectroscopy, and cyclic voltammetry (CV) in RuHex. The correlation of sp^2/sp^3 content and surface oxygen groups to electrochemical behavior informs which carbon is the best choice for electrode material, which was synthetic graphite fabricated from petroleum coke. Chapter five takes the choice carbon substrate and explores the deposition of Pt and PANI on the surface. The catalytic activity of both C/Pt and C/Pt-PANI are also evaluated in Chapter five through recorded CVs of the oxidation of n-propanol in KOH. It was found that the Pt and PANI deposition on the carbon were suitable as support for possible metal clusters inserted into PANI.

Chapters six and seven outline the interaction of palladium and polyaniline. In chapter six, the speciation of the chloropalladate ion is explained and each dominant species $PdCl_2(H_2O)_2$, $PdCl_3(H_2O)^-$, and $PdCl_4^-$, is evaluated for the strongest interaction with PANI using Raman spectroscopy, XPS, and CV in $HClO_4$. Results show that of the three species, the $PdCl_3(H_2O)^-$ complex interacts most fully with PANI. Chapter seven delves into the nature of the interaction of the PANI and Pd in the composite electrodes. XPS provides detailed information about the atomic percentages of each element, the oxidation state of the Pd, and the ratios of imines to amines. Correlating information from XPS, Raman spectra and CVs show that there is a possible irreducible complex between the PANI nitrogen-containing groups and the palladium (II) chlorocomplex.

Chapter eight, the final chapter, outlines the possible future work for this project. Understanding the nature of interactions between PANI and noble metals, such as Pd, is key to creating composite materials with atomic metal clusters supported in the PANI.

These composite materials using carbon and electrodeposited PANI as the support matrix for the insertion of metals serve as versatile catalytic materials for use in sensors, batteries, and fuel cells.

CHAPTER 1. INTRODUCTION

1.1 Objective

The main objective of this thesis is to understand the interactions between palladium, a noble metal, and polyaniline, a conducting polymer. With a better understanding of these interactions, they can be controlled and tuned to create sub-nanometer sized metal clusters supported by the polymer matrix. The aim of this work is to optimize, characterize, and understand the nature of polyaniline matrix as well as the palladium (II) chlorocomplexes used, and to tune the interactions between them. A precisely controlled electrochemical method for the insertion of palladium metal into the polyaniline is presented, as well as the process optimization, and the follow-up characterizations using cyclic voltammetry (CV), X-ray photoelectron spectroscopy (XPS), Raman spectroscopy, and secondary electron microscopy (SEM).

1.2 Polyaniline

Polyaniline (PANI) is of interest for this study due to is stability, ease of electropolymerization and redox properties.[1,2] This conducting polymer was chosen because it provides the ability to control the state through adjusting potentials. Polyaniline is made up of repeating quinoid and benzenoid units, as seen in the emeraldine base form of Figure 1.1.

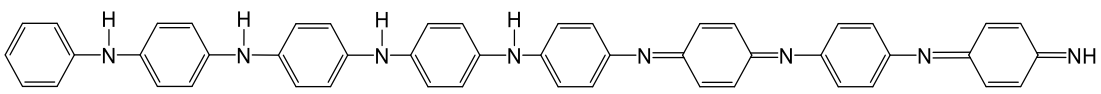

Figure 1.1: Emeraldine base form of polyaniline

1.2.1 Aniline polymerization

Radical polymerization of aniline leads to the formation of polyaniline. Extensive studies have been done regarding the mechanism for aniline polymerization.[3–6] These studies suggest that polymerization occurs through radical-cation – radical-cation pathways involving possible intermediates of p-aminodiphenylamine in a "head-to-tail" polymerization, or benzidine in a "tail-to-tail" mechanism. In basic media, even "head-to-head" mechanisms have been reported through the anilino radical.[7] These are summarized in Figure 1.2.

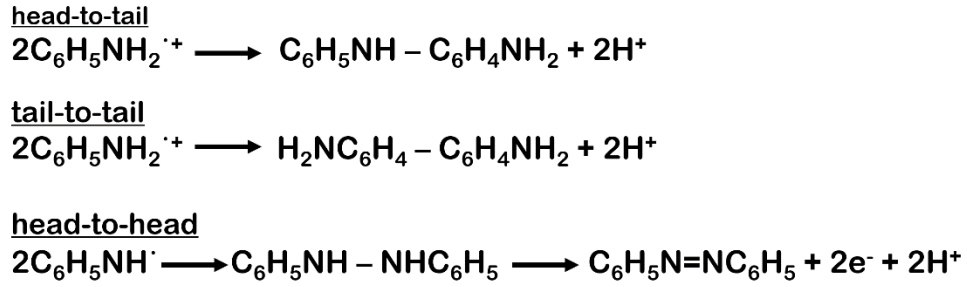

Figure 1.2: Possible polymerization pathways of polyaniline

1.2.2 States of PANI

In acidic solution, the nitrogen-containing groups undergo protonation, with the imines protonating first. The reported pK_a values for imine is 5.5 and amine is 2.5[8] and the various redox states of PANI can be seen in Figure 1.3. This figure shows three main oxidation states: pernigraniline (fully oxidized), emeraldine (partially oxidized), and leucoemeraldine (fully reduced). Also, with each of these oxidation states, there is a protonated salt and a base form.

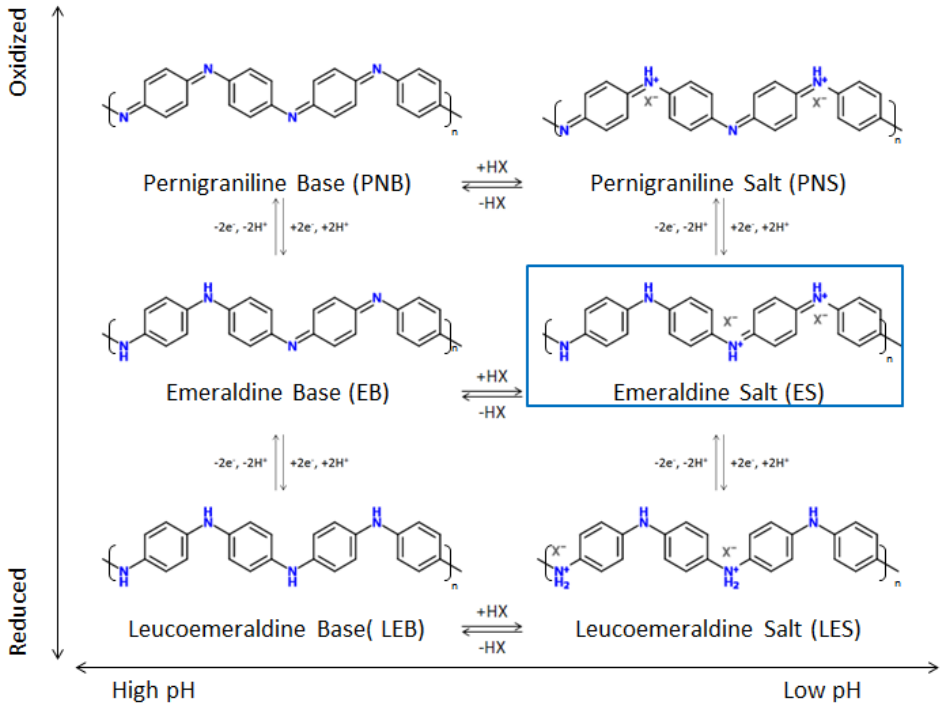

Figure 1.3: Oxidation states of polyaniline. Adapted from Harbottle.[9]

The electropolymerization of aniline from an acidic solution is used in this thesis to give the conducting emeraldine salt form. This form of PANI is crucial for the insertion of metal due to the need for precise control of the polymer state via potential changes. In the emeraldine salt form, the protonated imine bipolaron delocalizes into a polaron lattice (Figure 1.4), spreading the charge through the conjugated chains, resulting in the conducting polymer.[10,11]

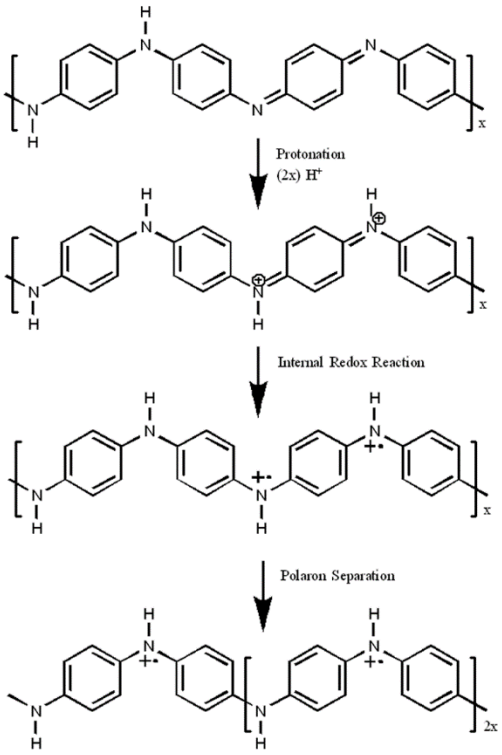

Figure 1.4: Polyaniline before protonation and after protonation resulting in the formation of the bipolaron and polaron lattice forms. Adapted from Stafstrom.[11]

1.3 Palladium (II) chlorocomplexes

For this study, the palladium was introduced into the PANI matrix through chloropalladate anions. The uptake of anions into polyaniline is necessary to maintain charge balance and the methods presented here take advantage of this thermodynamically favored process. Many other studies considering PANI-Pd complexes have used $PdCl_2$ with addition of HCl to control species in solution; this change in pH will affect the protonation level of the polymer.[12–15]

Palladium salts such as K_2PdCl_4, are known to form multiple complexes in aqueous solution.[16] The chloride ligands are labile and can be exchanged with water, thus changing

the charge of the resulting aquo complex.[17,18] The $PdCl_4^{2-}$ square planar complex can hydrolyze to form complexes of $PdCl_n(H_2O)_{4-n}^{2-n}$ where n = 0-4.[16,19,20] These species can also be monitored by UV-Visible spectroscopy to determine the dominant species in solution. The ligand-to-metal charge transfer (LMCT) can be seen by absorbance in the 200 nm – 700 nm range, as well as *d-d* ligand absorption bands and will be outlined in more detail in Chapter 6.[19]

The reduction of these chlorocomplexes can be experimentally determined on both a carbon electrode and a C/PANI electrode, as seen in Figure 1.5. With each -Cl ligand exchange with H_2O, the reduction potential shifts more negative, as seen in literature.[21] The equations for the reduction with the experimentally determined potentials are listed as Equations 1.1, 1.2, and 1.3.

$$[PdCl_4]^{2-} + 2e^- \rightarrow Pd^0 + 4Cl^- \qquad E = 0.46V \qquad (1.1)$$

$$[PdCl_3(H_2O)]^- + 2e^- \rightarrow Pd^0 + 3Cl^- + H_2O \qquad E = 0.44V \qquad (1.2)$$

$$[PdCl_2(H_2O)_2] + 2e^- \rightarrow Pd^0 + 2Cl^- + 2H_2O \qquad E = 0.42V \qquad (1.3)$$

Palladium reduction on C/PANI can also be determined through linear sweep voltammetry. Using the $PdCl_3(H_2O)^-$ complex in perchloric acid solution, and scanning at 50 mV/s, the reduction occurs at E = 0.47V (Figure 1.6). Understanding where the reduction potentials occur for each of the palladium (II) chlorocomplexes is an important

parameter for the process of metal insertion into PANI in order to avoid spontaneous reduction as outlined in Chapter 2.

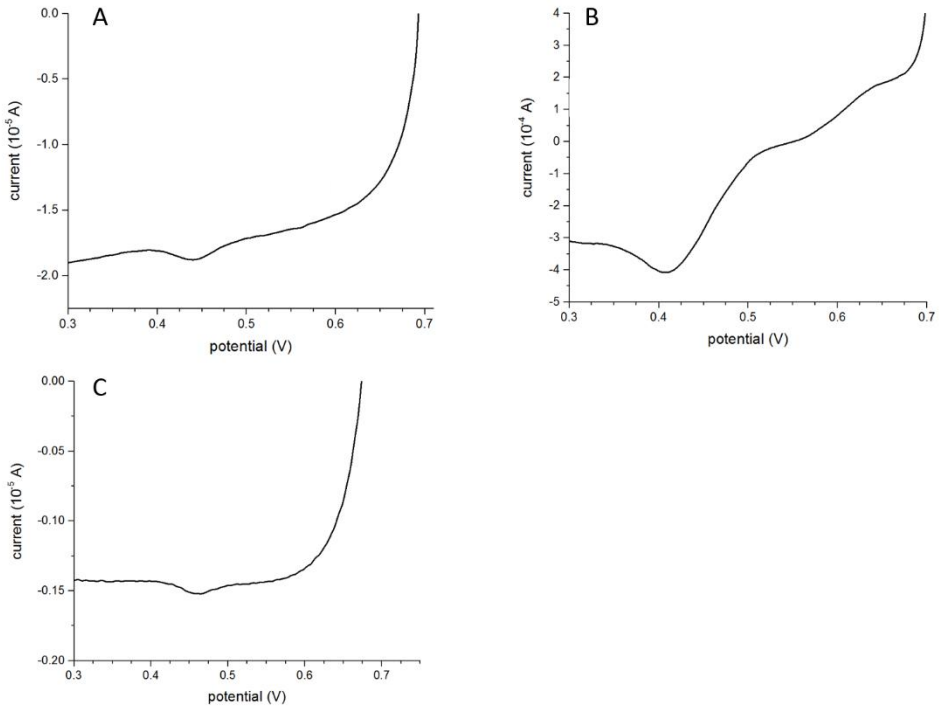

Figure 1.5: Palladium (II) chlorocomplex reduction on a carbon electrode by linear sweep voltammetry at 50mV/s. (A) $PdCl_2(H_2O)^-$ reduces at E = 0.44V, (B) $PdCl_2(H_2O)_2$ at E = 0.42V, and (C) $PdCl_4^-$ at E = 0.46V.

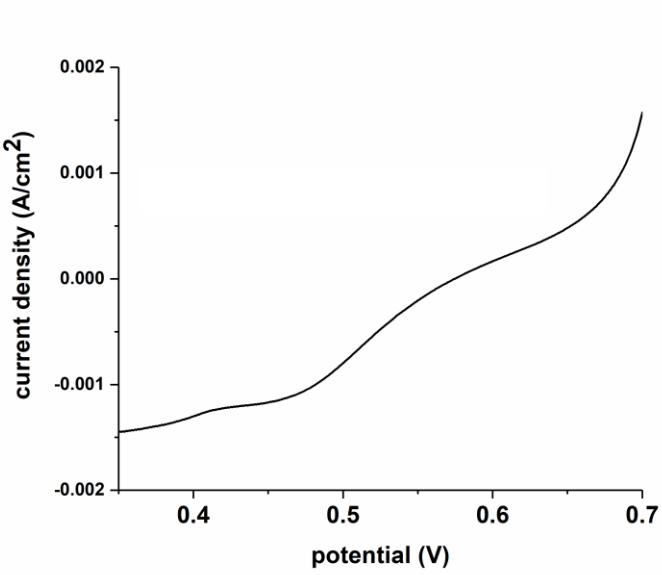

Figure 1.6: Linear sweep voltammogram of Pd reduction on C/PANI at 50mV/s using the $PdCl_3(H_2O)^-$ complex.

1.4 Characterization

Three main characterization techniques were used for this study: X-ray photoelectron spectroscopy (XPS), Raman spectroscopy, and cyclic voltammetry (CV). XPS provides surface information without any added sample preparation. The information most useful to this study that XPS provides is the composition of the samples, chemical analysis, and the oxidation state of metals such as Pd. The deconvolution of core-level scans can provide information about the environment of the Pd inserted into the PANI. Analysis reveals the oxidation state of the polymer in the ratio of amines to imines, and protonation of those nitrogen-containing groups using the N1s scans. The C1s scans provide information about the polaron and biopolaron states and the Pd3d scans give the oxidation state of the Pd as well as the association to either Cl or N atoms.

Resonance Raman spectroscopy will provide information regarding the structure of the polymer and how the addition of the metal will change the vibrations of bonds and character of the polymer. This study used the 785 nm laser which enhances the semi-quinone radical structures due to the laser line and vibrational modes coinciding with permitted electron transitions.[22] Through this technique, monitoring the changes in the polaronic structure, as well as vibrations associated with benzenoid and quinoid structures, gives information about the polymer before and after the insertion of Pd metal. The changes in the vibrations of the polyaniline structure seen through Raman can also be correlated to the changes seen in XPS.

Cyclic voltammetry aids in characterizing the PANI film after the electrodeposition on carbon, after conditioning and again after the insertion of Pd metal. Figure 2.4 shows a typical CV for deposited PANI. By monitoring the change in peak potentials and currents, a change in conformation and the oxidation state of the PANI can be detected. Other electrochemical characteristics of the PANI film, such as resistance and exchange of ions can also be studied.

1.5 PANI as a support matrix

Polyaniline is an electronically conducting polymer whose redox state can be precisely controlled. The nitrogen groups in the polymer are weak bases, which can be protonated and because of the redox and acid –base properties, it can be used as a matrix for insertion of various metal complexes. In previous work it was shown that insertion of haloaurate and halopalladate complexes under precise pH and potential control leads to formation of metal clusters, which have low total number of metal atoms.[23] Such metal clusters exhibit quantized behavior, which was predicted theoretically[24–26] and observed

experimentally by mass isolation spectroscopy.[27–29] This approach to formation of conducting polymer/metal composites differs fundamentally from the common approach in which the metal clusters are considered purely from the viewpoint of their size.[24–26] The aim of that approach is to differentiate between "surface" and "bulk" metal atoms. It may, and indeed does, lead to a considerable saving of the mass of precious metals. Moreover, nanometer sized metal clusters may exhibit plasmonic behavior, which may lead to additional interesting catalytic behavior.[13,30–32] However, the quantized behavior of these inserted metal atoms belongs only to PANI-metal composites with low number of metal atoms. In order to differentiate our atom-by-atom deposition from conventional metal/polymer composites we call the final materials "atomic metals". An excellent agreement between theory and experiment has been confirmed for $Au_{1\text{-}7}$[25], $Pd_{2\text{-}7}$[33] and for Pd, Au "atomic alloys" containing a total of seven atoms.[34–36] In continuation of this work, the conditions for insertion of palladium complexes have been examined in detail.

The anion insertion used in our approach relies on the uptake of anions into a PANI film and the subsequent interaction of the palladium species with the protonated nitrogen-containing groups on the polymer. The dominating requirement is the condition of charge neutrality of the final composite. Previous studies by Drelinkiewicz et. al.[15] used as starting materials deprotonated PANI and Pd chlorocomplex solutions with added HCl in order to achieve the desired speciation. Using that method leads to an undefined degree of protonation of the matrix. In this study, PANI in the protonated, emeraldine salt form is used in 0.1M strong acid in order to take advantage of the conducting form of the polymer. The desired Pd speciation is achieved by addition of NaCl in order to avoid changing the pH.

The preparation in this thesis uses the conducting form of PANI with precisely controlled potentials and solution conditions in order to insert Pd into the polymer matrix. The composition of the solution is controlled through the use of a flow-injection system and potentiostat connected to a three-electrode flow cell using a previously published method.[23] In order to further minimize the use of precious metals, carbon was used as the electrode material for the electropolymerization of PANI. Carbon has additional advantages in its light weight, good conductivity, and low cost.

The goals of this study were to choose and characterize an appropriate carbon substrate (Chapters 4 and 5) and identify which Pd species in aqueous acidic solution results in the most favorable interactions with the polymer (Chapter 6), and to elucidate the nature of these interactions for the controlled and systematic way (Chapter 7). The level of interaction can be discerned with the use of cyclic voltammograms (CVs), Raman spectroscopy and X-ray photoelectron spectroscopy (XPS), as will be explained in the chapters of this work.

1.6 References

(1) Huang, W.-S.; Humphrey, B. D.; MacDiarmid, A. G. Polyaniline, a Novel Conducting Polymer. Morphology and Chemistry of Its Oxidation and Reduction in Aqueous Electrolytes. *J. Chem. Soc. Faraday Trans. 1* **1986**, *82* (8), 2385.

(2) Golczak, S.; Kanciurzewska, A.; Fahlman, M.; Langer, K.; Langer, J. J. Comparative XPS Surface Study of Polyaniline Thin Films. *Solid State Ionics* **2008**, *179* (39), 2234–2239.

(3) Wang, B.; Tang, J.; Wang, F. Electrochemical Polymerization of Aniline. *Synth. Met.* **1987**, *18* (323).

(4) Zotti, G.; Cattarin, S.; Comisso, N. Cyclic Potential Sweep Electropolymerization of Aniline. The Role of Anions in the Polymerization Mechanism. *J. Electroanal. Chem.* **1988**, *239* (1–2), 387–396.

(5) Sasaki, K.; Kaya, M.; Yano, J.; Kitani, A.; Kunai, A. Growth Mechanism in the Electropolymerization of Aniline and P-Aminodiphenylamine. *J. Electroanal. Chem.* **1986**, *215* (1–2), 401–407.

(6) Yang, H.; Bard, A. J. The Application of Fast Scan Cyclic Voltammetry. Mechanistic Study of the Initial Stage of Electropolymerization of Aniline in Aqueous Solutions *. *Elsevier Sequoia S.A* **1992**, *339*, 423–449.

(7) Genies, E. M.; Lapkowski, M. Spectroelectrochemical Evidence for an Intermediate in the Electropolymerization of Aniline. *J. Electraanal. Chem* **1987**, *236*, 189–197.

(8) Ray, A.; Richter, A. F.; MacDiarmid, A. G.; Epstein, A. J. Polyaniline: Protonation/deprotonation of Amine and Imine Sites. *Synth. Met.* **1989**, *29* (1), 151–156.

(9) Harbottle, A. M. POLYANILINE SORPTION OF RUTHENIUM, Georgia Institute of Technology, 2016.

(10) Dmitrieva, E.; Dunsch, L. How Linear Is " Linear " Polyaniline? *J. Phys. Chem. B* **2011**, *115*, 6401–6411.

(11) Stafström, S.; Brédas, J. L.; Epstein, A. J.; Woo, H. S.; Tanner, D. B.; Huang, W. S.; MacDiarmid, A. G. Polaron Lattice in Highly Conducting Polyaniline: Theoretical and Optical Studies. *Phys. Rev. Lett.* **1987**, *59* (13), 1464–1467.

(12) Hasik, M.; Bernasik, A.; Drelinkiewicz, A.; Kowalski, K.; Wenda, E.; Camra, J. XPS Studies of Nitrogen-Containing Conjugated Polymers–palladium Systems. *Surf. Sci.* **2002**, *507*, 916–921.

(13) Drelinkiewicza, A.; Waksmundzka, A.; Makowski, W.; Sobczak, J. W.; Król, A.; Zięba, A. Acetophenone Hydrogenation on Polymer-Palladium Catalysts. The Effect of Polymer Matrix. *Catal. Letters* **2004**, *94* (3–4), 143–156.

(14) Drelinkiewicz, A.; Hasik, M.; Choczynski, M. Preparation and Properties of Polyaniline Containing Palladium. *Mater. Res. Bull.* **1998**, *33* (5), 739–762.

(15) Drelinkiewicz, A.; Hasik, M.; Quillard, S.; Paluszkiewicz, C. Infrared and Raman Studies of Palladium—nitrogen-Containing Polymers Interactions. *J. Mol. Struct.* **1999**, *511–512*, 205–215.

(16) Elding, L. I. Palladium (II) Halide Complexes. I. Stabilities and Spectra of Palladium (II) Chloro and Bromo Aqua Complexes. *Inorganica Chim. Acta* **1972**, *6* (4), 647–651.

(17) Elding, L. I. Palladium(II) Halide Complexes, II. Acid Hydrolyses and Halide Anations of palladium(II) Chloro and Bromo Aqua Complexes. *Inorganica Chim. Acta* **1972**, *6* (C), 683–688.

(18) Cruywagen, J. J.; Kriek, R. J. Complexation of palladium(II) with Chloride and Hydroxide. *J. Coord. Chem.* **2007**, *60* (4), 439–447.

(19) Drew Tait, C.; Janecky, D. R.; Rogers, P. S. Z. Speciation of Aqueous palladium(II) Chloride Solutions Using Optical Spectroscopies. *Geochim. Cosmochim. Acta* **1991**, *55* (5), 1253–1264.

(20) Boily, J.-F.; Seward, T. M. Palladium(II) Chloride Complexation: Spectrophotometric Investigation in Aqueous Solutions from 5 to 125°C and Theoretical Insight into Pd-Cl and Pd-OH 2 Interactions.

(21) Kriek, R. J.; Mahlamvana, F. Dependency on Chloride Concentration and "in-Sphere" Oxidation of H 2 O for the Effective TiO 2 -Photocatalysed Electron Transfer from H 2 O to [PdCl N (H 2 O) 4−n] 2−n (N = 0–4) in the Absence of an Added Sacrificial Reducing Agent. *"Applied Catal. A, Gen.* **2012**, *423–424* (424), 28–33.

(22) Morávková, Z.; Trchová, M.; Exnerová, M.; Stejskal, J. The Carbonization of Thin Polyaniline Films. *Thin Solid Films* **2012**, *520* (19), 6088–6094.

(23) Jonke, A. P.; Josowicz, M.; Janata, J.; Engelhard, M. H. Electrochemically Controlled Atom by Atom Deposition of Gold to Polyaniline. *J. Electrochem. Soc.* **2010**, *157* (10), P83–P87.

(24) Jonke, A. P.; Josowicz, M.; Janata, J. Odd-Even Pattern Observed in Polyaniline/(Au-0 - Au-8) Composites. *J. Electrochem. Soc.* **2012**, *159* (3), P40–P43.

(25) Hakkinen, H.; Landman, U. Gold Clusters (Au-N, 2 <= N <= 10) and Their Anions. *Phys. Rev. B* **2000**, *62* (4), R2287–R2290.

(26) Guo, J.-J.; Shi, J.; Yang, J.-X.; Die, D. Ab Initio Study of Small AunPd− (n=1–5) Cluster Anions. *Phys. B Condens. Matter* **2007**, *393* (1–2), 363–367.

(27) Gilb, S.; Weis, P.; Furche, F.; Ahlrichs, R.; Kappes, M. M. Structures of Small Gold Cluster Cations (Au+n, n<14): Ion Mobility Measurements versus Density Functional Calculations. *The Journal of chemical physics*. 2002, pp 4094–4101.

(28) Bondybey, V. E.; English, J. H. Laser Induced Fluorescence of Metal Clusters Produced by Laser Vaporization: Gas Phase Spectrum of Pb_2. *J. Chem. Phys.* **1981**, *74* (12), 6978–6979.

(29) Brucat, P. J.; Zheng, L.; Pettiette, C. L.; Yang, S.; Smalley, R. E. Metal Cluster Ion Photofragmentation. *J. Chem. Phys.* **1986**, *84* (6), 3078.

(30) Higuchi, M.; Ikeda, I.; Hirao, T. A Novel Synthetic Metal Catalytic System. *J. Org. Chem.* **1997**, *62* (4), 1072–1078.

(31) Amaya, T.; Saio, D.; Hirao, T. Versatile Synthesis of polyaniline/Pd Nanoparticles and Catalytic Application. In *Macromolecular Symposia*; WILEY-VCH Verlag, 2008; Vol. 270, pp 88–94.

(32) Islam, R. U.; Witcomb, M. J.; Van Der Lingen, E.; Scurrell, M. S.; Otterlo, W. Van; Mallick, K. In-Situ Synthesis of a Palladium-Polyaniline Hybrid Catalyst for a Suzuki Coupling Reaction. *J. Organomet. Chem.* **2011**, *696*, 2206–2210.

(33) Nava, P.; Sierka, M.; Ahlrichs, R.; Chemie, T. Density Functional Study of Palladium Clusters. *Phys. Chem. Chem. Phys.* **2003**, *5* (16), 3372–3381.

(34) Jonke, A. P.; Steeb, J. L.; Josowicz, M.; Janata, J. Atomic Clusters of Pd and AuNPdM in Polyaniline. *Catal. Letters* **2013**, *143* (6), 531–538.

(35) Jonke, A. P.; Josowicz, M.; Janata, J. Polyaniline Electrodes Containing Tri-Atomic Au/Pd Clusters: Effect of Ordering. *Catal. Letters* **2013**, *143* (12), 1261–1265.

(36) Ai-Jie, M.; Xiao-Yu, K.; Gang, C.; Ya-Ru, Z.; Yan-Fang, L.; Peng, L.; Chi, Z. *Ab Initio* Calculation of the Geometric, Electronic and Magnetic Properties of Neutral and Anionic $Au_N Pd$ ($N = 1–9$) Clusters. *Mol. Phys.* **2011**, *109* (11), 1485–1494.

CHAPTER 2. PALLADIUM INSERTION INTO A POLYANILINE MATRIX

2.1 Polyaniline Deposition and Conditioning

All PANI electrodepositions were done in a standard three-electrode configuration. The working electrode consisted of a graphite rod (Graphtek, Buffalo Grove, IL) with a synthetic graphite plate made from petroleum coke (Advanced Carbon Engineered Solutions, North Bay, ON Canada) glued to the surface using carbon epoxy (Atom Adhesives, AA-CARB-61, Ft. Lauderdale, FL). The working electrode can be seen in Figure 2.1. The other two electrodes in the system are a platinum counter electrode and a Ag/AgCl in 1M KCl//1M $NaNO_3$ reference.

Figure 2.1: Carbon working electrode. Synthetic graphite plate (from petroleum coke) carbon epoxied to the surface of a graphite rod. Screw hole machined into the back.

2.1.1 PANI Electrodeposition

Electrodepositions were done at constant potential using a 0.1M solution of aniline in 2M HBF_4. They were completed on a CH Instruments 660 workstation (Austin, TX). After holding the working electrode at the open cell potential (OCP) for 200s, a linear sweep voltammogram (LSV) was completed from OCP to +1.0V to find the optimal potential for the deposition, Figure 2.2.

.

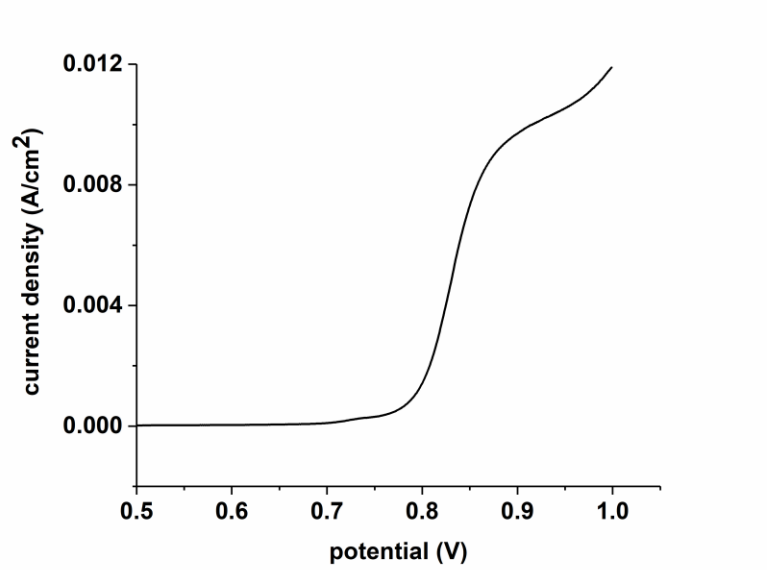

Figure 2.2: Linear sweep voltammogram in 0.1M aniline/2M HBF_4.

The optimal potential was found to be E = 0.85V. After completion of the LSV, deposition was carried out holding the potential until a charge of 500 mC was achieved (Figure 2.3A). Following the deposition, one cycle in the aniline solution was run between -0.25V and +0.95V in order to "set" the PANI layer (Figure 2.3B).

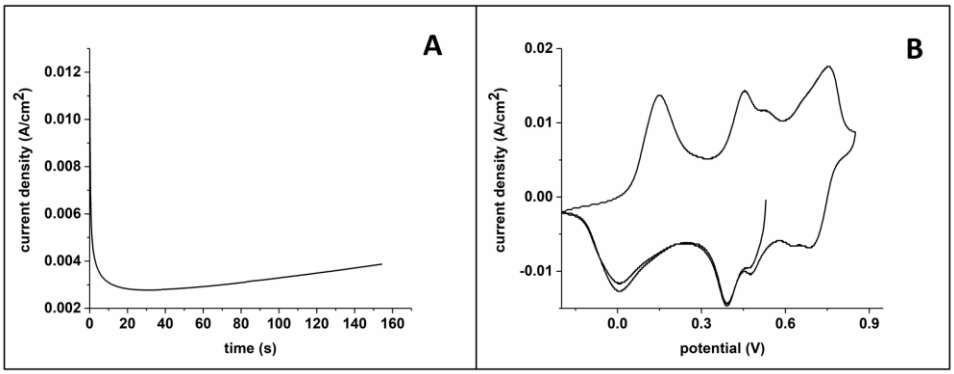

Figure 2.3: Deposition of PANI using 0.1M aniline in 2M HBF_4 (A) and one cycle in the aniline solution to "set" the PANI film (B).

Lastly, the PANI was characterized by running a cyclic voltammogram (CV) from -0.35V to +0.95V in 0.1M $HClO_4$ until the film was stable (Figure 2.4). This final step of cycling in 0.1M $HClO_4$ also served to exchange the anion from BF_4^- to ClO_4^- since all subsequent work was done in 0.1M $HClO_4$ solutions.

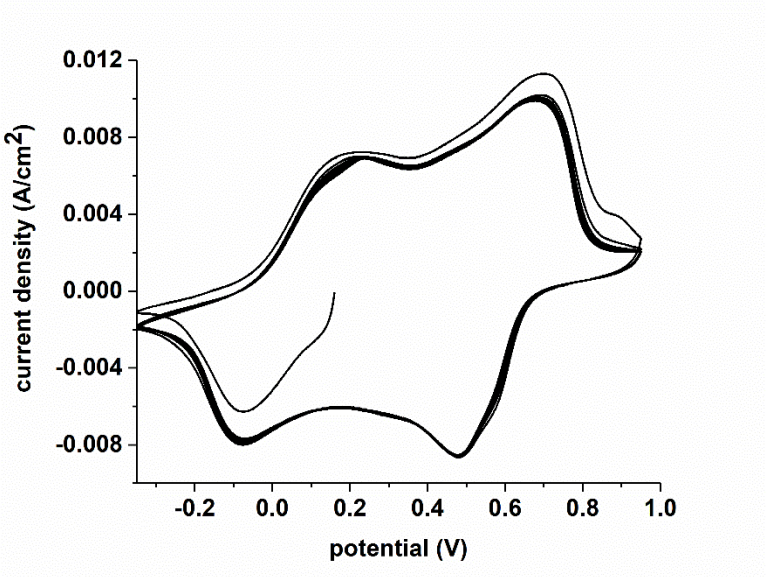

Figure 2.4: CV of PANI in 1M $HClO_4$ at 50mV/s.

2.1.2 PANI Conditioning

PANI electrodes that were used for palladium insertion were all run through a 'conditioning' process. The 'conditioning' made minor changes to the structure of the PANI matrix and ensured a consistent point with which to start the palladium insertion process. Figure 2.5 shows a CV of the conditioned PANI in 1M $HClO_4$. During the conditioning process, the H^+ exchange peaks and the anion exchange peaks decrease in current and shift closer together. This indicates a change in conformation of the polymer during the conditioning process that leads to these processes becoming more simultaneous.

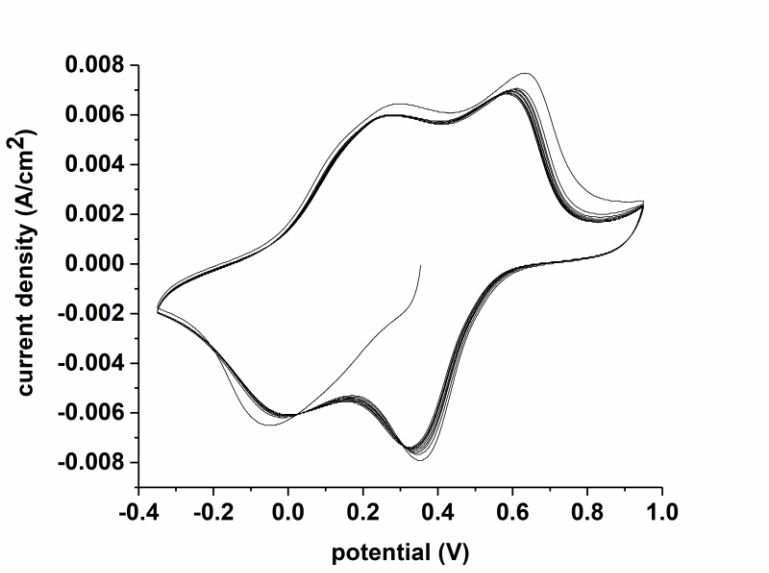

Figure 2.5: CV of conditioned PANI in 1M $HClO_4$ at 50 mV/s

2.2 Palladium Insertion Scheme

A controlled method of palladium insertion has been modified from previous studies using gold.[1] In this method, a specially machined flow cell is connected to a FIALab flow- injection analysis (Alitea Instruments, Medina, WA) system (Figure 2.6) and an OMNI 90 potentiostat (Cypress Systems, Lawrence KS) for precise control of the solutions and potential during the insertion process. Master control of the entire system is through LabView by National Instruments (Austin, TX).

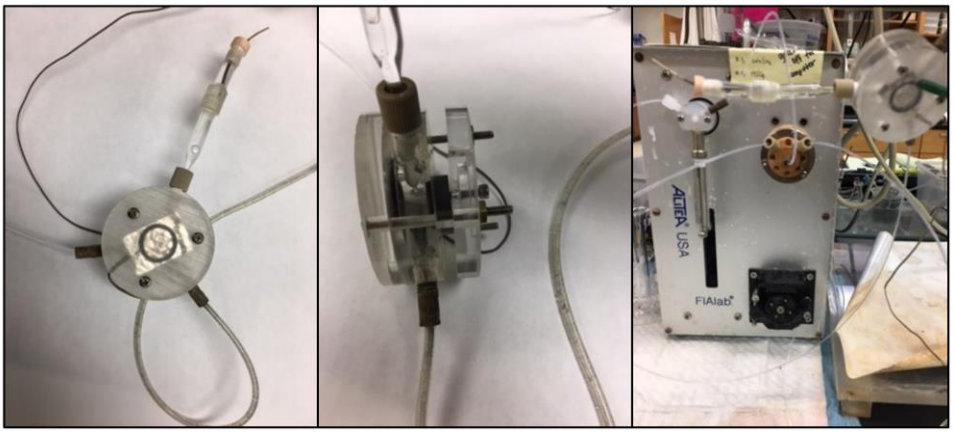

Figure 2.6: Flow cell machined from acrylic and connected to FIA System and potentiostat.

The controlled insertion of one palladium complex per nitrogen-containing site of PANI requires that there is no interruption of the electrochemical contact to the PANI film, scheme shown in Figure 2.7. The process begins with the flow cell containing 0.1M $HClO_4$ at open cell potential of +0.4 followed by a sweep up to the holding potential of +0.7V (A). The PANI film starts in the emeraldine salt form, PANI(ES), and is oxidized to the

pernigraniline form, PANI(PN) during this step. As the PANI is being held in the oxidized state at +0.7V in 0.1M $HClO_4$, a solution of K_2PdCl_4 is injected into the cell and the PANI exposure to the $PdCl_4^{2-}$ anion continues for 2 minutes (B). During this time, a stoichiometric PANI(PN)*$PdCl_4^{2-}$ complex is formed. However, due to the PANI being held in the oxidized state, the $PdCl_4^{2-}$ is not spontaneously reduced to Pd(0) metal. The excess $PdCl_4^{2-}$ anions that have not complexed with the PANI(PN) are rinsed with excess volume of 0.1M $HClO_4$ (C).

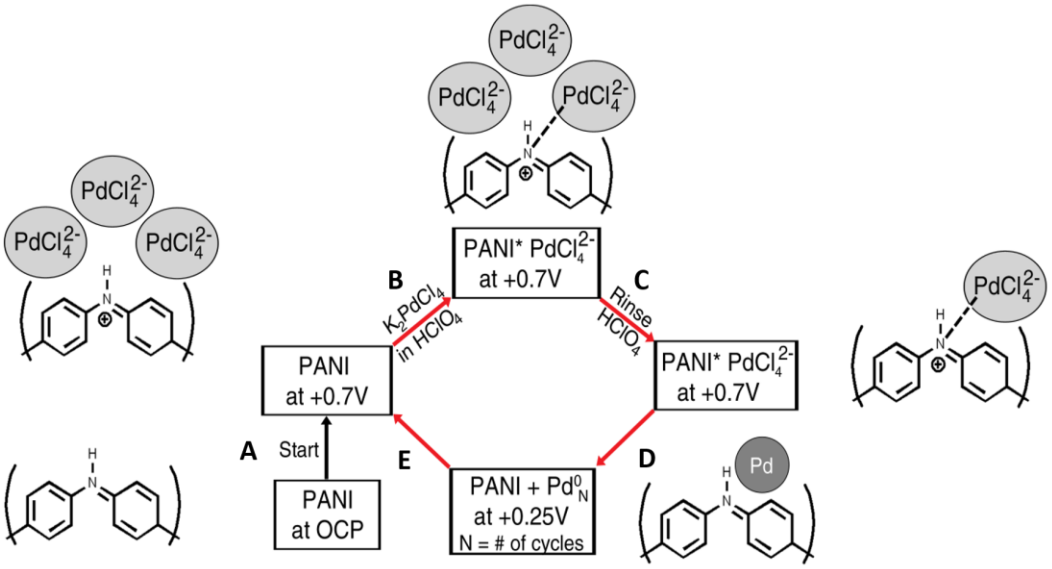

Figure 2.7: Scheme for palladium (II) chlorocomplex insertion into PANI.

Following the rinse, a negative sweep of the potential to +0.2V reduces the PANI(PN)*$PdCl_4^{2-}$ to Pd(0) and a reduced form of PANI (D). After the palladium is reduced, it frees up the nitrogen-containing groups to accept another $PdCl_4^{2-}$ anion in the

subsequent cycle. With each cycle described, another Pd atom should add to the previous Pd atoms and build clusters within the PANI matrix.

The steps shown in Figure 2.7 are also shown as part of the timing diagram for the insertion of palladium (Figure 2.8).

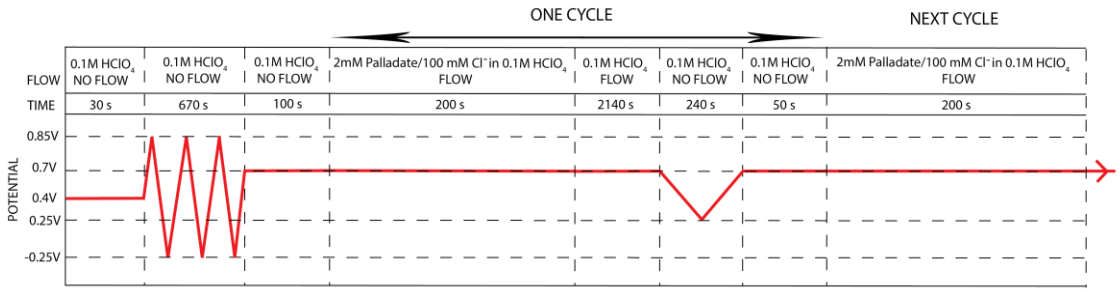

Figure 2.8: Timing diagram for the insertion cycles of palladium into PANI.

The process begins with the flow cell being filled with 0.1M $HClO_4$ and held with no flow. PANI starts at +0.4V and is scanned up to +0.7V, followed by three CVs in order to initially characterize the PANI film prior to palladium insertion. After cycling, the potential is held at +0.7V for another 100s with no flow. While the potential is held at +0.7V, a solution of 2.0mM $PdCl_4^{2-}$/100mM Cl^- in 0.1M $HClO_4$ is injected into the flow cell with the contact time between PANI and the palladate solution reaching two minutes. Following contact with palladate solution, the flow cell is sufficiently rinsed with 0.1M $HClO_4$ while the potential is still held at +0.7V. For the last step, flow of 0.1M $HClO_4$ is stopped and the potential is swept from +0.7V down to +0.25V and then brought back to +0.7V. After this reduction step, the process is then repeated with the injection of more $PdCl_4^{2-}$.

2.3 Electrode Characterization

All of the electrodes were characterized using any combination of Raman spectroscopy, X-ray photoelectron spectroscopy (XPS), and scanning electron microscopy (SEM). The electrodes were characterized at each stage of preparation: the bare carbon support, carbon-PANI, carbon-conditioned PANI, and carbon-PANI with inserted palladium. The $PdCl_4^{2-}$ solution and speciation for use in the insertion cycles was found using UV-Vis spectroscopy.

2.3.1 UV-Vis

Ultraviolet-visible spectroscopy (UV-Vis) measurements were performed using a Shimadzu UV-3101PC double beam instrument (Kytoto, Japan) with a quartz cuvette of a 1 cm path length, in the range of 190-800 nm.

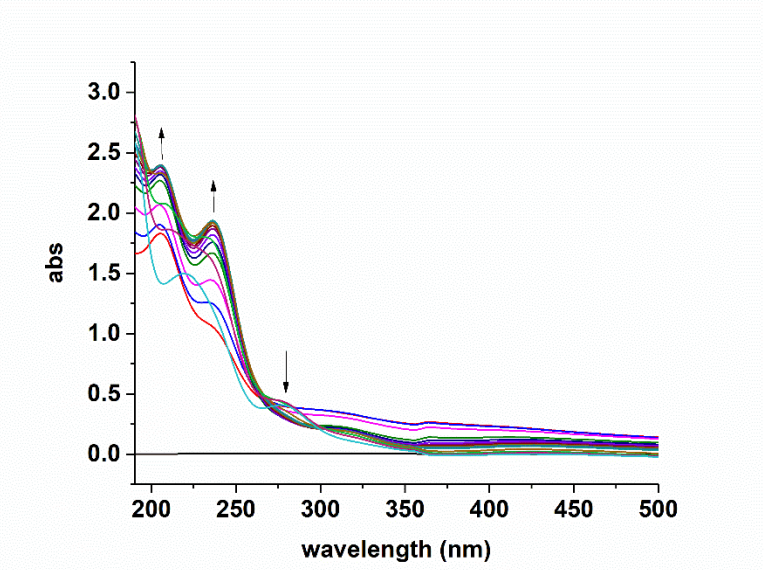

Figure 2.9: UV-Vis spectra of $PdCl_4^{2-}$ in 0.1M $HClO_4$ recorded with each 20µL addition 5M NaCl in 0.1M $HClO_4$.

UV-Vis spectroscopy was used in order to monitor the speciation of the $PdCl_4^{2-}$ in 0.1M $HClO_4$ as 20µL aliquots of 5M NaCl in 0.1M $HClO_4$ were added (Figure 2.9). The speciation of the palladium (II) chlorocomplex plays an important role in the interaction with PANI which will be outlined in detail in Chapter 7.

2.3.2 Raman spectroscopy

Resonance Raman spectra were collected using a Renishaw inVia Raman spectrometer (Wotton-under-Edge, UK) coupled onto a Leica DM 2500M microscope containing a 20X/0.4 N.A. objective and a 1200 lines/nm grating. The measurements were completed using a 785 nm diode laser with an integration time of 25 s. Signals were collected on a CCD detector in the range of 100-1800 cm^{-1}. Spectra were collected over five locations on each sample to evaluate overall consistency. The spectra were normalized, averaged, and smoothed using OriginPro 9.0 (Northampton, MA).

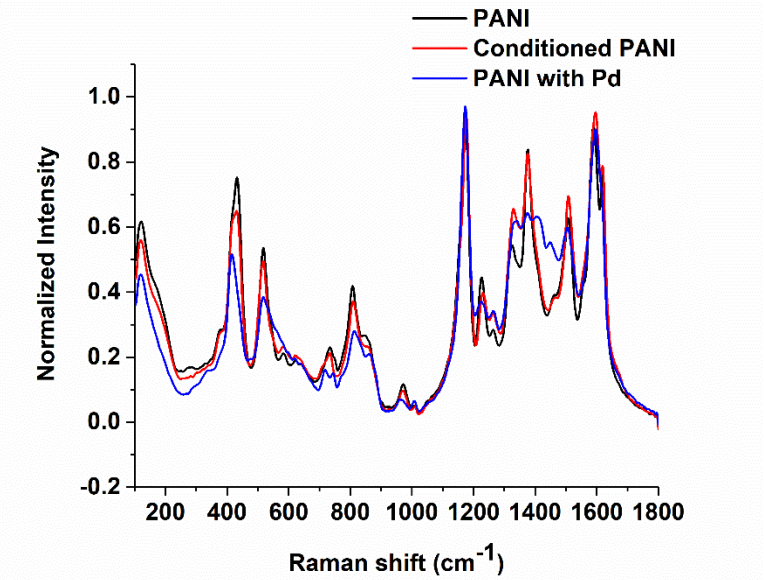

Figure 2.10: Raman spectra of PANI, conditioned PANI, and PANI after Pd insertion.

Raman spectra were recorded after each stage in the development of the composite electrode (Figure 2.10). The black spectrum shows the PANI after it was deposited on the carbon substrate, and the red spectra shows the PANI after the conditioning process. The spectra before and after conditioning are relatively similar with some slight changes in the intensity of the polaron peak at 1375 cm^{-1}. However, after Pd is inserted into the PANI matrix, several changes in the spectra can be seen. Two peaks appear at 1408 cm^{-1} and 1450 cm^{-1} that are not present without Pd, and can be tentatively assigned to C=N vibrations.[2] Raman spectroscopy studies will be explained in more detail in Chapters 6 and 7.

2.3.3 XPS

X-ray photoelectron spectroscopy (XPS) measurements were made using a ThermoFisher Scientific spectrometer (Waltham, MA) with an Al Kα X-ray photon source. The instrument was calibrated using a gold (Au) standard giving a binding energy (BE) of 83.96 eV for the Au $4f_{7/2}$. The vacuum in the analysis chamber was maintained at 3×10^{-7} mbar or lower. A flood gun consisting on low energy ionized Ar gas was used to neutralize any surface charges. Data were collected from the samples using a 400 μm X-ray spot size, pass energies of 200 eV for the survey scan, and 50 eV for the elemental scans. Spectra were deconvoluted and analysed using ThermoScientific Avantage Software.

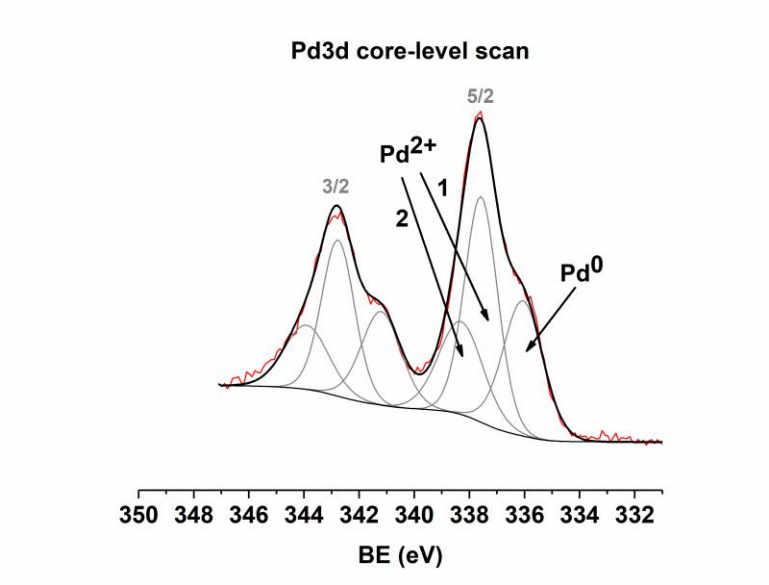

Figure 2.11: XPS Pd3d core-level scan of PANI after Pd insertion.

The Pd3d scans can be deconvoluted into three peaks (Figure 2.11). The peak centered around binding energy (BE) 335 eV corresponds to the Pd(0) reduced metal. The peak around BE=337 eV corresponds to the Pd(II) ion bound to Cl, and the peak at BE= 339 eV is also identified at Pd(II) but bound to a N or O.[3] More details of the XPS interpretation are outlined in Chapter 6.

2.3.4 SEM

Micrographs were acquired on a Hitachi SU8230 FE-SEM (Tokyo, Japan) using incident beam energies between 1.0 and 3.0 kV. The SEM images are evaluated using ImageJ software from NIH. The thickness of PANI fibers, the size of other PANI features, and the features of electrodeposited metal can be measured and compared (Figure 2.12).

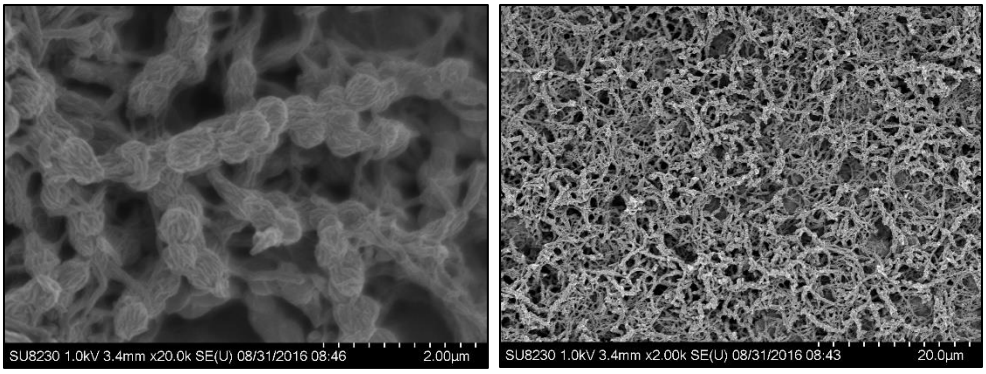

Figure 2.12: SEM images of PANI after Pd insertion at 20.0x magnification (left) and 2.00x magnification (right).

2.4 References

(1) Jonke, A. P.; Josowicz, M.; Janata, J.; Engelhard, M. H. Electrochemically Controlled Atom by Atom Deposition of Gold to Polyaniline. *J. Electrochem. Soc.* **2010**, *157* (10), P83–P87.

(2) Drelinkiewicz, A.; Hasik, M.; Quillard, S.; Paluszkiewicz, C. Infrared and Raman Studies of Palladium—nitrogen-Containing Polymers Interactions. *J. Mol. Struct.* **1999**, *511–512*, 205–215.

(3) Hasik, M.; Bernasik, A.; Drelinkiewicz, A.; Kowalski, K.; Wenda, E.; Camra, J. XPS Studies of Nitrogen-Containing Conjugated Polymers–palladium Systems. *Surf. Sci.* **2002**, *507*, 916–921.

CHAPTER 3. OPTIMIZATION OF THE PALLADIUM INSERTION PROCESS

3.1 Introduction

Chapter 2 outlines the experimental procedures used. However, during each step of the outlined insertion process, there is need for optimization of the parameters with the intention of fine-tuning the interaction between palladium and polyaniline. Also through changing various parameters in the insertion process, a better understanding of the nature of the palladium-PANI interaction can be gained. Many comparisons were made using Raman spectroscopy and X-ray photoelectron spectroscopy (XPS) while considering the state of the polymer, the effect of Pd presence on the bond vibrations, and the extent of Pd reduction within the polymer matrix. In particular, Figure 2.7 and Figure 2.8 should be referred to for each change in parameter.

3.2 Evaluation of parameters through Raman Spectra

3.2.1 Effect of multiple conditioning cycles

The original intent for conditioning of the polyaniline in previous work was to oxidize the film to shed oligomers and obtain a stable starting film for the insertion of palladium.[1] It was also necessary to run "blank" insertion cycles (without the presence of Pd) to find out if there were changes to the polymer that resulted from the insertion process itself. A series of one through four "blank" conditioning cycles were run to see if the number of cycles had an effect on the polymer matrix, Figure 3.1. The number of conditioning cycles does have a slight effect on the polymer Overall, the oxidation state of the polymer does not drastically change due to all of the runs using +0.7V as the holding

potential. This is also seen in the unchanging ratio of the intensity of the peaks at 1230 cm^{-1} and 1265 cm^{-1} tentatively assigned to the quinoid and benzenoid C-N stretches.[2,3]

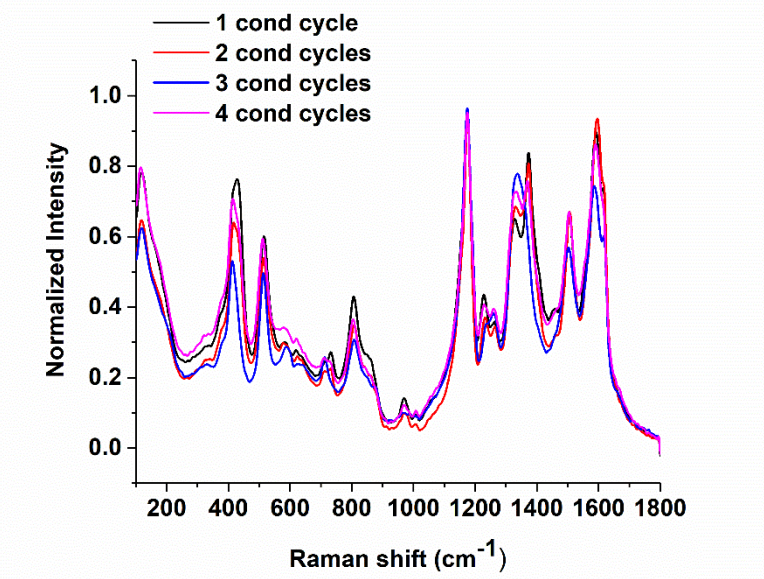

Figure 3.1: Raman spectra of multiple conditioning cycles of PANI. The effects of one through four cycles are shown.

However, the polaron C-$N^{\cdot+}$ stretch at 1375 cm^{-1} shows a difference in intensity, indicating a difference in the protonation level of the PANI.

The effects of the number of conditioning cycles was also checked by inserting Pd into the matrix after each set of conditioning cycles and is shown in Figure 3.2. After Pd insertion, the clearest indicator that Pd is interacting with the PANI is in the region of 1400 cm^{-1} to 1500 cm^{-1}. Namely, 1410 cm^{-1} and 1450 cm^{-1} tentatively attributed to the change in conjugation length of the C=N stretch when Pd is present. [2,4] In Figure 3.2, it can also be seen that the intensity of the polaron stretch at 1375 cm^{-1} is also changing with each

cycle as when Pd was absent in Figure 3.1. This makes it difficult to see if the changes in PANI causing differences in the Raman spectra are due to the effects of the number of cycles or due to the presence of Pd. Therefore, two conditioning cycles was chosen as the standard starting point for all further studies.

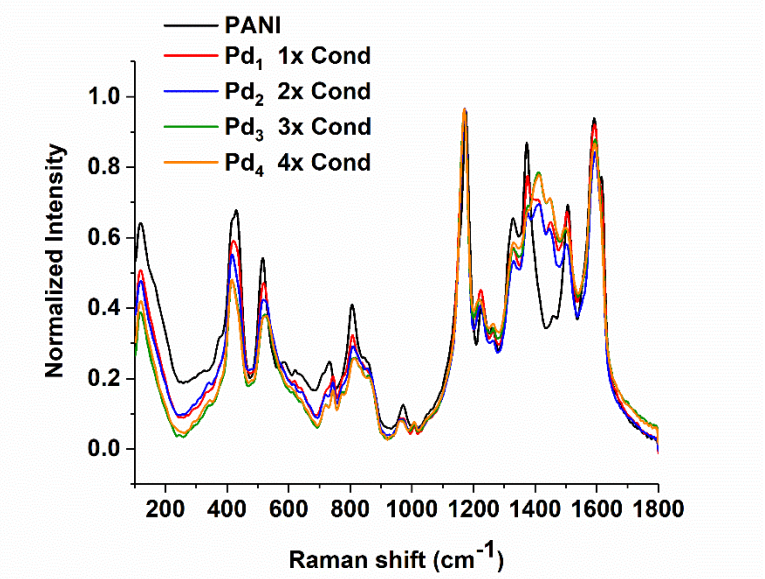

Figure 3.2: Insertion of Pd after each set of conditioning cycles. 1-4 Pd insertion cycles were run after 1-4 corresponding conditioning cycles

3.2.2 Effect of holding potential

The next parameter to be optimized was the potential to which the PANI was held in the oxidized state during the Pd insertion cycles. As seen in Figure 3.3 (right), the CV of PANI in 0.1M $HClO_4$ was recorded right before the start of the insertion cycles. At 0.6V, the PANI is in the emeraldine salt form, while at the 0.7V and 0.8V marks, the PANI is in the pernigraniline form. The state of PANI at these potentials will have an effect on the

insertion of the $PdCl_4^{2-}$ anion due to the level of protonation of the polymer. The anions are inserted into the film as a balance of charge to the protonation of imines and amines in the PANI. If the polymer is less protonated, less palladium (II) anion will be drawn into the film. It has also been reported that imine groups are protonated first due to the pKa value of 2.3 as opposed to 5.1 for amines[5] and that noble metals preferentially associate with imines.[6,7] Since 0.6V is in the emeraldine state form with less imine units, and 0.8V leaves PANI in an over-oxidized and degradative state,[1] 0.7V was chosen as the optimal holding potential.

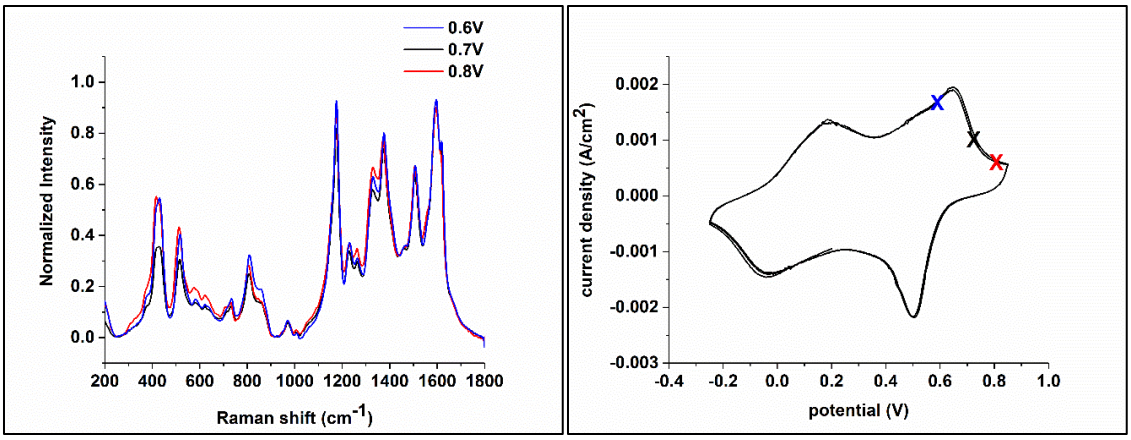

Figure 3.3: Raman spectra (left) of PANI after 2 conditioning cycles at holding potentials of 0.6V, 0.7V, and 0.8V and the CV (right) in 0.1M $HClO_4$ with the corresponding potentials marked.

3.2.3 Effect of acid concentration

The pH level of the perchloric acid solution was varied for both the conditioning step and the palladium insertion cycles. The results of the insertion are seen in the Raman spectra of the PANI-Pd shown in Figure 3.4. It is clear that the Pd is interacting more with

the polymer when 0.1M $HClO_4$ is used. As previously stated in section 1.2.1, the Raman bands at 1410 cm^{-1} and 1450 cm^{-1} are visible, indicating the modification of the C=N vibration by the presence of Pd. Those bands are absent in the spectra of the PANI-Pd prepared with 0.01M $HClO_4$. This is most likely due to the lack of protonation of the PANI at the higher pH. With less protonation, less Pd(II) anions will enter into the film to balance the charge, and the lack of Pd(II) means less effect on the C=N bond vibration.

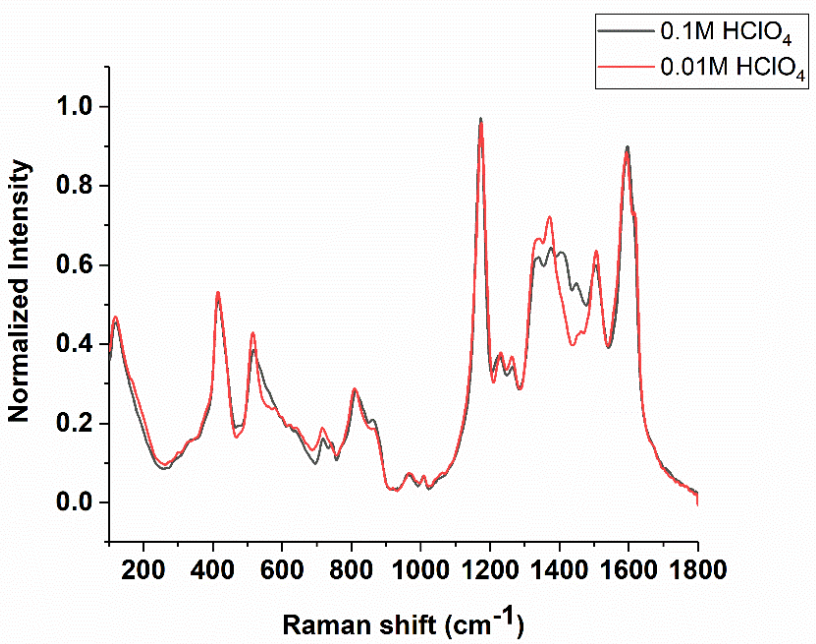

Figure 3.4: Effect of pH on the insertion of Pd. Raman spectra shown of PANI-Pd that were prepared using 0.1M $HClO_4$ and 0.01M $HClO_4$.

3.2.4 Effect of E_{min} for reduction of Pd

Initially, the reduction sweep started at +0.7V down to +0.25V. It was initially assumed that all of the Pd(II) chlorocomplex that was associated with the nitrogen-

containing groups in the PANI would reduce. Further studies with XPS revealed that a majority of the palladium in the PANI matrix remained Pd(II) and there was very little Pd(0) present. In an attempt to reduce a greater percentage of Pd(II) to Pd(0), the minimum potential that reduction sweep reaches was changed to more negative potentials of -0.25V and -1.3V, and a run with no reduction sweep was recorded as a control. In the Raman spectra of Figure 3.5, the intensity of the 1410 cm^{-1} and 1450 cm^{-1} peaks were monitored as an indicator of the extent of Pd(II) interaction in the PANI matrix. The most intense peaks are for the control, indicating that no Pd(0) was formed and that there is a great amount of C=N vibration disruption based on Pd(II) still interacting with the nitrogen-containing groups. The +0.25V and -0.25V reductions are very similar in intensity but are lower than the control. This indicates there is still a majority of Pd(II) in the matrix interacting with the nitrogen-containing groups, but the decrease in intensity indicates that some Pd(0) did form. In Table 3.1, XPS Pd3d core-level scan results confirm that only about 15% of the total palladium content in these samples was Pd(0). The most interesting finding was after the reduction was swept to -1.3V. The Raman spectrum would indicate that perhaps a large percentage of the Pd(II) did reduce as indicated by disappearance of the peaks at 1410 cm^{-1} and 1450 cm^{-1}. In order to confirm that the Pd was reduced, the XPS Pd3d core-level spectrum was taken. The results, shown in Table 3.1 indicate that even less Pd(0), 11%, is present as compared to the +0.25V and -0.25V samples. This suggests a major conformational change in the PANI matrix at such negative potentials that may prevent the reduction of Pd. Based on these results, the potential for the reduction sweep was kept at +0.25V.

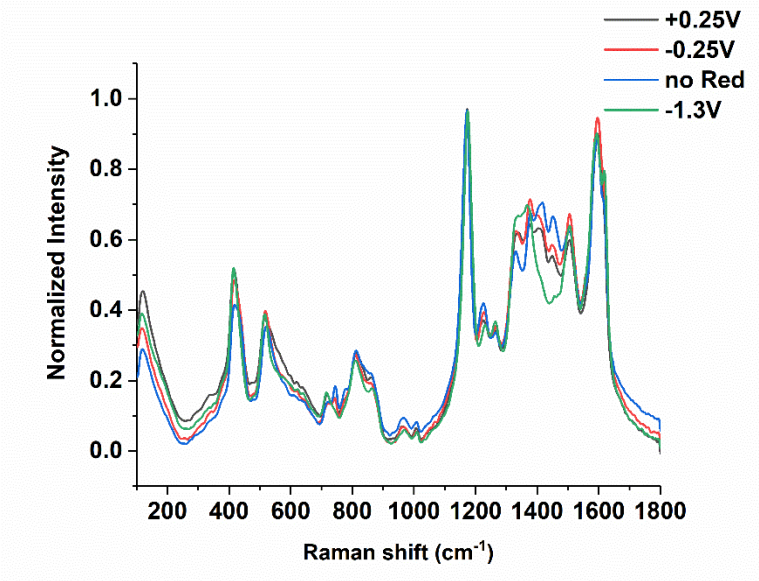

Figure 3.5: Raman spectra of PANI-Pd after each change in final potential of the reduction sweep, E_{min}.

3.2.5 Effect of Pd(II) chlorocomplex solution

Given the final parameter to be changed was the concentration of the palladium (II) chlorocomplex solution. The Raman spectra of the PANI-Pd prepared with 0.2 mM, 2.0 mM, and 20 mM solution is seen in Figure 3.6. Again, considering the bands at 1410 cm^{-1} and 1450 cm^{-1}, the PANI-Pd prepared with 2.0mM Pd(II) solution shows the greatest interaction with the nitrogen-containing groups in the PANI. It was found through XPS and SEM measurements that the 0.2mM solution was not concentrated enough for Pd(II) to interact with enough nitrogen-containing groups that would have an effect on the C=N conjugation seen in Raman spectra. From Table 3.1, the N/Pd ratio is reported as 1 Pd atom for every 61 N atoms. This confirms very little interaction between Pd and the nitrogen-containing groups of PANI. Also, with the low concentration of Pd(II) in the PANI matrix, only 5.6% of the total Pd is being reduced to Pd(0), also seen in Table 3.1. For the PANI-

Pd prepared with 2.0mM and 20mM solutions, more detail regarding the difference in Raman spectra will be explained in Chapters 6 and 7. For the PANI-Pd prepared with 20 mM solution, 21% of the total Pd content was reduced to Pd(0), and when using 2.0 mM solution, the reduction to Pd(0) was 41.5%. It is also seen in the N/Pd ratio that for every 5 or 6 N atoms, there is a Pd, confirming greater interaction. However, as discussed in later chapters, there is more involved in the interaction of Pd to nitrogen-containing groups in PANI that may account for the lack of full reduction to Pd(0).

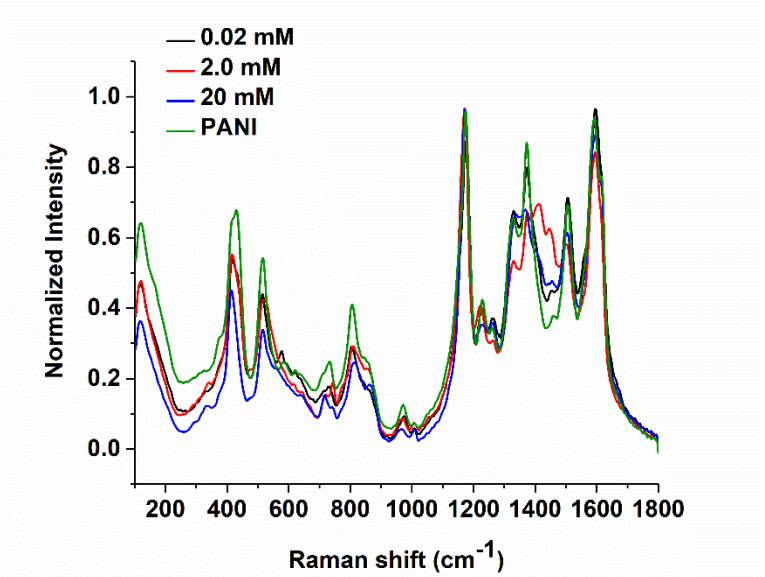

Figure 3.6: Raman spectra of PANI-Pd that was prepared with varying concentrations of Pd(II) chlorocomplex solution.

3.3 Correlation of Raman and XPS results

Table 3.1: Change of parameters, Pd ratios and Raman peak ratios

		Raman		XPS			Notes
Sample #	Description	1410cm^{-1} /1175cm^{-1}	1450cm^{-1} /1175cm^{-1}	N/Pd	Pd^{2+}/Pd^{0}	atom % Pd^{0}	
70	Pd1	0.61	0.52	-	-	-	0.6V to 0.25V 1xRed
69	Pd2	0.64	0.56	4.9	1.4	41.5	
68	Pd3	0.69	0.62	-	-	-	
67	Pd4	0.82	0.72	-	-	-	
71	Pd5	0.70	0.60	3.4	1	49.4	
69	Pd2 0.1M $HClO_4$	0.65	0.57	4.9	1.4	41.5	0.6V to 0.25V 1xRed
82	Pd2 0.01M $HClO_4$	0.52	0.44	6.3	20.6	4.6	
69	Pd2 0.1M $HClO_4$	0.65	0.57	4.9	1.4	41.5	0.6V to 0.25V 1xRed
84	Pd2 HCSA (+)	0.76	0.69	-	-	-	
35	Pd2 (0.2mM Pd)	0.62	0.51	61	17	5.6	0.6V to 0.25V 1xRed
69	Pd2 (2mM Pd)	0.65	0.57	4.9	1.4	41.5	
76	Pd2 (20mM Pd)	0.57	0.49	6	3.8	20.9	
79	no Red	0.72	0.69				0.6V to -0.25V
78	1x Red	0.70	0.61	7	5.8	14.72	
81	3x Red	0.55	0.47	4.7	2.7	24.4	
41	1C PANI	0.72	0.65	-	-	-	0.6V to 0.25V 1xRed
51	500mC PANI	0.70	0.61	-	-	-	
80	no aging	0.64	0.57	-	-	-	0.6V to 0.25V 1xRed
69	2xCon	0.65	0.57	4.9	1.4	41.5	
85	90 min	0.63	0.56	-	-	-	
120	120min	0.75	0.68	3.5	8.4	10.7	
98	no aging	0.67	0.59	3.5	3.7	21.48	0.6V to 0.25V 3xred
97	2xCon	0.78	0.71	3.5	10.9	8.37	
117	0.1M$HClO_4$ + 0.1M NaCl Rinse	0.77	0.67	12.9	22.2	4.3	0.6V to 0.25V 1xRed
101	0.1M HCl	0.81	0.76	-	-	-	
102	0.01M HCl	0.95	0.93	-	-	-	
114	.7V to -0.25V	0.87	0.79	-	-	-	1x Red
87	0.6V to -1.3V	0.51	0.45	11.8	7.7	11.5	
78	0.6V to -0.25V	0.70	0.61	7	5.8	14.72	
118	$PdCl_2(H_2O)_2$	0.60	0.51	11.8	9.3	9.7	0.7V to 0.25V 1xRed
125	$PdCl_3(H_2O)^-$	0.75	0.66	6.36	8.5	9.8	
121	$PdCl_4^{2-}$	0.56	0.47	10.18	49.5	2	

Table 3.1 summarizes all of the studies involving parameter changes in the Pd insertion process. For the Raman columns, the intensities of the two main peaks, 1410 cm^{-}

[1] and 1450 cm^{-1}, are reported in a ratio with the normalized peak at 1175 cm^{-1} which corresponds to the C-H stretch in quinoid units.[2,4] The XPS data for the N/Pd ratio is reported from the survey scans of each sample and the calculated atomic % of each element. The total % of Pd(0) and the Pd^{2+}/Pd^{0} ratio are calculated from atomic % data from deconvoluted Pd3d core-level scans.[8]

The greatest interaction be between the PANI and the palladium can be marked by the N/Pd ratio and the ratio of the Raman peaks. The lower the N/Pd ratio indicates more Pd per nitrogen-containing group and also correlates to higher intensities in the Raman peak ratios. The conditions with the highest conversion of Pd(II) to Pd(0) are highlighted in yellow.

3.4 Conclusions

Various parameters were studied, such as the number of conditioning cycles, the pH of the acidic solutions, holding potential, the ending potential of the reduction sweep, and the concentration of the Pd(II) chlorocomplex solution. The PANI and PANI-Pd samples prepared with the varying parameters were evaluated using Raman spectroscopy and XPS. It was found that using 0.1M $HClO_4$ with 2.0 mM $PdCl_4^{2-}$, two conditioning cycles, a holding potential of 0.7V, and a reduction sweep to +0.25V was favorable for further studies.

3.5 References

(1) Jonke, A. P.; Josowicz, M.; Janata, J. Polyaniline Doped with Atomic Gold. *J. Electrochem. Soc.* **2011**, *158* (12), E147–E151.

(2) Lindfors, T.; Ivaska, A. Raman Based pH Measurements with Polyaniline. *J. Electroanal. Chem.* **2005**, *580* (2), 320–329.

(3) Trchová, M.; Morávková, Z.; Bláha, M.; Stejskal, J. Raman Spectroscopy of Polyaniline and Oligoaniline Thin Films. *Electrochim. Acta* **2014**, *122*, 28–38.

(4) Louarn, G.; Lapkowski, M.; Quillard, S.; Pron, A.; Buisson, J. P.; Lefrant, S. Vibrational Properties of Polyaniline - Isotope Effects. *J. Phys. Chem.* **1996**, *100* (17), 6998–7006.

(5) Ray, A.; Richter, A. F.; MacDiarmid, A. G.; Epstein, A. J. Polyaniline: Protonation/deprotonation of Amine and Imine Sites. *Synth. Met.* **1989**, *29* (1), 151–156.

(6) Jonke, A. P.; Josowicz, M.; Janata, J.; Engelhard, M. H. Electrochemically Controlled Atom by Atom Deposition of Gold to Polyaniline. *J. Electrochem. Soc.* **2010**, *157* (10), P83–P87.

(7) Hatchett, D. W.; Josowicz, M.; Janata, J.; Baer, D. R. Electrochemical Formation of Au Clusters in Polyaniline. *Chem. Mater.* **1999**, *11* (10), 2989–2994.

(8) Hasik, M.; Bernasik, A.; Drelinkiewicz, A.; Kowalski, K.; Wenda, E.; Camra, J. XPS Studies of Nitrogen-Containing Conjugated Polymers–palladium Systems. *Surf. Sci.* **2002**, *507*, 916–921.

CHAPTER 4. EFFECT OF CARBON SUPPORT ON THE PROPERTIES OF ELECTROCHEMICALLY DEPOSITED PLATINUM AND POLYANILINE

In order create the optimal conditions for the insertion of atomic metal clusters into PANI, it is necessary for the PANI matrix to have the most ideal electrochemical properties. The quality and nature of the carbon support plays a role in the properties of the electrodeposited PANI. This chapter outlines the characterization of the carbon support and the correlation to the electrochemical properties of the PANI.

4.1 Introduction

Carbon used as a support material in fuel cells and batteries can vary in properties depending on the structure and impurities present. Reviews on carbon supports have indicated that graphite is commonly chosen to support catalytic metals due to its inert character and conductivity, and the support itself can affect performance of the fuel cell. [1–4] Composite electrodes can be produced from potentiostatic depositions of platinum and/or polyaniline (PANI) directly onto the carbon surface. Carbon supported platinum (C/Pt) is widely used for its known activity toward alcohol oxidation,[5–7] and carbon supported PANI (C/PANI), or even carbon-platinum supported PANI (C/Pt-PANI) electrodes are also attractive for the fabrication of composite catalyst materials.[8,9] Previous studies have shown that PANI can be used as a viable matrix for the insertion of catalytically active atomic-sized metal clusters, using platinum as support.[10–12] We have focused our recent studies on using carbon as a support due to its benefits of being conductive, lightweight and inexpensive.[13] However, in order to choose the appropriate carbon for a support

electrode, understanding the effects that the substrate has on the PANI film is necessary. Dinh and Birss have compared the effects of differing types of support materials, such as noble metals and glassy carbon, on PANI properties. Impedance and CV studies on PANI grown by cycling revealed that the growth rate of the films and redox kinetics are affected by the differing supports. [14] The present study focuses on carbon substrates and the deposition of platinum on the surface as well as the growth of PANI film at constant potential on both the carbon and platinum-on-carbon surfaces.

For this study, we are using a novel synthetic graphite produced from petroleum coke in a process that results in an intended crystalline structure. As a comparison, a widely available extruded graphite rod was also included. From here on, the substrates will be referred to as 'coke' and 'graphite' respectively. Initial characterization of both substrates was completed using X-ray photoelectron spectroscopy (XPS) and Raman spectroscopy. Characterization of the two carbon samples reveal differences in the surfaces as well as in the overall crystalline structure that could account for differences in electrochemical behaviors of the samples.

4.2 Preparation of Electrodes

The petroleum coke was purchased from Advanced Carbon Engineered Solutions (North Bay, Ontario) with dimensions of 13 mm OD and 1 mm thick, with a resistivity of 5.5 μΩ*m, and bulk density of 1.88 g/cm^3. The extruded rod was purchased from Graphtek, L.L.C. (Buffalo Grove, IL) with dimensions of 12.7mm OD and 5 mm thick with a resistivity of of 7.6 μΩ*m and a bulk density of 1.70 g/cm^3. Each was mechanically polished with 30 μm paper (Aluminum Oxide, Allied), rinsed with iso-propanol (70%,

EMD), and dried in oven at 65°C before use. Electrodepositions of platinum and polyaniline (PANI), and electrochemical characterizations were done with an electrochemical workstation (660, CH Instruments) in a three-electrode cell, using a platinum wire mesh counter electrode, and Ag/AgCl in 1M KCl/1M $NaNO_3$ as a reference. Platinum depositions were carried out at E_{const} = 0.02V using a solution of 1 x 10^{-2}M $H_2PtCl_6 \cdot 6H_2O$ (99.9%, Strem) in 0.1M $HClO_4$ (70%, Macron). PANI depositions were done at E_{const} = 0.85V from 0.1M aniline (99+%, Alfa Aesar) in 2M HBF_4 (48%, Strem) and subsequently cycled in 0.1M $HClO_4$. RuHex solution used for carbon characterization was made with equal molar hexaaminеruthenium (III) chloride (Aldrich, 98%) and hexaminеruthenium (II) chloride (Aldrich, 99.9+%) in 1M KNO_3. Characterization of the carbon was carried out using X-ray photoelectron spectroscopy (XPS, Kratos), Raman spectroscopy (confocal, WITec GmbH), and scanning electron microscopy (SU-8230, Hitachi). The thickness of the PANI fibers and Pt features were estimated using ImageJ software from NIH.

4.3 Carbon Characterization

The XPS survey scans of both substrates reveal that the only significant bands present were from carbon and oxygen with possible trace metals present in the graphite substrate. The core-level C1s spectrum (Figure 4.1A) shows a narrower and more intense peak for coke at binding energy (BE) of 283.8 eV; this indicates a majority of sp^2 carbon in the sample.

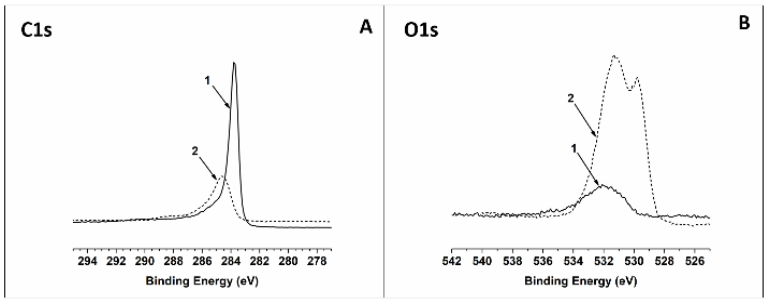

Figure 4.1: XPS spectra for coke (1) and graphite (2) substrates showing the core-level C1s (A) and O1s (B) scans.

The graphite surface has a broader, less intense peak at BE of 284.7 eV, which indicates both sp^2 and sp^3 carbons are present, with the majority being sp^3.[15–17] For the core-level O1s spectrum the broader peak of graphite indicates more surface oxygen groups (Figure 4.1B). For the coke samples, the broad O1s peak centered at a BE of 532 eV indicates both C-O and C=O groups are present on the surface. For graphite, C-O is seen from the peak at BE of 531.3 eV, however, the peak at BE of 529.8 eV may indicate the presences of trace metal oxides that are also on the surface.[17,18] The atomic % ratios of O:C differ greatly between the two samples. For the graphite sample, the O:C ratio is 0.56 and for the coke sample it is 0.05, confirming that the oxygen content of the graphite sample is 11 times greater. With the increase in intensity of the O1s scan for graphite, the greater oxides on the surface as well as the presence of possible metal oxides shows a less pure starting surface for the deposition of PANI. This could inhibit the PANI ever reaching a state of continued growth through uneven adsorption of the monomers on the graphite surface.

The atoms in graphitic carbon are arranged in sheets as a system of bonded hexagons ideally with sp^2 hybridization. With three valence electrons used in the sp^2

hybridization, the fourth forms a π bond, giving the carbon its conductivity.[1] Disruptions and disorder in the hexagonal structure can change the hybridization and the overall properties of the substrate. These differences in the structure of carbon samples can be seen in the Raman spectra (Figure 4.2). The D band near 1350 cm^{-1} is attributed to the breathing mode of rings, while the G band near 1575 cm^{-1} is attributed to bond stretching of the sp^2 of both rings and chains.[19] The D band can be considered a measure of the disorder in a system, therefore the greater the number of defects of the sp^2 structure in the carbon, the more intense the D band.[16,19]

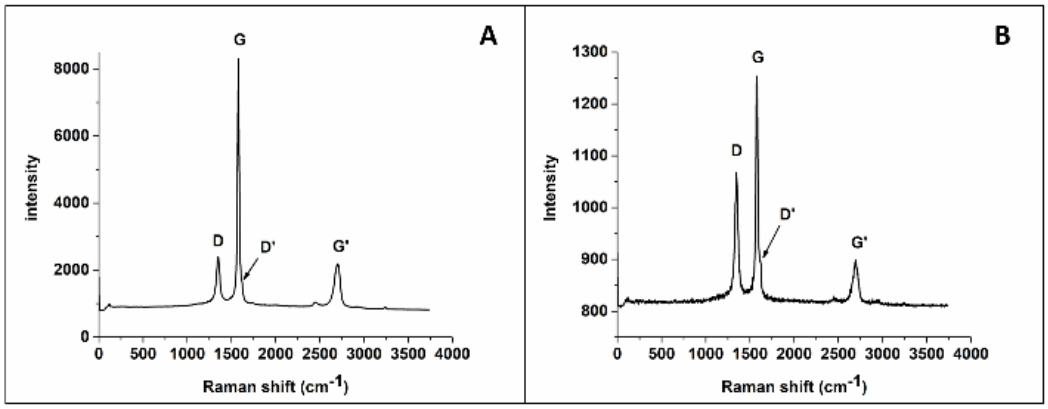

Figure 4.2: Raman spectra of G band for coke (A) and graphite (B). Four different positions were sampled on the carbon surface in (A), while two were sampled on the surface in (B). Spectra were collected using Nd:YAG laser at 532 nm and a 600 g/mm diffraction grating with an acquisition time of 0.01s.

Also, the D' band around 1620 cm^{-1} is seen for graphite in Figure 4.2B but is not seen for coke in Figure 4.2A. This D' band is caused by sufficient defects in the carbon causing a phonon confinement where normally the phonons would be Raman inactive.[20] The D/G intensity ratio can give an indication of the sp^2 or sp^3 character as referenced to pure graphene, though the D band can be due to other defects in the sample.[15] The coke

sample (Figure 4.2A) shows a less intense D band compared to G but the graphite (Figure 4.2B) has a smaller D/G intensity ratio, this suggests a possible higher sp^3 content in the graphite sample. This is consistent with the XPS results in Figure 4.1, which also suggest a higher sp^3 character for graphite.

Since the XPS studies reveal more oxygen groups on the surface, and the Raman spectra show an increase in structural defects in the sp^2 character for the graphite sample, there is a correlation to a small increase in resistance.[21] This resistance will affect Pt deposition efficiency and could inhibit PANI polymerization by keeping the film from reaching a state of continued growth. The greater surface oxygen groups can also affect Pt deposition by causing the nucleation seeds from the H_2PtCl_6 precursor to be unevenly dispersed on the surface. These surface groups can also increase hydrophilicity of the carbon and therefore keep aniline monomers from adsorbing on the surface, resulting in a thinner polymerized PANI film.[21,22]

Each carbon sample was also characterized by CV in 2.5 mM RuHex in $1MKNO_3$. The redox peak potentials appear at -0.19V and -0.27V respectively, Figure 4.3. The 80mV peak separation for both substrates confirms that the rate of electron transfer is not affected by the difference in structure or molecular differences of the electrode surfaces.

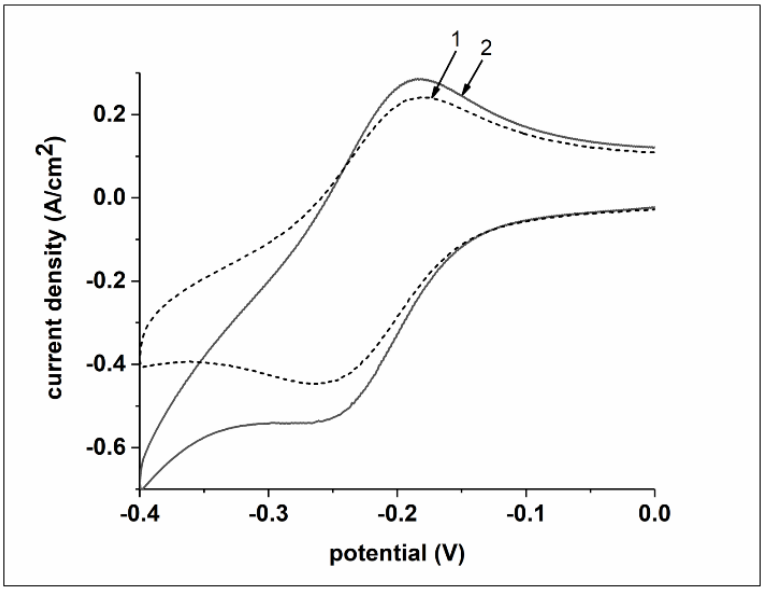

Figure 4.3: Cyclic voltammogram of coke (1) and graphite (2) substrates in 2.5mM RuHex in 1MKNO_3 at 50mV/s. Shown is last scan after reaching steady state.

4.4 Platinum deposition on carbon

In order to compare the electrochemically active surface, a platinum layer was deposited on each of the carbon surfaces using a constant potential (E = 0.02V), Figure 4.4A.

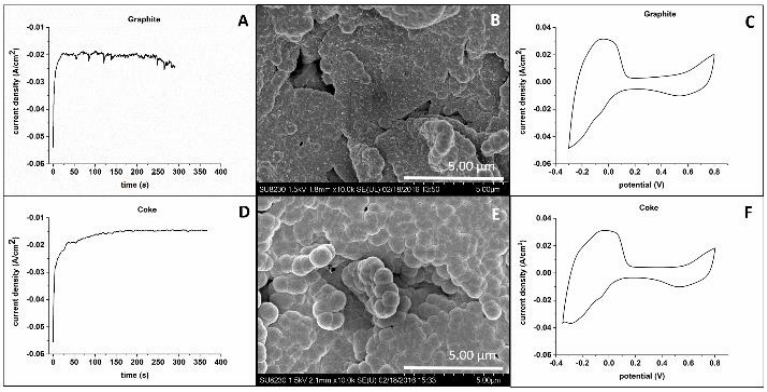

Figure 4.4: Deposition of platinum on graphite (A) and coke (D) at E_{const} = 0.02V until 5 C/cm^2 is achieved. Top row: graphite, bottom row: coke. The corresponding SEM images of the platinum are also shown for graphite support (B) and coke support (E). CVs in 1M H_2SO_4 were recorded at 100mV/s for graphite (C) and coke (F).

The choronoamperogram for graphite shows evidence of hydrogen evolution and a slight decrease in current over time.[23] This hydrogen evolution leads to faster nucleation, and uneven growth of the Pt layer, seen in the SEM image (Figure 4.4B). The platinum deposition on the coke sample results in the opposite. The chronoamperogram in Figure 4.4D has an exponential increase of current over time, signaling a 2D or 3D growth process. The SEM of deposited platinum has a more bulbous structure indicating greater surface area coming from slower growth and larger nucleation sites (Figure 4.4E). The CV of each C/Pt, shown in Figure 4.4C and Figure 4.4F, is similar in the anodic region, showing the hydroxide adsorption, and the cathodic region showing the reduction potential of the oxide formed during the anodic sweep to +0.75V. In the cathodic region, the coke sample shows slightly greater resolution in the hydrogen adsorption and desorption peaks between -0.4V to 0.0V, most likely due to the more structured facets seen in the SEM image after conditioning in 1M H_2SO_4 by fast cycling at 1V/s, in Figure 4.5B and Figure 4.5D.

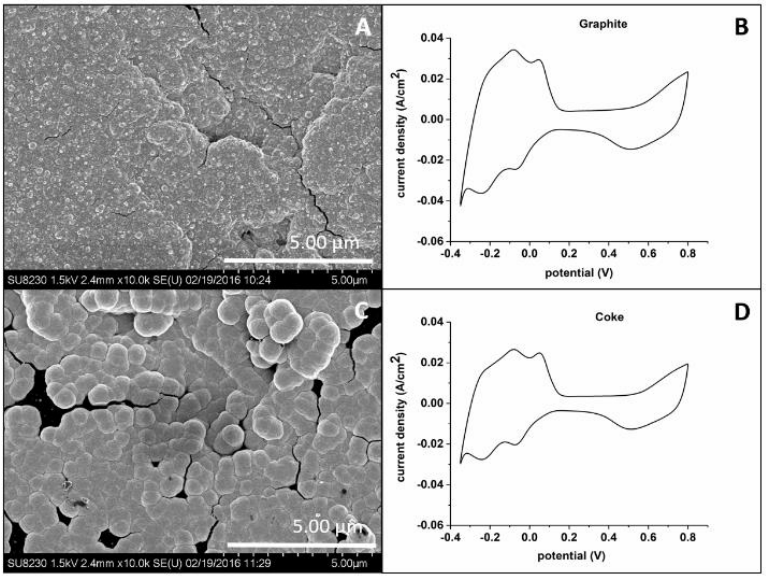

Figure 4.5: SEM and electrochemistry of Pd depositions on graphite (A,B) and coke (C,D). The CVs were recorded in 1M H_2SO_4 at 100 mV/s.

For the coke sample, the structure of the Pt surface did not undergo large physical changes but the bulbous areas reduced in size from approximately 850 nm to 700 nm (Figure 4.5C). However, the Pt on the graphite showed greater rearrangement to a more flat and continuous sheet (Figure 4.5A). Furthermore, the conditioning process rearranged the structure of both samples to allow better hydrogen adsorption on the surface as seen by the peaks at E= -0.5V, Pt(100) facet, and E = -0.25V, Pt(110) facet, Figure 4.5B. For graphite, there is greater hydrogen adsorption on the Pt(100) facet than for coke sample with values of 2.41 mC/cm^2 and 2.15 mC/cm^2 respectively. Conversely, there is greater adsorption on the Pt(110) facet for coke at 2.0 mC/cm^2, over graphite, 1.66 mC/cm^2.[24,25] The coke sample shows approximately the same adsorption for both facets after conditioning.

4.5 Electropolymerization of aniline on carbon and C/Pt

Figure 4.6 shows the polymerization of aniline from 2M HBF_4 at E_{const} = +0.85V onto the surface of each carbon. The PANI films were cycled in 0.1M $HClO_4$ to exchange the BF_4^- anion inserted during polymerization, and as characterization of the film.

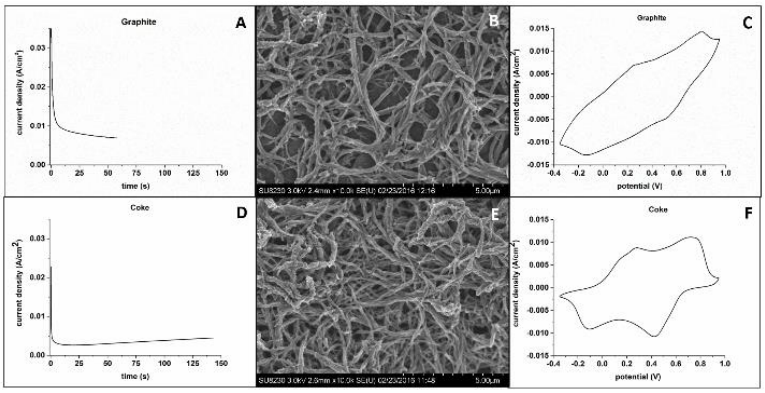

Figure 4.6: Comparison of PANI deposited directly onto graphite (top) and coke (bottom) surfaces. The i-t curves shown are for constant potential deposition (E = 0.85V, Q = 0.42 C/cm^2) from aniline solution described in Experimental. Characterization of the films was done by CVs in 0.1M $HClO_4$ at 50 mV/s for graphite support (C) and coke support (F).

The downward slope of the PANI on the graphite sample (Figure 4.6A) indicates that the polymerization never reaches a state with continued growth and branching[26]. In contrast, the upward slope of the deposition on the coke sample (Figure 4.6D) indicates steady growth of the polymer film. In this sense, polymerization on the graphite surface may take longer to reach the state of continued growth.[22] The SEM images of the PANI film on each carbon sample show differences in the openness of the structure between the graphite support (Figure 4.6B) and the coke support (Figure 4.6E), with Figure 4.6B even showing the carbon support through the matrix. The PANI structure is also slightly more two-dimensional in the coke sample (Figure 4.6E) as compared to graphite (Figure 4.6B). The PANI fiber thickness on the coke electrode is also slightly smaller at approximately 150 nm compared to the graphite electrode at 200nm. In the CVs for the PANI on carbon surfaces (Figure 4.6C and Figure 4.6F), the characteristic peaks corresponding to the insertion and expulsion of protons (E ≈ 0.25V and -0.2V) and the insertion and expulsion of anions (E ≈ 0.8V and 0.4V) are different. The PANI-on-graphite sample shows smaller

peak areas, which indicates a thinner film and less protonation of the polymer. The upward slope of the PANI-on-graphite CV indicates a larger resistance, which is estimated from the CV to be twice that of the PANI-on-coke sample. The separation in the peak potentials of the PANI-on-graphite electrode are also 100mV greater than in the PANI-on-coke electrode showing a different conformation of the polymer.

Similar results are seen with PANI deposition on the C/Pt surfaces (Figure 4.7). For the polymerization curves, the graphite/Pt electrode shows only a slight increase in slope, while the coke/Pt electrode has a greater increase in slope, again indicating the lack of continued growth of PANI on the graphite sample. Similar results are seen in the CVs of PANI on the C/Pt surfaces regarding decreased peak areas, larger separation of peak potentials, and larger resistance of the graphite/Pt support (Figure 4.7C and Figure 4.7F). The SEM images reveal that the PANI film on graphite/Pt support is very thin with much of the underlying platinum layer showing through (Figure 4.7B).

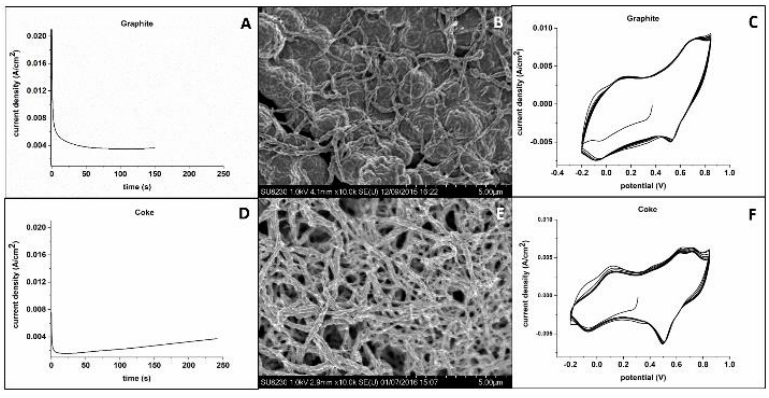

Figure 4.7: Comparison of PANI deposition on to carbon surfaces (A) and onto C/Pt surfaces (C). The curves shown are for constant potential deposition (E = 0.85V, Q = 0.42 C/cm^2) from aniline solution described in Experimental. Characterization is done by CVs in 0.1M $HClO_4$ at 50 mV/s.

The PANI on the coke/Pt support shows a much thicker and more compact layer that is almost twice as thick (Figure 4.7E). Calculation of the PANI layer using method described in Genies and Tsintavis[27] show that the PANI on graphite-platinum support is 3.2 μm thick while the PANI on coke-platinum is 7.5 μm.

4.6 Conclusion

This study shows differences on two carbon samples: a synthetic graphite plate from a novel petroleum coke process, and an extruded graphite rod. These show differences in graphitic structure and surface characteristics which contribute to differences in the electrodeposition of Pt and PANI on the surfaces. The surface oxygen content and the defects in the sp^2 character were key in determining which carbon sample is sufficient for use in further studies using PANI as a support matrix for atomic metal clusters. The effects in the Pt and PANI depositions can be clearly seen in the CVs of the deposited PANI films in 0.1M$HClO_4$. The PANI deposited on the coke substrate gives resolved characteristic peaks of the H^+ and anion exchanges, showing that the sp^2 structure is more ideal for PANI film growth. The graphite substrate is less desirable, most likely due to the increase in sp^3 content and the concomitant loss of π bonding which results in a less conducting material. Of the two carbon substrates used in these experiments, the synthetic graphite from the novel petroleum coke process proved to be optimal because of its higher sp^2 carbon content and less surface oxygen content.

Thanks to Ángela López Lorente of Ulm University, Germany for collecting the Raman data.

4.7 References

(1) Dicks, A. L. The Role of Carbon in Fuel Cells. *Journal of Power Sources*. 2006, pp 128–141.

(2) McCreery, R. L. Advanced Carbon Electrode Materials for Molecular Electrochemistry. *Chem. Rev.* **2008**, *108* (7), 2646–2687.

(3) Kinoshita, K.; Zaghib, K. Negative Electrodes for Li-Ion Batteries. In *Journal of Power Sources*; 2002; Vol. 110, pp 416–423.

(4) Antolini, E.; Giorgi, L.; Cardellini, F.; Passalacqua, E. Physical and Morphological Characteristics and Electrochemical Behaviour in PEM Fuel Cells of PtRu /C Catalysts. *J. Solid State Electrochem.* **2001**, *5* (2), 131–140.

(5) Gloaguen, F.; Leger, J. M.; Lamy, C. Electrocatalytic Oxidation of Methanol on Platinum Nanoparticles Electrodeposited onto Porous Carbon Substrates. *J. Appl. Electrochem.* **1997**, *27* (9), 1052–1060.

(6) Ma, L.; Chu, D.; Chen, R. Comparison of Ethanol Electro-Oxidation on Pt/C and Pd/C Catalysts in Alkaline Media. *Int. J. Hydrogen Energy* **2012**, *37* (15), 11185–11194.

(7) Xie, S. W.; Chen, S.; Liu, Z. Q.; Xu, C. W. Comparison of Alcohol Electrooxidation on Pt and Pd Electrodes in Alkaline Medium. *Int. J. Electrochem. Sci.* **2011**, *6* (4), 882–888.

(8) Hatchett, D. W.; Wijeratne, R.; Kinyanjui, J. M. Reduction of PtCl62- and PtCl42- in Polyaniline: Catalytic Oxidation of Methanol at Morphologically Different Composites. *J. Electroanal. Chem.* **2006**, *593* (1–2), 203–210.

(9) Niu, L.; Li, Q.; Wei, F.; Chen, X.; Wang, H. Electrochemical Impedance and Morphological Characterization of Platinum-Modified Polyaniline Film Electrodes and Their Electrocatalytic Activity for Methanol Oxidation. *J. Electroanal. Chem.* **2003**, *544* (SUPPL.), 121–128.

(10) Jonke, A. P.; Josowicz, M.; Janata, J. Polyaniline Doped with Atomic Gold. *J. Electrochem. Soc.* **2011**, *158* (12), E147–E151.

(11) Jonke, A. P.; Josowicz, M.; Janata, J.; Engelhard, M. H. Electrochemically Controlled Atom by Atom Deposition of Gold to Polyaniline. *J. Electrochem. Soc.* **2010**, *157* (10), P83–P87.

(12) Jonke, A. P.; Steeb, J. L.; Josowicz, M.; Janata, J. Atomic Clusters of Pd and AuNPdM in Polyaniline. *Catal. Letters* **2013**, *143* (6), 531–538.

(13) Gawron, E. L.; Krizek, T.; Kowalik, M. A.; Josowicz, M.; Janata, J. Preparation of a Carbon-Platinum-Polyaniline Support for Atomic Metal Deposition. *J. Electrochem. Soc.* **2015**, *162* (7), H423–H427.

(14) Dinh, H. N.; Birss, V. I. Effect of Substrate on Polyaniline Film Properties A Cyclic Voltammetry and Impedance Study. *J. Electrochem. Soc.* **2000**, *147* (10), 3775.

(15) Giorgi, R. Evaluation of the sp2 / sp3 Ratio in Amorphous and XAES Carbon Structure by XPS. *Appl. Surf. Sci.* **1991**, *47* (1), 17–21.

(16) Chu, P. K.; Li, L. Characterization of Amorphous and Nanocrystalline Carbon Films. *Mater. Chem. Phys.* **2006**, *96* (2–3), 253–277.

(17) NIST X-ray Photoelectron Spectroscopy Database Version 4.1. NIST X-Ray Photoelectron Spectroscopy Database, Version 4.1. National Institute of Standards and Technology: Gaithersburg 2012.

(18) Biniak, S.; Szymański, G.; Siedlewski, J.; Światkoski, A. The Characterization of Activated Carbons with Oxygen and Nitrogen Surface Groups. *Carbon N. Y.* **1997**, *35* (12), 1799–1810.

(19) Ferrari, A. C.; Robertson, J. Resonant Raman Spectroscopy of Disordered, Amorphous, and Diamondlike Carbon. *Phys. Rev. B* **2001**, *64* (7), 75414.

(20) Kudin, K. N.; Ozbas, B.; Schniepp, H. C.; Prud'homme, R. K.; Aksay, I. A.; Car, R. Raman Spectra of Graphite Oxide and Functionalized Graphene Sheets. *Nano Lett.* **2008**, *8* (1), 36–41.

(21) Pandolfo, A. G.; Hollenkamp, A. F. Carbon Properties and Their Role in Supercapacitors. *Journal of Power Sources*. 2006, pp 11–27.

(22) Bade, K.; Tsakova, V.; Schultze, J. W. Nucleation, Growth and Branching of Polyaniline from Microelectrode Experiments. *Electrochim. Acta* **1992**, *37* (12), 2255–2261.

(23) Domínguez-Domínguez, S.; Arias-Pardilla, J.; Berenguer-Murcia, Á.; Morallón, E.; Cazorla-Amorós, D. Electrochemical Deposition of Platinum Nanoparticles on Different Carbon Supports and Conducting Polymers. *J. Appl. Electrochem.* **2008**, *38* (2), 259–268.

(24) Frelink, T. ; Visscher, W. H. M. ; Van Veen, J. A. R.; Acta, E.; Frelink, T.; Vrsscm, W. The Third Anodic Hydrogen Peak on Platinum; Subsurface H2 Adsorption. *Electrochim. Acta Ekcrrochimica Acta* **1995**, *40* (5), 545–549.

(25) Stevens, D. A.; Dahn, J. R. Electrochemical Characterization of the Active Surface in Carbon-Supported Platinum Electrocatalysts for PEM Fuel Cells. *J. Electrochem. Soc.* **2003**, *150* (6), A770–A775.

(26) Sapurina, I.; Riede, A.; Stejskal, J. In-Situ Polymerized Polyaniline Films - 3. Film Formation. *Synth. Met.* **2001**, *123* (3), 503–507.

(27) Genies, E. M.; Tsintavis, C. Electrochemical Behaviour, Chronocoulometric and Kinetic Study of the Redox Mechanism of Polyaniline Deposits. *J. Electroanal. Chem.* **1986**, *200* (1–2), 127–145.

CHAPTER 5. PREPARATION OF A CARBON-PLATINUM-POLYANILINE SUPPORT

Similarly to Chapter 4, the carbon support plays a crucial role in the quality of the PANI matrix used for the insertion of metal. The subject of this chapter characterizes electrodeposited platinum on the carbon support, as well as the PANI film electrodeposited on the platinum. The catalytic activity of the C/Pt-PANI was evaluated for appropriateness as a composite support for atomic metal clusters.

5.1 Introduction

Our previous experience with preparation of PANI-Pd composites on Pt[1–3] has shown that the order of deposition determines the location of the metal inside the composite.[4] Therefore, starting with the synthetic graphite as the support, the sequence of platinum and PANI depositions was investigated. The result is shown in Figure 5.1. The depositions were carried out at constant potential and controlled by applied charge. Platinum was deposited from 0.001M K_2PtBr_4 in 1M $HClO_4$ at potential E=-0.1 V and PANI was deposited from 0.2M aniline in 1M $HClO_4$ at potential E = 0.8V. The charge used for the deposition of polyaniline was 1.43 C/cm^2, and the charge for Pt was 5.38 x 10^{-2} C/cm^2.

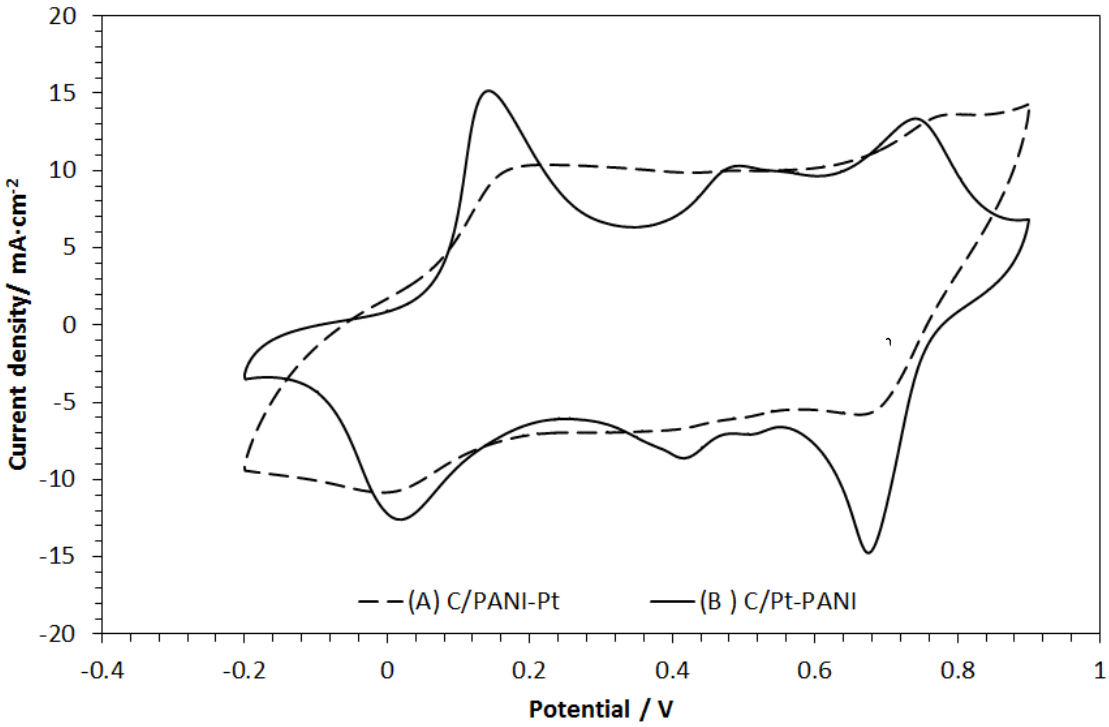

Figure 5.1: Effect of the deposition sequence of Pt and PANI on the voltammetry of the carbon electrodes: (A) PANI followed by Pt deposition on carbon support, C/PANI-Pt (B) Platinum deposition followed by aniline polymerization on carbon support, C/Pt-PANI. Cyclic voltammograms were recorded in 0.1M $HClO_4$ with 20 mV/s.

The cyclic voltammetry of C/Pt-PANI electrode resembles that of PANI film deposited directly onto a polycrystalline platinum electrode.[5] Distinct oxidation/reduction peaks around 0.15 V/0.05 V can be seen for the expulsion/insertion of H^+ ion attributed to the transition between leucoemeraldine and emeraldine form of polyaniline, and around 0.75 V/ 0.70 V for the ClO_4^- anion insertion/expulsion attributed to the redox transition between emeraldine and pernigraline forms. The middle redox peaks arise from crosslinking of low molecular intermediates. In contrast, the PANI redox transitions in the C/PANI-Pt are suppressed by the presence of the Pt particles. Furthermore, peaks in the potential range of hydrogen adsorption/desorption, are broad but symmetrical, indicating

polycrystalline structure of the deposited Pt. The overlap of hydrogen sorption-desorption processes with the redox transition of PANI results in a pseudocapacitive behavior of the electrode; this observation agrees with that already reported.[6] Based on this distinguished difference in behavior, all further studies were completed solely with the C/Pt-PANI composite electrode on which the behavior is dominated by PANI electrochemistry in an acidic medium.

5.2 Preparation of the C/Pt and C/Pt-PANI electrodes

5.2.1 Electrodeposition

Electrochemical experiments were done with an electrochemical workstation (CH Instruments 406, Austin, TX) in a three-electrode cell. The double-junction reference electrode was Ag/AgCl in 1M KCl//1M KNO_3. All potentials mentioned in this work are referred to this electrode (E= 0.235 V vs. SHE). Thin synthetic graphite plates from Advanced Carbon Engineered Solutions (North Bay, Ontario) with bulk density of 1.88 g/cm^3 and specific resistivity of 10 μΩm were used as counter and working electrodes. Before use, each 3.5 cm x 1.0 cm x 0.05 cm electrode was polished with alumina lapping pads (30, 12 and 0.05 μm), obtained from Allied High Tech Products Inc. and was thoroughly rinsed with 2-propanol. The working electrode was then encased in Coleflex heat shrinkable tubing, and a geometric area of 0.5 cm x 0.7 cm was cut out. In order to ensure proper wetting of the exposed porous carbon material, each working electrode was evacuated in plating solutions for approximately 20 minutes, or until air bubbles were no longer seen forming on the surface of the electrode. Immediately after this step, either platinum was deposited from 0.001M or 0.0085M K_2PtBr_4 in 1M $HClO_4$ or polyaniline was deposited from solutions of either 0.25 M aniline/1 M $HClO_4$ or 0.4 M aniline/2 M

HBF_4. Unlike the chloroplatinate salts, potassium tetrabromoplatinate solutions are more stable in acid and do not hydrolyze.[7] The K_2PtBr_4 stability in 1M $HClO_4$ was confirmed by UV absorbance measurements before use. Platinum was deposited on carbon, C/Pt, or on PANI, C/PANI-Pt, at a constant potential of -0.1 V, as specified in the Results. The polyaniline was either deposited directly on carbon, C/PANI, or on platinum, C/Pt-PANI, at constant potential of 0.8 V until a charge of 1.43 C/cm^2 was reached and was kept constant throughout this work. After each deposition, the electrode was rinsed with deionized water and cyclic voltammograms (CVs) were recorded in 1M $HClO_4$ at 20 mV/s between +0.9 V and -0.2 V.

5.2.2 CV and SEM analysis

Cyclic voltammograms were recorded in solutions of 0.5M 1-propanol in 1M KOH at 50 mV/s using Pt foil as counter electrode. CVs were recorded between +0.4 V and -0.7 V until a stable voltammogram was obtained. Further characterization of the electrodes was carried out with scanning electronic microscope (SEM) Hitachi SU8230 cold field-emission SEM (Tokyo, Japan).

5.2.3 HPLC analysis

HPLC measurements were performed on Agilent 1100 Series HPLC system (Agilent Technologies, USA) with HC-75 (H+) column, 7.8 × 305 mm, particle size 9 µm (Hamilton, USA). The mobile phase for isocratic elution was 5mM H_2SO_4 in water at a flow rate of 0.7 mL/min. The separation column was thermostated to 80 °C and a variable wavelength detector was used to measure the absorbance at 190 nm. For system control and data evaluation, Agilent ChemStation software, rev. B.04.02 SP1, (Agilent

Technologies, USA) was employed. Volume of sample injected on the column was 100 µl. Peaks were identified using standard addition method. Sensitivity of the method to 1-propanol (0.27 AU·L/mol) was significantly lower than sensitivity to propionic acid (7.97 AU·L/mol). Sensitivity to unknown product of aldol condensation as a marker of propionaldehyde was approximately 85 AU·L/mol, i.e. ten times higher than sensitivity to propionic acid.

Electrooxidation of 1M 1-propanol in 1M KOH was performed in a U-type glass cell with a frit separating the working and auxiliary electrode compartments of 3 and 15 mL, respectively. Platinum mesh (6.25 cm^2) was used as auxiliary electrode in the larger compartment. Both compartments were filled with the same solution. Oxidation of 1-propanol for HPLC analysis was conducted by applying potential step sequence described in the Results. This sequence of pulses was repeated 360 times making the cumulative time at the oxidation potential, -0.26 V, a total of one hour. Samples were analyzed after 12 hours of storage at room temperature.

5.3 Characterization of C/Pt and C/Pt-PANI

It has been generally accepted that the physico-chemical properties of the supporting carbon material and size and distribution of metal particles are important characteristics. Prior to the Pt-deposition the carbon electrodes were characterized by SEM and cyclic voltammetry. Figure 5.2A shows the SEM image of the polished synthetic graphite plate (see experimental section). It shows open surface structure that governs the low resistance and low double layer capacity observed in the CV in Figure 5.2C curve 1. The SEM image obtained after Pt deposition demonstrates that the growth of platinum

agglomerates is uneven with asymmetric, sharp edges (Figure 5.2B). In agreement with the accepted nucleation and growth theory, the irreversible growth of the nanocrystals is achieved through atomic addition until the reaction is terminated.[8] Figure 5.2C curve 2, shows a sharp peak corresponding to the underpotential deposition of protons on the Pt surface at potentials ranging from -0.25 to 0 V. Before the hydrogen evolution, on the reverse scan of the same potential range, the oxidative desorption of protons from the Pt surface generates a broad peak. The two peaks ~ 0.8 and ~ 0.5 V correspond to oxidation and reduction of Pt respectively. The CV shown as curve 3 changed profoundly after an electrochemical annealing treatment was applied in steps (of 10 cycles) between -1.0 and +1.0 V with a scan rate of 1 V/s. From the SEM micrograph shown in Figure 5.2D, it appears that during this treatment the nanoclusters coalesce, resulting in larger hemispherical (1.0 μm) platinum agglomerates. The corresponding CV is shown in Figure 5.2C, curve 3. It agrees with a voltammogram of the polycrystalline platinum electrode.[5] The distinct peaks due to strong hydrogen adsorption at 0.1 V and weaker hydrogen adsorption at -0.1 V indicate a high surface quality of deposited Pt.

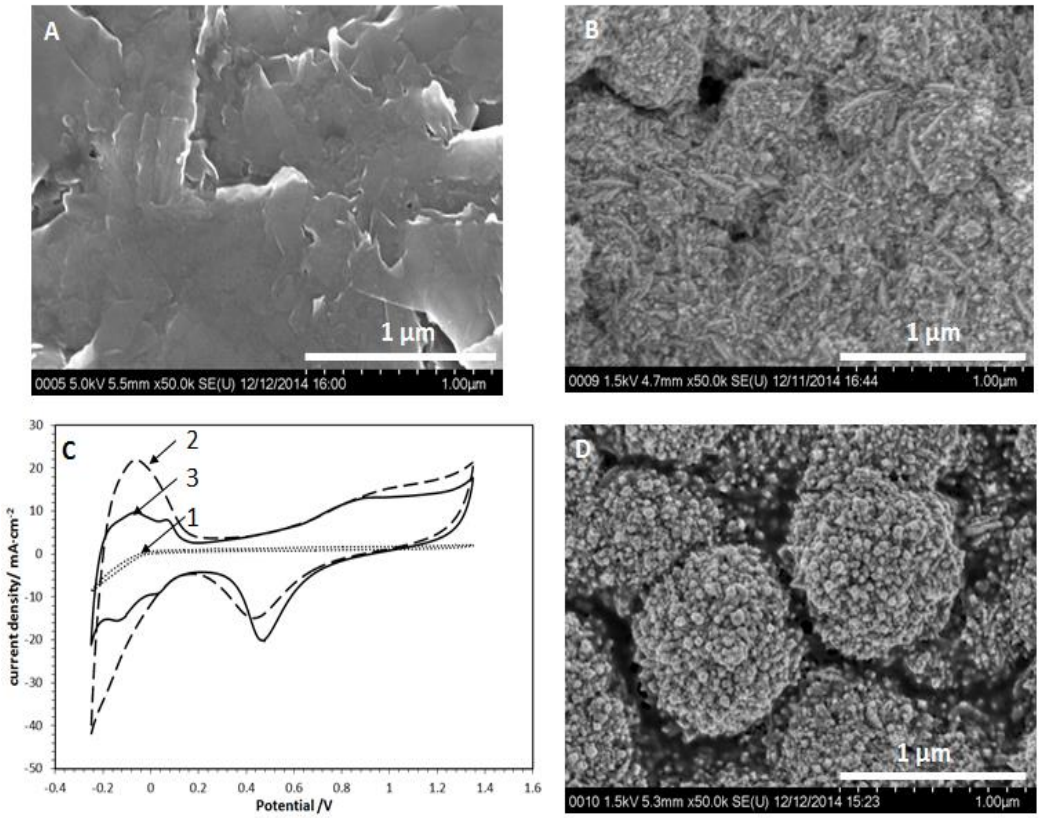

Figure 5.2: Platinum electrodeposited on carbon support: SEM images of polished carbon substrate (A), of C-support after Pt deposition from 0.0085M K_2PtBr_4 in 1M $HClO_4$ at constant potential of E=-0.1 V using 1.71 C/cm^2 (B), and after applied electrochemical annealing treatment in 1 M H_2SO_4 (D). CVs of electrodes shown as SEM images in (A), (B) and (D) were recorded sequentially as curve (1), (2) and (3), in 1M H_2SO_4 with 20 mV/s, shown in (C).

In order to examine the effect of the deposited platinum on the electrochemical surface area (ESA), voltammograms were recorded after the electrochemical annealing step, Figure 5.3. The inset in this figure shows a CV recorded after annealing, with the shaded region indicating the area of H-atom adsorption peaks. The integration of the charge within this region followed the method applied by Stevens and Dahn.[9] Figure 5.3 shows the dependency of the ESA upon the applied deposition charges, Q_{Pt}, from 0.07 to 7.14 C/cm^2.

With the increased Pt loading, the ESA begins slowly to level off. The diminishing increase of the ESA may result from an interplay between primary and the secondary nucleation centers (on the surface of the electrodeposited Pt nanoparticles) leading to complex nanograined deposits. The latter limits the number of specific crystal faces that can be formed on the platinum during sulfate ion adsorption.[10]

In order to examine the effect of Pt-loading on PANI activity, the polymerization of aniline was always carried out from the same electrolyte at constant potential E = 0.8 V and controlling the thickness of the deposition using charge of 1.42 C/cm^2. It was observed that the shape of the CV shown in Figure 5.1 as curve B does not undergo fundamental changes by varying the Pt-loading. The average charge under the oxidation peak at 0.15 V for all the different Pt-loadings was determined to be 90.0 ± 1 mC/cm^2. That reveals the expected consistency for PANI deposition, with no effect from varying the Pt deposition charge.

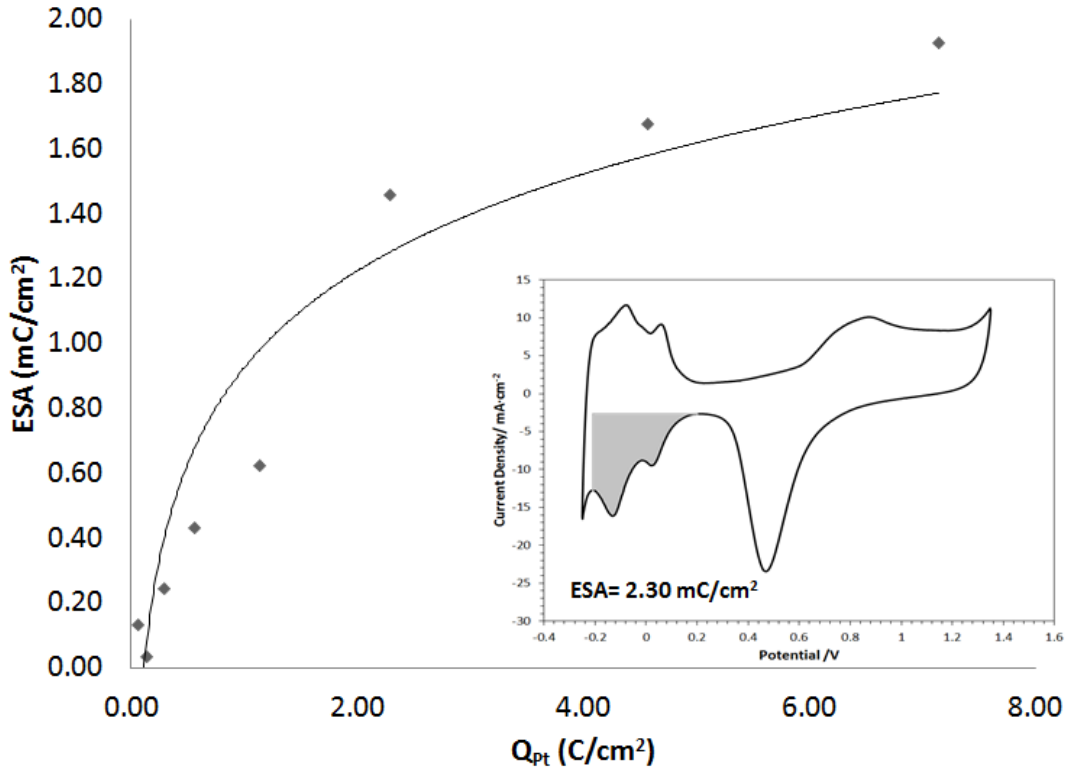

Figure 5.3: Dependence of ESA on the charge used for Pt deposition. Inset: Stable CV obtained for Pt-loading with QPt = 2.30 C/cm2. All platinum depositions were carried out at 60°C and followed the plating conditions given in Figure 5.2.

5.4 Behavior of the electrodes in 1-propanol

The platinum loaded carbon support in the absence and presence of PANI in 1M KOH was compared in Figure 5.4A and Figure 5.4C. The hydrogen adsorption/ desorption peak potentials were shifted in the alkaline medium towards the more negative potentials as compared to Figure 5.1. The pH change provides more insights into the Pt-loading effect on the carbon support; at the higher Pt-content the shape of the CV curves is better resolved. The electrode surface becomes more sensitive to other electrochemical reactions such as the oxygen reduction around -0.3 V that may coincide with the hydrogen peroxide

oxidation/reduction. The C/Pt-PANI electrode also mirrors that behavior. A peak at the same potential is also seen on the reverse scan, suggesting that it is a reversible process. However, when the potential is scanned in a more positive direction, new oxidation peaks are observed. They all are irreversible and can likely be assigned to the formation of $Pt(OH)_x$ and PtO_x.[11]

Oxidation of 0.5M n-propanol in 1M KOH on C/Pt and C/Pt-PANI electrodes is compared in Figure 5.4B and Figure 5.4D. It is observed that with increased platinum loading, there is an increase in activity toward 1-propanol oxidation with the potential remaining around -0.2V. Furthermore, at large Pt loadings of 4.5 C/cm^2, the peaks corresponding to hydrogen adsorption on platinum can also be seen between -0.4 and -0.7 V (curve 4 of Figure 5.4B and Figure 5.4D). Comparing the absence and presence of PANI (Figure 5.4B and Figure 5.4D), having a PANI film present tends to slightly suppress the peak currents, but does not disturb the general trend due to platinum loadings.

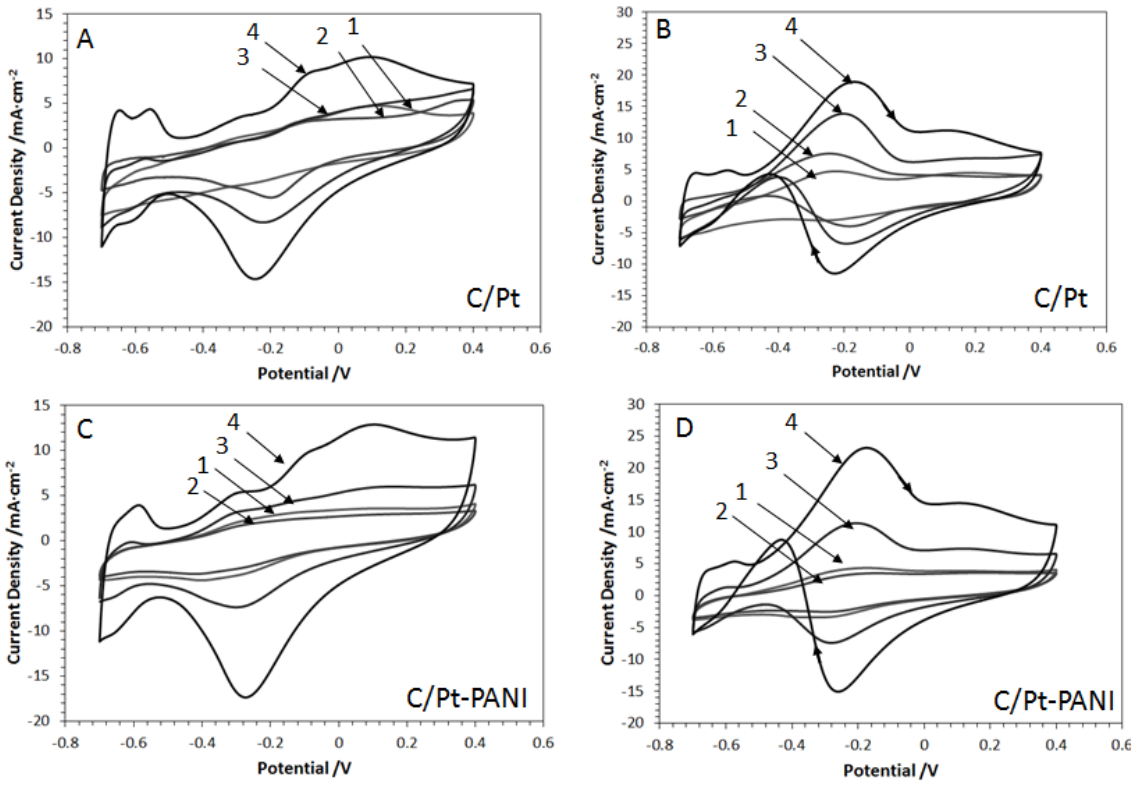

Figure 5.4: Voltammograms of C/Pt and C/Pt-PANI in 1M KOH are shown in (A) and (C). The response of the same electrodes to 0.5M 1-propanol/1M KOH are shown in (B) and (D). Platinum deposition charges were: (1) 0.29 C/cm^2, (2) 1.14 C/cm^2, (3) 2.29 C/cm^2, (4) 4.57 C/cm^2. All CVs were recorded at 50 mV/s.

In order to examine the effect of the deposited platinum on the electrochemical surface area (ESA), voltammograms were recorded after the electrochemical annealing step, Figure 5.3. The inset in this figure shows a CV recorded after annealing, with the shaded region indicating the area of H-atom adsorption peaks. The integration of the charge within this region followed the method applied by Stevens and Dahn.[9] Figure 5.3 shows the dependency of the ESA upon the applied deposition charges, Q_{Pt}, from 0.07 to 7.14 C/cm^2.

With the increased Pt loading, the ESA begins slowly to level off. The diminishing increase of the ESA may result from an interplay between primary and the secondary nucleation centers (on the surface of the electrodeposited Pt nanoparticles) leading to complex nanograined deposits. The latter limits the number of specific crystal faces that can be formed on the platinum during sulfate ion adsorption.[10]

In order to examine the effect of Pt-loading on PANI activity, the polymerization of aniline was always carried out from the same electrolyte at constant potential E= 0.8 V and controlling the thickness of the deposition using charge of 1.42 C/cm^2. It was observed that the shape of the CV shown in Figure 5.1 as curve B does not undergo fundamental changes by varying the Pt-loading. The average charge under the oxidation peak at 0.15 V for all the different Pt-loadings was determined to be 90.0 ± 1 mC/cm^2. That reveals the expected consistency for PANI deposition, with no effect from varying the Pt deposition charge.

5.5 Product Analysis

A most direct test of the electrocatalytic efficiency is the electrolysis and analysis of the products of 1-propanol oxidation on C/Pt and C/Pt-PANI electrodes. For that purpose an HPLC analysis of the electrolyte containing oxidation products from 1M 1-propanol in 1M KOH was developed. The characteristic feature of oxidation of propanol in strongly alkaline medium is the blockage of the working electrode with oxidation product resulting in greatly reduced current efficiency and characteristic cyclic voltammograms (insets of Figure 5.5A and Figure 5.5B). The peak around -0.2 V observed during the forward scan indicates the catalytic oxidation of 1-propanol. The products of the oxidation are adsorbed

on the electrode surface in the region of 0.0 to 0.4 V and block further oxidation. A periodic application of "cleaning" pulse removes the blocking products and restores the electrolysis. Thus, electrolysis was carried out using pulsing regime shown in Figure 5.5C. The repetitive pulses were initiated at -0.26 V (for 10 s) then stepped to 0.4 V (for 0.1 s) and terminated at -0.6 V (for 0.2 s). The resulting chronoamperometric response for the last applied oxidation pulse at -0.26 V in the series is shown in Figure 5.5A and Figure 5.5B. Electrocatalytic activity for C/Pt-PANI electrodes is generally somewhat lower than that for the bare C/Pt. That can be explained by the limited mass transport of propanol due to the layer of PANI. At the same time, electrodes with higher Pt loading tend to show higher catalytic activity as can be seen in Figure 5.5, curves 1-4.

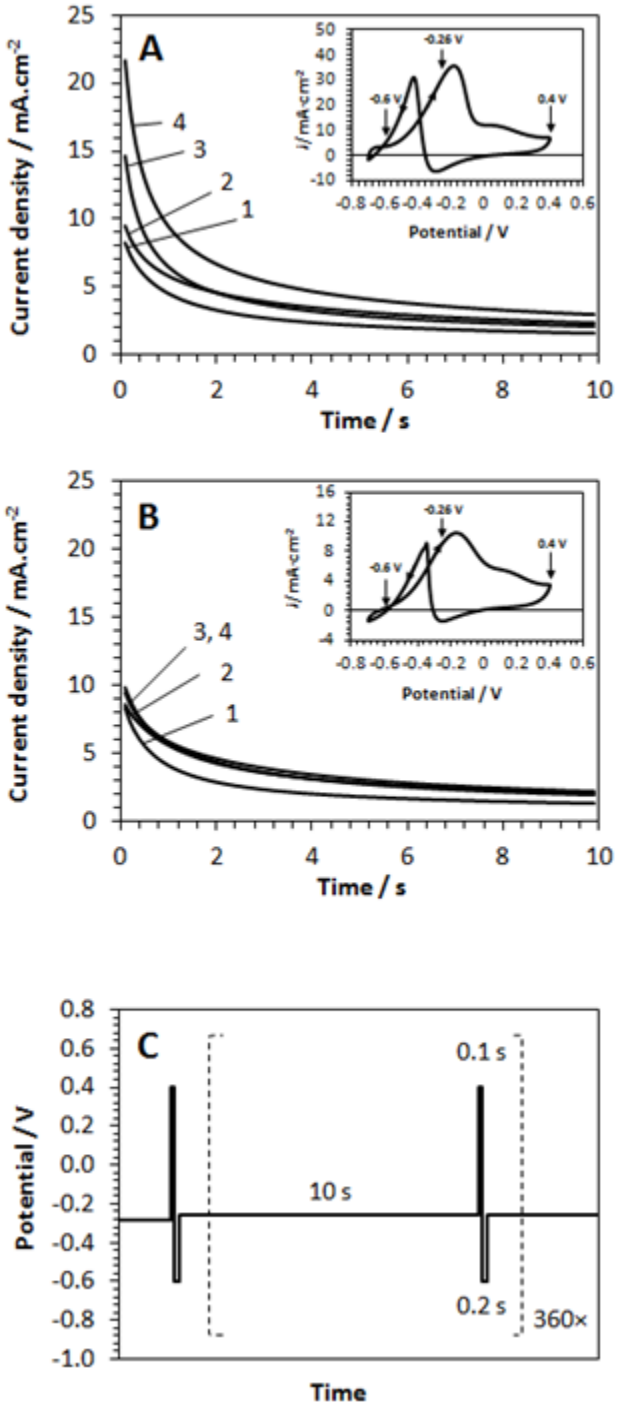

Figure 5.5: Pulse oxidation of 1M 1-propanol on (A) C/Pt and (B) C/Pt-PANI in 1M KOH. Charge used for the deposition of Pt was Q = (1) 0.29, (2) 1.14, (3) 2.29 and (4) 4.57 C/cm^2. Insets show corresponding CVs recorded for Q = 4.57 C/cm^2 with scan rate 50 mV/s. (C) Diagram of applied potential pulses.

Figure 5.6 shows HPLC chromatograms of samples taken after one hour of pulsed electrooxidation using C/Pt and C/Pt-PANI electrodes. As a result of 1-propanol (peak 2) oxidation, propionic acid (peak 1) was detected. Another expected product, propionaldehyde, could not be solely identified due to the competing aldol condensation reaction.[12] However, the presence of peak 3 and several minor peaks prove propionaldehyde being one of the products. These peaks were also found in chromatograms of samples prepared by adding propionaldehyde to 1M KOH and 1M 1-propanol (data not shown). The peak 1 (propionic acid) is approximately two times higher for C/Pt than for C/Pt-PANI electrode. That indicates that PANI layer on the Pt electrode does not contribute to catalytic activity of the oxidation. The ratio of peak 1 to peak 3 is roughly the same for both electrodes indicating that oxidation on either electrode is governed by the same mechanism.

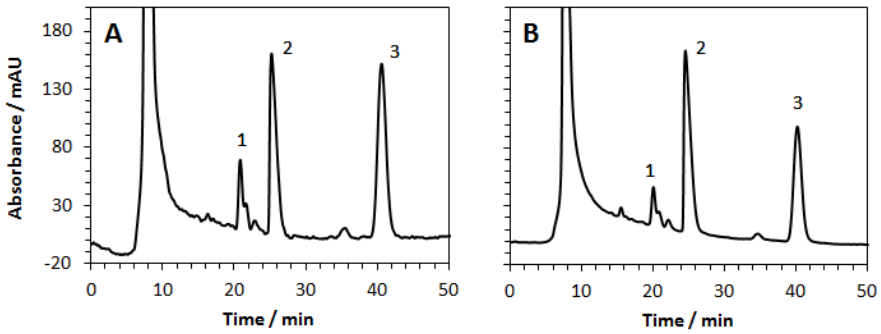

Figure 5.6: HPLC chromatograms of sample collected after pulse electrolysis discussed above (Figure 5.5). (A) C/Pt, (B) C/Pt-PANI. On both electrodes, Pt was deposited using 4.57 C/cm^2. Peak identification: (1) propionic acid, (2) 1-propanol, (3) unknown product of aldol condensation of propionaldehyde.[12]

5.6 References

(1) Schwartz, I. T.; Jonke, A. P.; Josowicz, M.; Janata, J. Polyaniline Electrodes with Atomic Au (N) Pd-1 Alloys: Oxidation of Methanol and Ethanol. *Catal. Letters* **2013**, *143* (7), 636–641.

(2) Jonke, A. P.; Steeb, J. L.; Josowicz, M.; Janata, J. Atomic Clusters of Pd and AuNPdM in Polyaniline. *Catal. Letters* **2013**, *143* (6), 531–538.

(3) Jonke, A. P.; Josowicz, M.; Janata, J. Polyaniline Electrodes Containing Tri-Atomic Au/Pd Clusters: Effect of Ordering. *Catal. Letters* **2013**, *143* (12), 1261–1265.

(4) Li, H. S.; Josowicz, M.; Baer, D. R.; Engelhard, M. H.; Janata, J. Preparation and Characterization of Polyaniline-Palladium Composite Films. *J. Electrochem. Soc.* **1995**, *142* (3), 798–805.

(5) Bard, A. J.; Faulkner, L. R. *Electrochemical Methods: Fundamentals and Applications*, 2nd ed.; John Wiley & Sons: Hoboken.

(6) Hu, C. C.; Chen, E.; Lin, J. Y. Capacitive and Textural Characteristics of Polyaniline-Platinum Composite Films. *Electrochim. Acta* **2002**, *47* (17), 2741–2749.

(7) Davidson, C. M.; Jameson, R. F. Complexes Formed between Platinum Metals and Halide Ions .2. Extraction of Haloplatinates by Solutions of Salts of Amberlite La-2 in Carbon Tetrachloride and in Cyclohexane. *Trans. Faraday Soc.* **1965**, *61* (505P), 133-.

(8) Ustarroz, J.; Hammons, J. A.; Altantzis, T.; Hubin, A.; Bals, S.; Terryn, H. A Generalized Electrochemical Aggregative Growth Mechanism. *J. Am. Chem. Soc.* **2013**, *135* (31), 11550–11561.

(9) Stevens, D. A.; Dahn, J. R. Electrochemical Characterization of the Active Surface in Carbon-Supported Platinum Electrocatalysts for PEM Fuel Cells. *J. Electrochem. Soc.* **2003**, *150* (6), A770–A775.

(10) Kolics, A.; Wieckowski, A. Adsorption of Bisulfate and Sulfate Anions on a Pt(111) Electrode. *J. Phys. Chem. B* **2001**, *105* (13), 2588–2595.

(11) Tripković, A. V.; Popović, K. D.; Lović, J. D. The Influence of the Oxygen-Containing Species on the Electrooxidation of the C1–C4 Alcohols at Some Platinum Single Crystal Surfaces in Alkaline Solution. *Electrochim. Acta* **2001**, *46* (20), 3163–3173.

(12) Wade Jr., L. G. *Organic Chemistry*, 7th ed.; Pearson Prentice Hall: Upper Saddle River.

CHAPTER 6. EFFECTS OF PALLADIUM (II) CHLOROCOMPLEX SPECIATION ON THE CONTROLLED INTERACTION WITH POLYANIINE FILM IN ACID

To optimize the fabrication of the C/PANI-Pd electrode, the carbon was characterized (Chapter 4) and the catalytic activity of the carbon and PANI was evaluated (Chapter 5). This chapter focuses on the palladium (II) chlorocomplexes used and which species in acidic solution shows the strongest interaction with PANI.

6.1 Introduction

It is known that the tetrachloropalladate anion generated from the $PdCl_4^{2-}$ will hydrolyze to form multiple species in acidic aqueous solution.[1] The goal of determining the species of chloropalladate that has maximum interaction with PANI therefore requires adjustment of the equilibrium with an addition of free Cl^- to generate predominant species in solution.

6.2 Electrode preparation and palladium chlorocomplex insertion into polyaniline

The working electrode in the three electrode cell was a thin (1.0mm) synthetic graphite plate from Advanced Carbon Engineered Solutions (North Bay, Ontario). This carbon has a bulk density of 1.88 g/cm^3 and specific resistivity of 10 μΩm. The plates were polished with 30μm grit paper, rinsed with isopropyl alcohol, and dried in an oven at 65°

C. A platinum mesh cage served as a counter electrode. The double-junction reference electrode was Ag/AgCl in 1M KCl//1M $NaNO_3$ and all potentials mentioned in this work are referred to this electrode (E = 0.235 V vs. SHE). The PANI was deposited onto carbon using a solution of 0.1M aniline in 2M HBF_4 at a constant potential of 0.85 V until a charge of 0.4 C/cm^2 was reached. The polymerization from HBF_4 provides a more stable film with less degradation, but due to further experimentation in perchloric acid, the BF_4^- anion was exchanged for ClO_4^- by cyclic voltammetry (CV) in 0.1M $HClO_4$.[2–5] Ten CVs were recorded at a scan rate of 50 mV/s, but only the last steady-state cycle is shown here. All data were collected with a CH Instruments 660 electrochemical workstation (Austin, TX).

This procedure required the potential of PANI and the contact time of the Pd species in acidic K_2PdCl_4 solutions to be precisely controlled, and that the electrical contact to the PANI film was never interrupted while the Pd species was present in solution. This procedure follows what is described in Jonke, et. al.[6] with minor modifications for this study. To follow these requirements, a special flow cell was manufactured from acrylic with a volume of 1.27 mL. The PANI-coated carbon served as the working electrode and was placed on one side of the flow cell. Contact to the electrode was made through the back of the carbon. Platinum foil served as the counter electrode and was placed on the other side of the flow cell. The potential was controlled by an OMNI 90 potentiostat (Cypress Systems, Lawrence, KS) and the solution delivery was controlled with a FIAlab flow-injection system (Alitea Instruments, Medina, WA). The operations of both the potentiostat and flow-injection system were controlled through use of LabView (National Instruments, Austin, TX).

Each insertion cycle consists of holding the potential at 0.7 V in 0.1M $HClO_4$ while a palladium(II) chlorocomplex solution is introduced to the flow cell for a two-minute contact time, followed by rinsing with 110 mL 0.1M $HClO_4$, and a sweep to 0.25 V for the reduction of Pd(II) to Pd(0). The potential in the cell is then swept back to 0.7 V to repeat these previously defined steps. All composite electrodes made for this study used two of these cycles for the Pd complex insertion. The PANI was 'conditioned' before Pd complex insertion by using two "blank" cycles run without the presence of a Pd(II) chlorocomplex solution.

Ultraviolet-visible spectroscopy (UV-Vis) measurements were performed using a Shimadzu UV-3101PC double beam instrument (Kytoto, Japan) with a quartz cuvette of a 1 cm path length, in the range of 190-800 nm.

Resonance Raman spectra were collected using a Renishaw inVia Raman spectrometer (Wotton-under-Edge, UK) coupled onto a Leica DM 2500M microscope containing a 20X/0.4 N.A. objective and a 1200 lines/nm grating. The measurements were completed using a 785 nm diode laser with an integration time of 25 s. Signals were collected on a CCD detector in the range of 100-1800 cm^{-1}. Spectra were collected over five locations on each sample to evaluate overall consistency. The spectra were normalized, averaged, and smoothed using OriginPro 9.0 (Northampton, MA). The mean and uncertainty in the Raman measurements are shown in Figure 6.1.

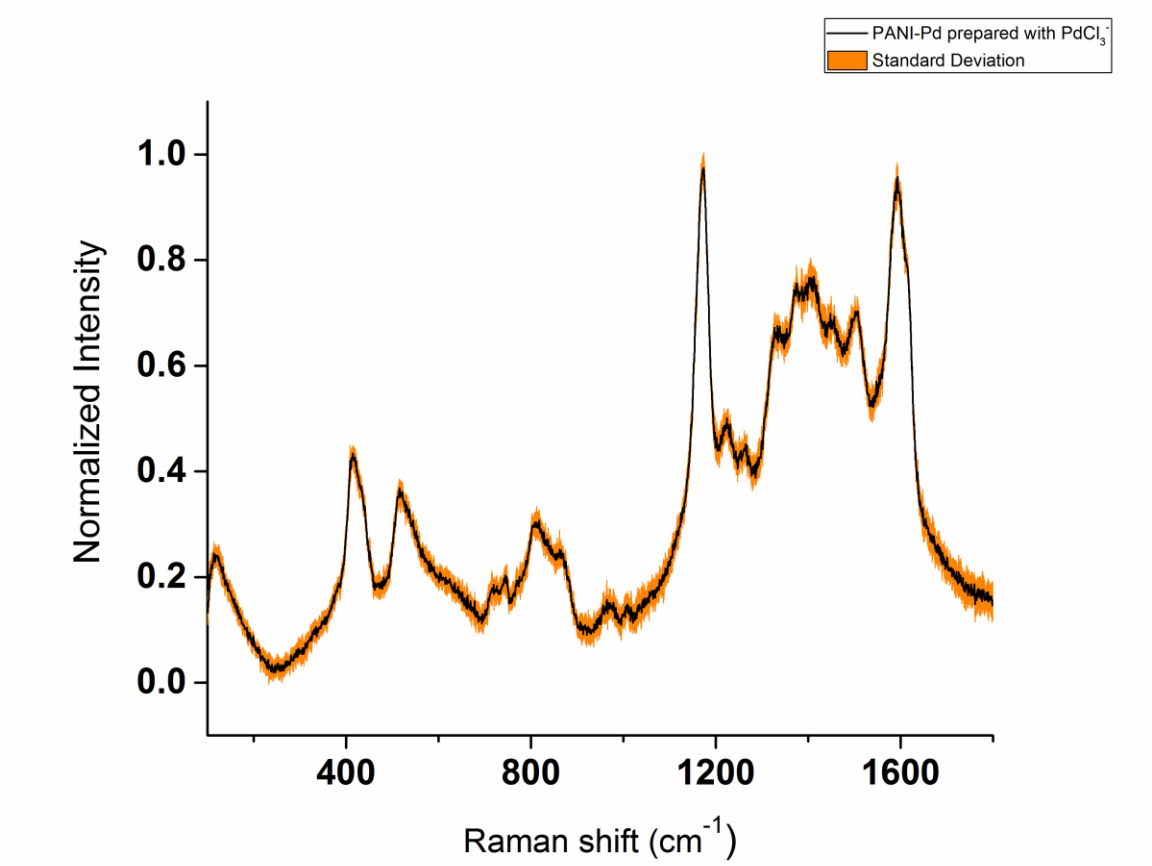

Figure 6.1: Averaged and normalized Raman spectra. Raman spectra taken at 5 individual spots on each electrode. Each spectrum was normalized, averaged, and then smoothed. Mean spectrum (black) with standard deviation (orange) shows consistency across the surface of the composite electrode. Reprinted with permission from American Chemical Society.[7]

X-ray photoelectron spectroscopy (XPS) measurements were made using a ThermoFisher Scientific spectrometer (Waltham, MA) with an Al Kα X-ray photon source. The instrument was calibrated using a gold (Au) standard giving a binding energy (BE) of 83.96 eV for the Au $4f_{7/2}$. The vacuum in the analysis chamber was maintained at 3×10^{-7} mbar or lower. A flood gun consisting of low energy ionized Ar gas was used to neutralize any surface charges. Data were collected from the samples using a 400 µm X-ray spot size, pass energies of 200 eV for the survey scan, and 50 eV for the elemental scans. Spectra

were deconvoluted and analyzed using ThermoScientific Avantage Software. An example of a survey scan can be seen in Figure 6.2.

Name	Peak BE	Height CPS	FWHM eV	Atomic %
C1s	284.56	201547.45	2.04	68.52
O1s	531.83	131267.95	2.75	14.23
N1s	399.45	48446.85	3.07	10.1
Cl2p	207.51	28791.13	3.41	5.56
Pd3d	337.79	59176.9	2.86	1.59

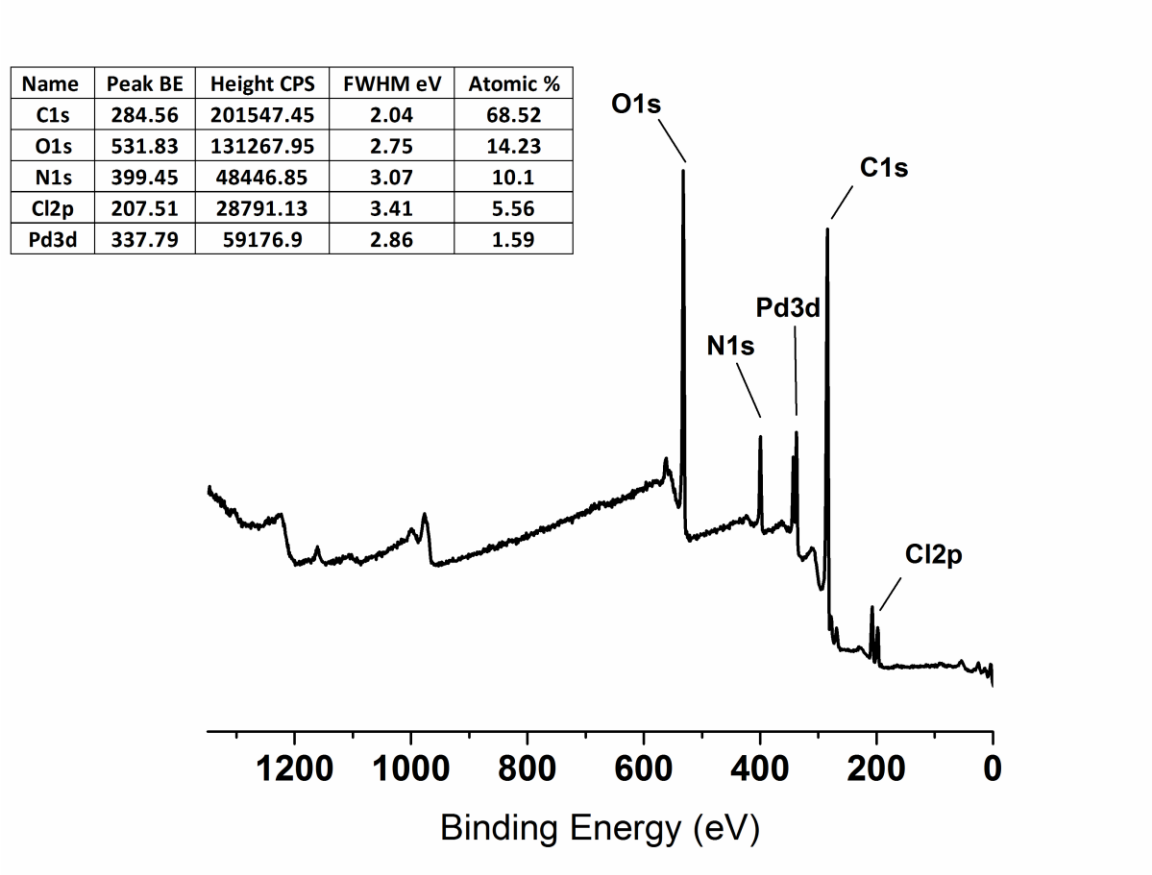

Figure 6.2: The XPS survey scan of the C/PANI-Pd composite electrode. Three scans with a dwell time of 50ms were averaged. All elements are present and shown in the table as relative atom % values. The N/Pd ratio is 6.4 atom %. Reprinted with permission from American Chemical Society.[7]

6.3 Palladium (II) chlorocomplex speciation in perchloric acid

The previous reports have made the adjustments with the use of HCl, without considering the change in pH caused from the additions of a strong acid.[8,9] For this work, chloride was added in the form of NaCl to eliminate any significant changes in pH and

therefore prevent changes in the degree of protonation of polyaniline. We conducted our experiments by adding 20 µL increments of 5M NaCl in 0.1M $HClO_4$ to 2.0mM K_2PdCl_4 dissolved in 0.1M $HClO_4$. The absorbance spectra were recorded with each addition of the NaCl solution. From these spectra, free Cl^- concentrations were chosen that defined three solutions, each of a differing dominating palladium chlorocomplex. These three solutions, as shown in Figure 6.3, were prepared as follows: (A) 2.0mM K_2PdCl_4 dissolved in 0.1M $HClO_4$ for $PdCl_2(H_2O)_2$, (B) 2.0mM K_2PdCl_4 and 0.100M NaCl dissolved in 0.1M $HClO_4$ for $PdCl_3(H_2O)^-$, and (C) 2.0mM K_2PdCl_4 and 1.0M NaCl dissolved in 0.1M $HClO_4$ for $PdCl_4^{2-}$. It should be noted that for solution A, the K_2PdCl_4 was used as received with no added Cl^-, therefore the initial distribution of species in solution is unknown. Studies by Elding[1] and Cruywagen[10] calculated stability constants and distributions for the chloro-species respectively.

Figure 6.3 shows the spectra acquired for each solution; for solution A at the given pH, and no added Cl-, the distribution of species is likely to include both $PdCl_2(H_2O)_2$ and $PdCl_3(H_2O)^-$. Solutions A and B have overlapping peaks with differing intensity at 208 nm and 236 nm due to the differing distributions of both $PdCl_3(H_2O)^-$ and $PdCl_2(H_2O)_2$ species, with $PdCl_2(H_2O)_2$ being the most prevalent species in solution A. These peaks correspond to the ligand-metal charge transfer.[11] Upon closer inspection of the peaks near 208nm, solution A has a slight shift (<1 nm) to a shorter wavelength compared to B, which confirms the exchange of Cl ligands to water.[10] Solution C shows absorbance at 280 nm and 222 nm also due to the ligand-metal charge transfer. The peaks at higher wavelengths are caused by (d,d) ligand field absorption and occur at 465 nm for solution C, 427 nm for solution B, and 305 nm and 420 nm for solution A,[1,12,11] and are shown in the inset of

Figure 6.3. After this verification of the speciation, each solution was used for Pd(II) chlorocomplex insertion into the PANI film using the flow cell as described in the experimental section.

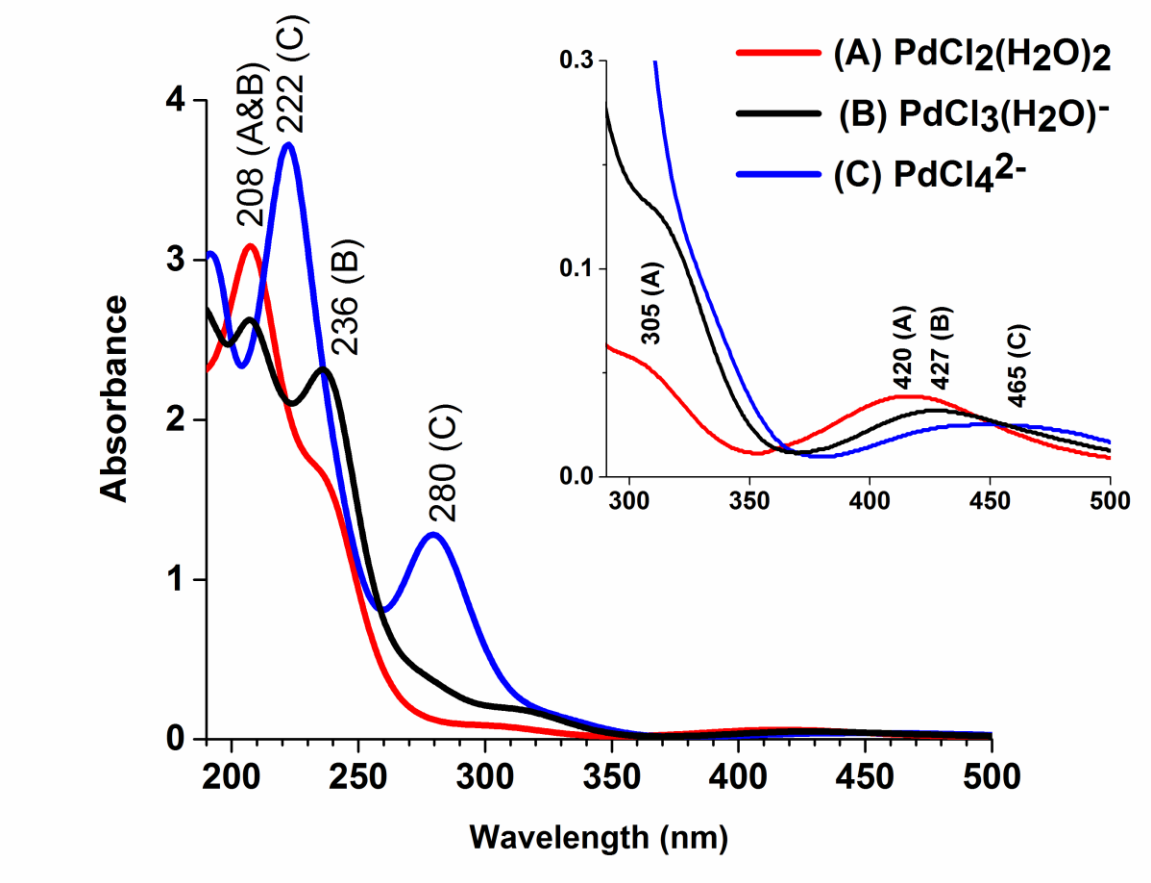

Figure 6.3: UV-Vis spectra of the $PdCl_4^{2-}$, $PdCl_3(H_2O)^-$, and $PdCl_2(H_2O)_2$ species. The inlay is an enlarged region between 300-500 nm for clarity of spectroscopic features. These solutions were used within 30 minutes of their preparation. Reprinted with permission from American Chemical Society.[7]

6.4 Stabilization of PANI matrix

In order to compare the PANI interaction with palladium (II) chlorocomplex species, it was necessary to examine the electrochemical stability of the PANI matrix. CVs

were recorded in 0.1M $HClO_4$ after PANI deposition, as shown in Figure 6.4A. PANI has four characteristic peaks for the exchange of protons (0.2 V, peak 1) and charge-compensating anions (0.75 V, peak 2), and the expulsion of anions (0.4 V, peak 3) and protons (-0.15 V, peak 4). The PANI was then subjected to a conditioning process in the flow cell which we defined as two "blank" Pd-insertion cycles without the presence of Pd(II) chlorocomplex. This conditioning process allows for a more consistent starting matrix for the insertion of Pd(II) chlorocomplex. After this step, peaks 1 and 2, as well as peaks 3 and 4 shift slightly closer together and decrease in current when compared with the previously recorded CV likely due to PANI becoming less protonated. For comparison, a CV of PANI film after interaction with $PdCl_3(H_2O)$- species is also shown in Figure 6.2A.

In addition to electrochemical characterization of the PANI matrix, Raman spectra were recorded on the samples using a wavelength of 785 nm, as shown in Figure 6.4B. Resonance Raman is known to occur at this wavelength, enhancing the semi-quinoid structures of PANI.[13] Spectra were recorded after PANI deposition, conditioning of the PANI matrix, and after Pd(II) chlorocomplex insertion. The differences observed in the Raman spectra of PANI and PANI after conditioning imply that the quinoid character of the PANI has increased.[13,14]

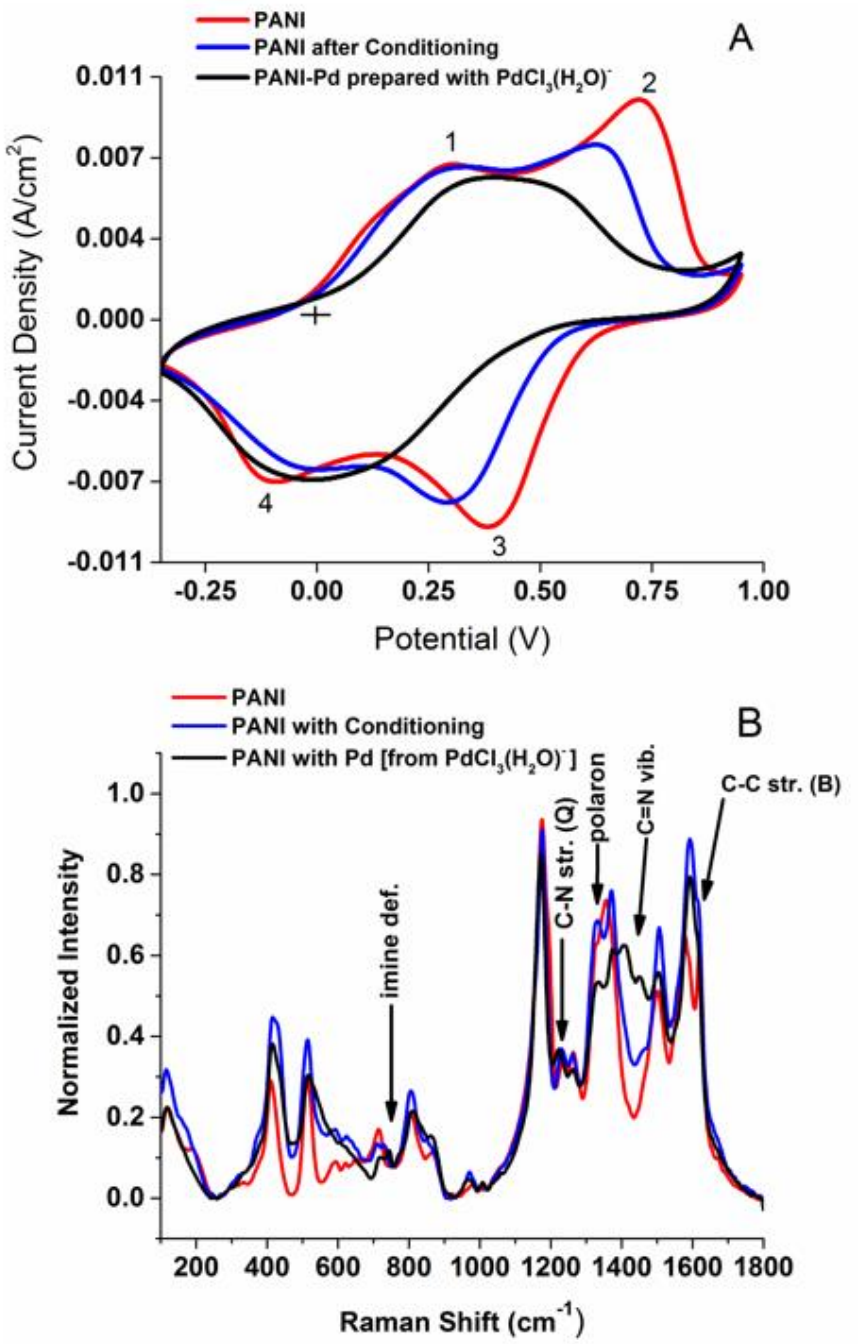

Figure 6.4: Characterization of PANI with (A) CV and (B) Resonance Raman spectroscopy. Both show PANI, PANI after conditioning treatment, and PANI after Pd insertion using $PdCl_3(H_2O)^-$ species. For the Raman spectra, tentative peak assignments are shown and PANI benzenoid (B) and quinoid (Q) character is also shown. Reprinted with permission from American Chemical Society.[7]

Most notably, there are increases in intensity at 1230 cm^{-1} and 745 cm^{-1}, tentatively assigned to C-N stretch (quinoid) and imine deformation respectively. Further evidence of

this enhanced quinoid character is seen in the disappearance of the peak at 1617 cm^{-1} which is due to C-C stretch in the benzenoid units.[15] This quinoid predominance is likely due to the polymer being held at a potential of 0.70 V where it is in an oxidized state. When $PdCl_3(H_2O)^-$ is present in PANI, significant changes occur in the 1400-1500 cm^{-1} range and other changes signify increased quinoid character. The imine deformation peak is even more pronounced, and shifted slightly to lower energy. There is also a shift to lower energy of the peak at 1175 cm^{-1}, attributed to C-H stretch in the quinoidal form, as well as a decrease in the delocalized polaron present at 1332 cm^{-1}.[15,16] The two peaks that appear at 1408 cm^{-1} and 1450 cm^{-1} are tentatively assigned to C=N bond vibrations and are due to changes in the conjugation length as a result of the Pd interacting with the nitrogen atoms.[16]

6.5 Effects of Pd species insertion into PANI matrix

To examine whether all Pd species, as defined in Figure 6.3, interact with the PANI in a similar manner, CVs and Raman spectra were compared in Figure 6.5. In Figure 6.5A, CVs of PANI in 0.1M $HClO_4$ were recorded after interactions with each of the Pd(II) chlorocomplexes. These CVs show that potential for H^+ and anion insertion (marked as 1 and 2) have shifted closer to each other for each of the cases. However, when Pd was inserted using $PdCl_4^{2-}$, there is still slight separation of broad peaks 1 and 2, as well as separation of broad peaks 3 and 4. This suggests that the species present in this solution did not interact as completely with the polymer; the PANI maintains some of its initial character in allowing protons and anions to enter and exit the film. For $PdCl_2(H_2O)_2$, there is also slight separation in peaks, especially 3 and 4, the expulsion of anions and protons respectively. For $PdCl_3(H_2O)^-$, there is no observed separation between them.

Although only slight differences are evident in the CVs between these samples, Raman spectra shown in Figure 6.5B highlights that the PANI-Pd composites prepared from solutions A and C have similar spectra, where the composite from solution B shows clear differences. The most notable differences in the spectra occur at 1408 cm^{-1}, 1450 cm^{-1}, and 745 cm^{-1}. Other studies report that these peaks are due to phenazine-like structures, however these peaks are not present in the spectra of PANI when Pd is absent.[13]

Furthermore, the presence of a peak at 745 cm^{-1}, attributed to imine deformation, is seen only when PANI interacts with solution B, but not with solutions A or C. This evidence suggests that Pd metal is present in the PANI and is locking the imine structure in place.[16] Further evidence of this imine structure is in the increased intensity of the 1230 cm^{-1} peak relative to the intensity of the 1265 cm^{-1} peak. These peaks are attributed to the quinoid and benzenoid moieties in PANI, respectively.[15,17] Similar spectra at different excitation wavelengths can be seen in Hien et. al. [18] The presence of Pd in the polymer can be indicated by peaks at 1408 cm^{-1} and 1450 cm^{-1} and can be tentatively attributed to changes in the polyaniline structure, specifically the C=N stretch, most likely due to interactions of Pd with the PANI. [16,19]

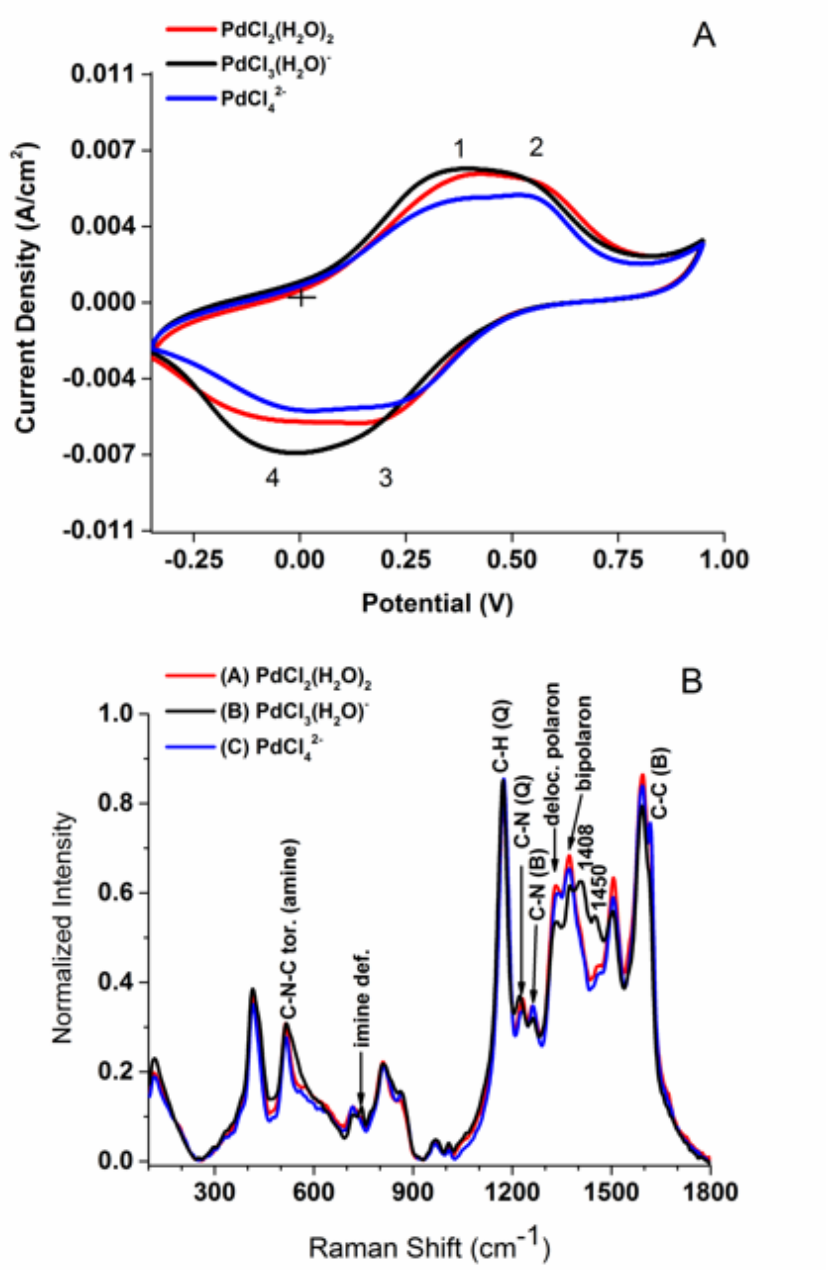

Figure 6.5: (A) CVs after the Pd(II) complex insertion into PANI, prepared with $PdCl_2(H_2O)_2$, $PdCl_3(H_2O)^-$, $PdCl_4^{2-}$as in Figure 6.1. Experimental conditions are the same as Figure 2A. (B) Resonance Raman spectra of PANI-Pd composites tentative peak assignments with and PANI benzenoid (B) and quinoid (Q) character are labeled. Reprinted with permission from American Chemical Society.[7]

6.6 XPS analysis of PANI after interaction with Pd(II) species

The evidence for the interaction of PANI with the Pd(II) species in our electrochemically controlled experiment is evaluated through deconvolution of the Pd3d core level spectrum (Figure 6.6), and summarized in Table 6.1. After deconvolution of the Pd3d doublet, the spectrum shows three doublets that provide analysis of the present oxidation states of Pd. The doublet at 336.4 eV corresponds to reduced Pd(0) metal, the doublet at 337.6 eV, labeled (1), corresponds to Pd-Cl interaction and the doublet at 338.8 eV, labeled (2), is due to Pd coordinated to nitrogen.[20]

Using data from the survey spectrum (Figure 6.2), the atomic % ratios of total palladium and nitrogen are compared for each of solutions A, B, and C. Sputtering technique was also used to determine distribution of Pd within the bulk PANI, and no change in the profile was observed.This comparison reveals that the interaction of PANI with solution B is favored as compared to solutions A and C. For the composite electrodes prepared with solutions A and B, close to 10 atom % of the total Pd at the surface is reduced to Pd(0), as seen in Table 6.1. For solution C, less than 2 atom % of the surface Pd is reduced to metal.

Table 6.1: Overview of the XPS data analysis from Pd3d and survey (Figure 6.2) scans. Reprinted with permission from American Chemical Society.[7]

Solution Species	BE Pd3d (eV)	Pd (at. %)	N:Pd	Pd^{2+}		Pd^{0}	
				BE(eV)	atom%	BE(eV)	atom%
(A) $PdCl_2(H_2O)_2$	337.6	0.8	11.8:1	(1) 337.6 (2) 338.8	74.2 16.1	336.5	9.7
(B) $PdCl_3(H_2O)^-$	337.8	1.6	6.4:1	(1) 337.7 (2) 338.9	70.9 12.7	336.3	9.84
(C) $PdCl_4^{2-}$	337.4	1.0	10.2:1	(1) 337.5 (2) 338.4	74.3 23.8	336.2	1.98

Considering the Pd-N doublet (2), the composite electrode prepared with Solution B, has 12.7 atom %, while the one prepared with solution A has 16.1 atom %, and with solution C has 23.7 atom % in that form (Table 6.1). It can also be seen that the Pd species with the lowest N/Pd atomic ratio is found for solution B. There are nearly twice as many Pd atoms interacting with N than in the other two Pd species. An XPS example for N1s is shown in Figure 6.7. This shows that the $PdCl_3(H_2O)^-$ species (solution B) gives the best result for interaction with PANI that leads to reduction of Pd(0) metal, as seen in Table 6.1. The incomplete conversion to Pd(0) may be due to the inserted Pd(II) forming a strong complex in the matrix, effectively "crosslinking" the N groups of two neighboring PANI chains. Such a complex is irreducible, similar to reported Ni and PANI complex[21].

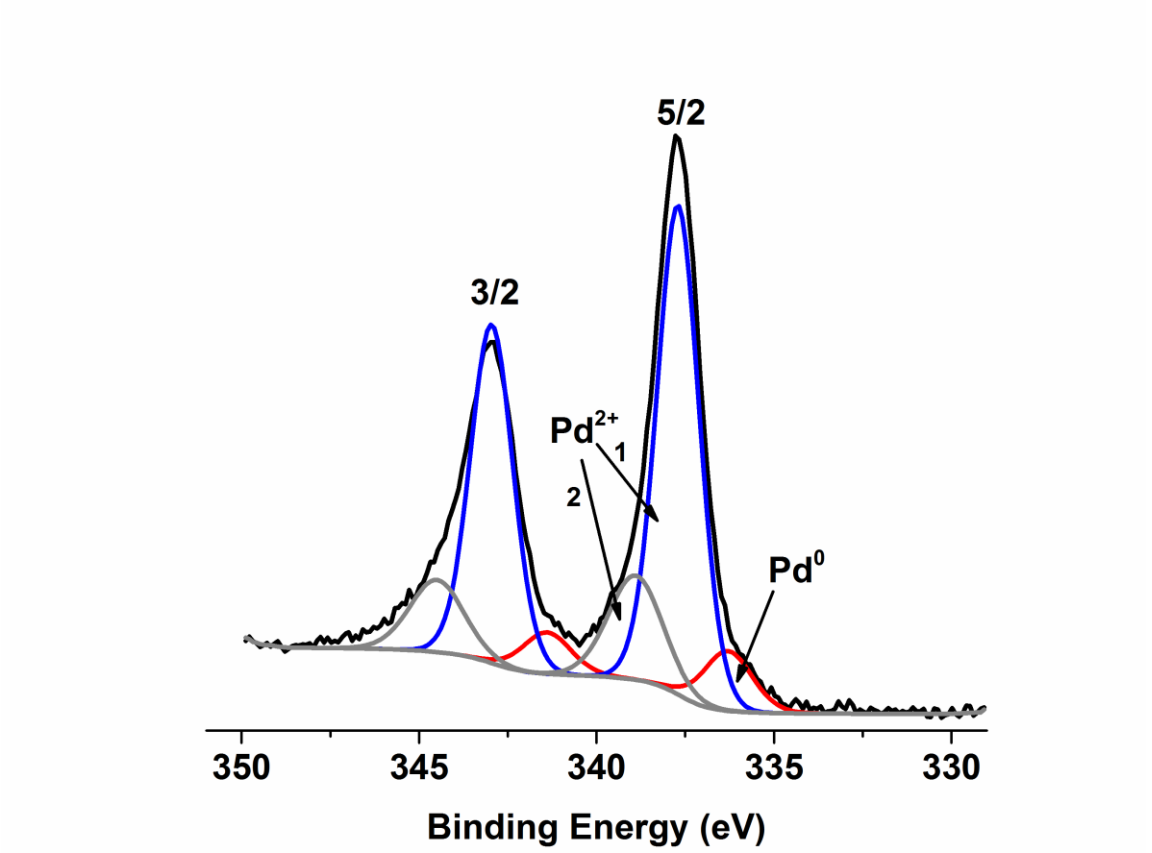

Figure 6.6: Palladium 3d XPS spectra of PANI-Pd composite prepared with $PdCl_3(H_2O)^-$ speciation. The observed doublets are fit and reveal Pd^{2+} and Pd^0 species present. For the two Pd^{2+} identified features, the peak at 337.7 eV is tentatively assigned to Pd-Cl (A) and the peak at 338.9 eV is tentatively assigned to Pd-N (B). Pd^0 has a single peak at 336.3 eV. Reprinted with permission from American Chemical Society.[7]

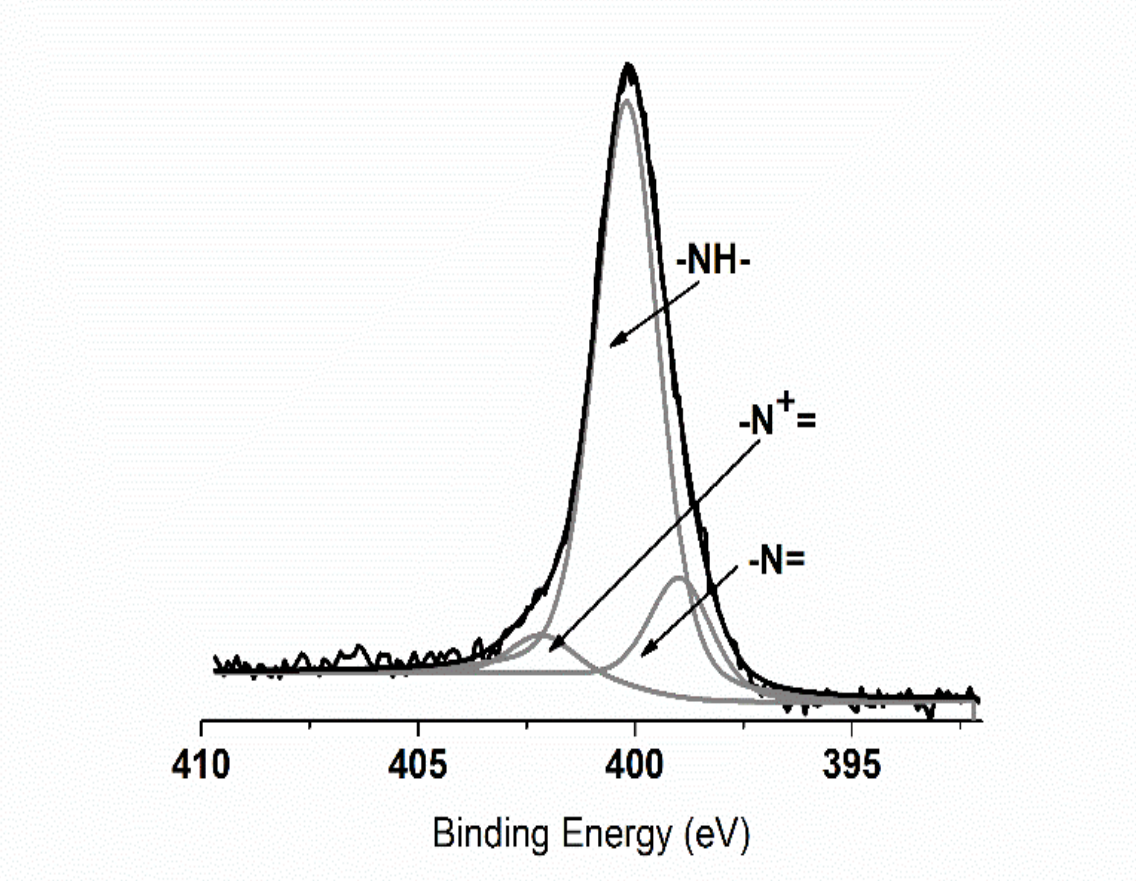

Figure 6.7: N1s scan of conditioned PANI. Deconvolution using Lorentzian/Gaussian mix of 30% shows protonated and non-protonated nitrogen-containing groups. Observation has shown that less protonated imine, correlates with a lessened interaction of the Pd species with the polyaniline. Reprinted with permission from American Chemical Society.[7]

6.7 Conclusions

We have confirmed through UV-Vis spectroscopy that $PdCl_4^{2-}$ will hydrolyze in aqueous acidic solution to form several Pd species: $PdCl_2(H_2O)_2$, $PdCl_3(H_2O)^-$, and $PdCl_4^{2-}$ and the equilibrium can be adjusted by adding free Cl^-. We have determined that the species, $PdCl_3(H_2O)^-$ interacts most effectively with polyaniline at low pH. This is most likely due to the required charge balance of the anion with the protonated polymer. Therefore, $PdCl_3(H_2O)^-$ is the best Pd species for the controlled and systematic formation of Pd clusters in a PANI matrix. The XPS results also show a smaller N:Pd ratio at 6.4

atoms of N per one atom of Pd for $PdCl_3(H_2O)^-$ while the other two species, $PdCl_2(H_2O)_2$ and $PdCl_4^-$ show N:Pd ratios of 11.8:1 and 10.2:1 respectively. The greater interaction of $PdCl_3(H_2O)^-$ with nitrogen is also seen in the Raman spectra with the appearance of C=N stretch at 1408 cm^{-1} and 1450 cm^{-1} resulting in increased quinoid character. The conformational changes in the PANI matrix are seen in the CV data, which show merging of the separate proton and anion peaks into a pair of broad peaks at 0.0V and +0.4V respectively, corresponding to the mixed ion exchange.

Considering data from cyclic voltammetry, Raman and XPS spectroscopies, the speciation of $PdCl_4^{2-}$ resulting in $PdCl_3(H_2O)^-$ is the most efficient for insertion of Pd(II) into the PANI matrix. We assume that this is due to this species, bearing the most favorable single negative charge, needed for the charge compensation of the H^+ in the doped polymer. However, given the high concentration of the ClO_4^- anion the charge compensation cannot be the only explanation for this result. The fact that a high fraction of Pd(II) cannot be reduced electrochemically or chemically suggests formation of a Pd complex which crosslinks suitably oriented PANI chains is the most likely explanation. We plan on more studies to probe this interaction further.

6.8 References

(1) Elding, L. I. Palladium (II) Halide Complexes. I. Stabilities and Spectra of Palladium (II) Chloro and Bromo Aqua Complexes. *Inorganica Chim. Acta* **1972**, *6* (4), 647–651.

(2) Abrantes, L. M.; Correia, J. P. Polymer Films Containing Metal Particles - Noble Metals in Polyaniline. *191*.

(3) Jonke, A. P.; Janata, J. Atomic Metal/Polyaniline Composites, Georgia Institute of Technology, 2013, Vol. Doctor of.

(4) Tang, H.; Kitani, A.; Shiotani, M. Effects of Anions on Electrochemical Formation and Overoxidation of Polyaniline. *Electrochim. Acta* **1996**, *41* (9), 1561–1567.

(5) Hatchett, D. W.; Josowicz, M.; Janata, J. Acid Doping of Polyaniline: Spectroscopic and Electrochemical Studies. *J. Phys. Chem. B* **1999**, *103* (50), 10992–10998.

(6) Jonke, A. P.; Josowicz, M.; Janata, J.; Engelhard, M. H. Electrochemically Controlled Atom by Atom Deposition of Gold to Polyaniline. *J. Electrochem. Soc.* **2010**, *157* (10), P83–P87.

(7) Gawron, E. L.; Hira, S. M.; Josowicz, M.; Janata, J.; Janata, J. Effects of Palladium (II) Chlorocomplex Speciation on the Controlled Interaction with Polyaniline Film in Acid. *Langmuir* **2017**.

(8) Drelinkiewicz, A.; Hasik, M.; Choczynski, M. Preparation and Properties of Polyaniline Containing Palladium. *Mater. Res. Bull.* **1998**, *33* (5), 739–762.

(9) Mourato, A.; Viana, A. S.; Correia, J. P.; Siegenthaler, H.; Abrantes, L. M. Polyaniline Films Containing Electrolessly Precipitated Palladium. *Electrochim. Acta* **2004**, *49*, 2249–2257.

(10) Cruywagen, J. J.; Kriek, R. J. Complexation of palladium(II) with Chloride and Hydroxide. *J. Coord. Chem.* **2007**, *60* (4), 439–447.

(11) Drew Tait, C.; Janecky, D. R.; Rogers, P. S. Z. Speciation of Aqueous palladium(II) Chloride Solutions Using Optical Spectroscopies. *Geochim. Cosmochim. Acta* **1991**, *55* (5), 1253–1264.

(12) Elding, L. I. Palladium(II) Halide Complexes, II. Acid Hydrolyses and Halide Anations of palladium(II) Chloro and Bromo Aqua Complexes. *Inorganica Chim. Acta* **1972**, *6* (C), 683–688.

(13) Morávková, Z.; Trchová, M.; Exnerová, M.; Stejskal, J. The Carbonization of Thin Polyaniline Films. *Thin Solid Films* **2012**, *520* (19), 6088–6094.

(14) Drelinkiewicz, A.; Hasik, M.; Quillard, S.; Paluszkiewicz, C. Infrared and Raman Studies of Palladium—nitrogen-Containing Polymers Interactions. *J. Mol. Struct.* **1999**, *511–512*, 205–215.

(15) Trchová, M.; Morávková, Z.; Bláha, M.; Stejskal, J. Raman Spectroscopy of Polyaniline and Oligoaniline Thin Films. *Electrochim. Acta* **2014**, *122*, 28–38.

(16) Louarn, G.; Lapkowski, M.; Quillard, S.; Pron, A.; Buisson, J. P.; Lefrant, S. Vibrational Properties of Polyaniline - Isotope Effects. *J. Phys. Chem.* **1996**, *100* (17), 6998–7006.

(17) Lindfors, T.; Ivaska, A. Raman Based pH Measurements with Polyaniline. *J. Electroanal. Chem.* **2005**, *580* (2), 320–329.

(18) Hien, H. T.; Giang, H. T.; Hieu, N. Van; Trung, T.; Tuan, C. Van. Elaboration of Pd-Nanoparticle Decorated Polyaniline Films for Room Temperature NH 3 Gas Sensors. *Sensors Actuators B. Chem.* **2017**, *249*, 348–356.

(19) Quillard, S.; Louarn, G.; Lefrant, S.; Mac Diarmid, A. G. Vibrational Analysis of Polyaniline: A Comparative Study of Leucoemeraldine, Emeraldine, and Pernigraniline Bases. *Phys. Rev. B* **1994**, *50* (17), 12496–12508.

(20) Hasik, M.; Bernasik, A.; Drelinkiewicz, A.; Kowalski, K.; Wenda, E.; Camra, J. XPS Studies of Nitrogen-Containing Conjugated Polymers-Palladium Systems. *Surf. Sci.* **2002**, *507–510*, 916–921.

(21) Dimitriev, O. P. Doping of Polyaniline by Transition-Metal Salts. *Macromolecules* **2004**, *37* (9), 3388–3395.

CHAPTER 7. POLYANILINE AND PALLADIUM INTERACTIONS IN ACIDIC CONDITIONS

For this final chapter, understanding the nuances of the interaction between PANI and palladium will aid in tuning the interaction, allowing the process of atomic metal insertion to be applied to a broader list of metals and polymers.

7.1 Introduction

The interaction with various transition metal species such as Au, Ni and Fe has been studied previously. It is known that transition metal salts will dope protonated nitrogen groups of the PANI structure.[1–6] These previous studies, however, do not take into account the precise and controlled insertion process outlined in this study. With such a controlled insertion process, understanding the interaction between metal and PANI fully allows for tuning the interaction to the metal used and the application needed. Not only does the metal anion speciation matter, as outlined in Chapter 6, the morphology of the PANI does also play a role. [7,8] In this chapter, the effects of PANI conditioning, change to PANI with the insertion of Pd, and the role of the perchlorate anion are presented.

7.2 Electrode Preparation and Characterization

The electrode preparation is the same as described in Chapter 6, however, all palladium insertion into PANI was completed with the $PdCl_3(H_2O)^-$ species. Characterization was also done using Resonance Raman spectroscopy, XPS, and CV, similarly to Chapter 6.

7.3 PANI conditioning effects

"Conditioning" the polymer, as explained in the experimental, is done by running "blank" insertion cycles. Running a blank cycle initially served as a control in order to see the changes in the PANI matrix that were caused by cycling potentials and flowing solutions. Knowing the effects of the process itself on the matrix allowed us to isolate any changes that were caused by the Pd complex insertion. A series of electrodes were tested using from one to four "blank" cycles. Raman spectra were recorded before and after each set of cycles. It was determined that these "blank" or "conditioning" cycles did change the oxidation state of the PANI as compared to the initial film as shown in our previous work.[9] It was also determined that slight changes in the intensities of Raman bands occurred with each additional conditioning cycle. In particular, the intensity of the C~N$^{\cdot+}$ vibration of the bipolaron increased with every cycle, and a decrease in intensity of the C-C benzenoid stretch occurs. Remaining studies were done using two conditioning cycles in order to have a consistent starting matrix.

The effects of conditioning the PANI matrix can be seen more closely in Figure 7.1. The non-conditioned PANI sample shows differences in the imine/amine ratio as well as the protonation of the nitrogen-containing groups as compared to the conditioned PANI sample.

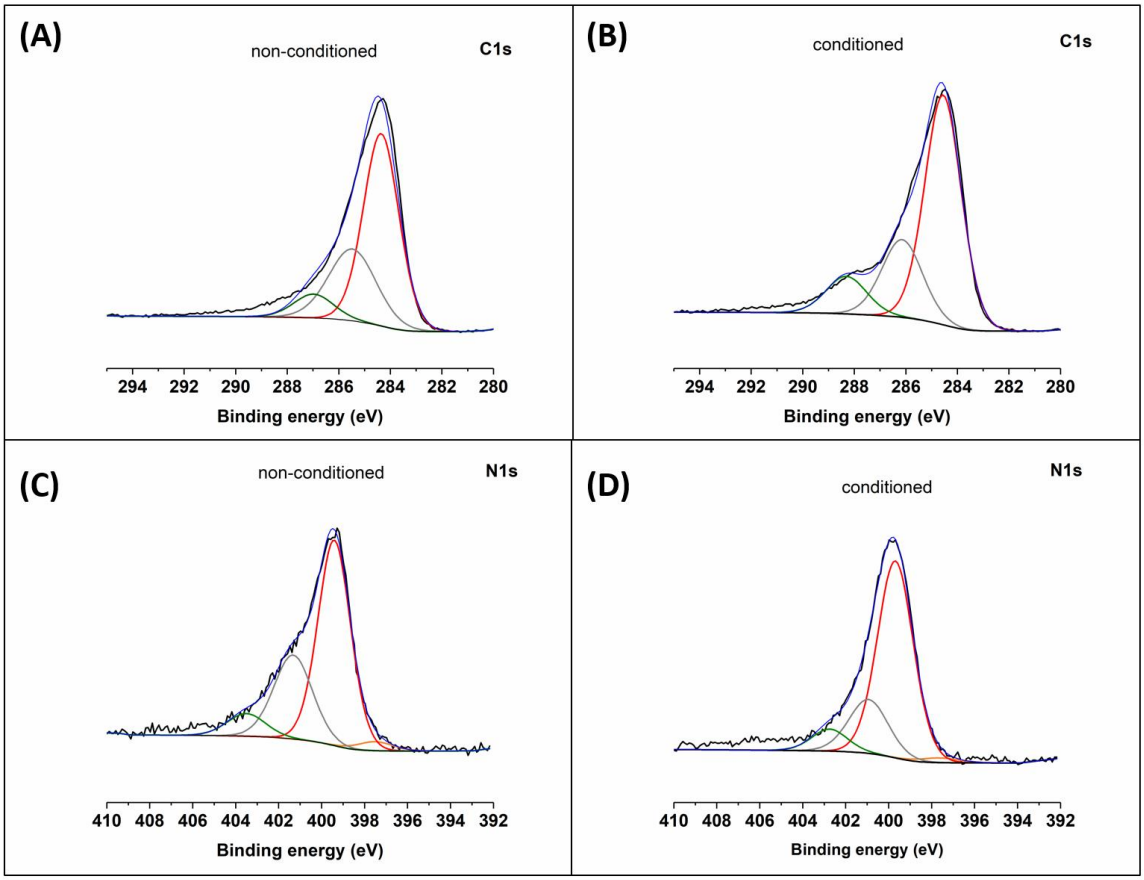

Figure 7.1: XPS core scans of non-conditioned and conditioned PANI. (A) and (C) show deconvoluted C1s and N1s spectra for non-conditioned polyaniline respectively. (B) and (D) show C1s and N1s for conditioned PANI respectively.

The deconvoluted carbon scan for the non-conditioned PANI, Figure 7.1A, shows that the majority of the carbon in the sample comes from the PANI backbone or C-C/C-H bonds with a binding energy of 284.4 eV. The C-N of the delocalized polaron makes up 30.4 atomic %, which the C-N of the bipolaron is 8.5 atomic %. For the C1s scan of the conditioned PANI, Figure 7.1B, the C-N delocalized polaron is 24.2 atomic %, while the C-N biplaron is 11.7 atomic %. This indicates that the conditioned PANI is less protonated overall. The data from the deconvoluted N1s scans of each PANI is contained in Table 7.1 and shows a similar trend. The deconvolution of the non-conditioned N1s scan (Figure

7.1C) reveals that a greater percentage of imine is present with an amine/imine ratio of 14.9 as compared to the 38.6 of the conditioned sample (Figure 7.1D). Also, the ratio of non-protonated to protonated nitrogen groups (N/N^+) shows that the conditioned sample is less protonated. However, in the conditioned PANI, a greater percentage of the total protonated nitrogen-containing groups is imine groups. The data from the survey scans of each PANI sample is also contained in Table 7.1.

Table 7.1: Atomic % ratios of elements and nitrogen-containing groups in non-conditioned and conditioned PANI

Sample	*Ratio of Atomic % from N1s Scans*			*Atomic % from Survey Scan*		
	$\frac{-NH-}{-N=}$	$\frac{-NH^+-}{-N^+=}$	$\frac{N}{N^+}$ (Protonation level)	$\frac{C}{N}$	$\frac{Cl}{N}$	$\frac{O}{Cl}$
PANI Non-conditioned	14.9	3.7	1.7	8.5	0.4	7.8
PANI Conditioned	38.6	2.7	2.5	6.4	0.3	6.2

The expected ratio of carbon/nitrogen is 6/1 and the expected ratio of oxygen/chlorine in a perchlorate doped sample is 4/1. This increase in carbon of the non-conditioned sample, and the increase of oxygen on both samples could be attributed to surface contamination. A higher than expected ratio of C/N and O/Cl could also indicate degradation of the polymer into benzoquinone units.[10] The level of protonation can also be evaluated through the Cl/N ratio. Perchlorate anions enter the PANI film in order to balance the charge of the protonated nitrogen-containing groups. Ideally, there would be

one perchlorate anion per protonated group, which indicates that there is a slightly higher level of protonation in the non-conditioned sample.

7.4 Palladium (II) Complex Insertion into PANI

7.4.1 Effect of PANI conditioning on Pd insertion and reduction

Figure 7.2 shows the effects of conditioning on the reduction of the palladium complex inserted into the PANI (PANI-Pd). After the palladium complex is inserted, the N1s scans reveal that there is minimal difference in the protonated nitrogen-containing groups between the non-conditioned (Figure 7.2A) and the conditioned (Figure 7.2B). This should be expected given that the palladium metal locks the polymer into more reduced state, and with the metal taking the nitrogen-containing sites, there is no longer an available site for protonation to take place.

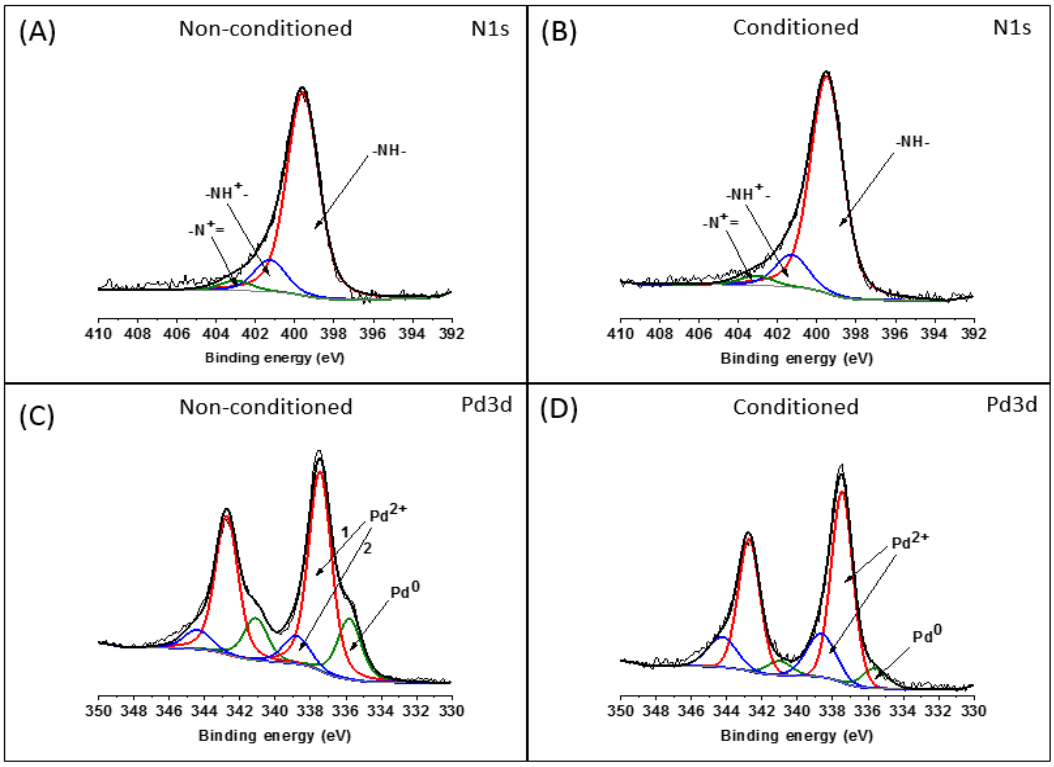

Figure 7.2: XPS scans of conditioned and non-conditioned PANI after palladium (II) complex insertion. (A) and (C) show the deconvoluted spectra for N1s and Pd3d of the non-conditioned PANI-Pd sample, respectively and the N1s (B) and Pd3d (D) of the conditioned PANI-Pd are also shown.

Both show approximately the same atomic % of protonated amine and protonated imine. The non-conditioned PANI-Pd has slightly less protonation than the conditioned PANI-Pd, as seen in Table 7.2, which is consistent with the N1s scan of non-conditioned PANI before palladium insertion (Figure 7.1).

It can be seen in the deconvoluted Pd3d scans of each of the PANI-Pd samples that the non-conditioned samples show greater reduction of the Pd(II) complex to Pd(0) metal, Figure 7.2C. This reduction could be explained by the greater level of protonation. The insertion of the palladium complex into the PANI film relies on the uptake of these $PdCl_3(H_2O)^-$ anions as a balance to the charge of the protonated nitrogen-containing groups

and then a subsequent interaction between the complex and nitrogen-containing groups. Having greater protonation means greater drive for charge balance resulting in an increase of palladium complex in the matrix. However, from Table 7.2, there is only approximately 21.5% reduction of the Pd(II) to Pd(0). This indicates there are other factors preventing the full reduction to metal. From the survey scans of each sample, the total atomic % of Pd in the conditioned sample is actually higher, at 21.38% versus the 11.07% in the non-conditioned sample. The deconvolution of the Pd3d scans reveal that even though there is less total Pd in the non-conditioned sample, there is more Pd(0). It is also seen that there is an inverse relationship between the percentage of reduced Pd(0) and the percentage of unreduced Pd^{2+} associated with nitrogen. In the conditioned sample there is a greater percentage of Pd^{2+}-- N and less Pd(0) as seen in Table 7.2. Also, of the total protonated nitrogen-containing groups in the conditioned sample, more are imine groups. This result is indicative of a strong interaction between the Pd(II) complex and the nitrogen-containing groups that leads to a lack of reduction to the Pd(0) metal.

Table 7.2: Atomic % values from N1s and Pd3d core scans for PANI-Pd samples

Sample	*Energy* / *%*	$-NH-$	$-NH^+-$	$-N^+=$	$\frac{N}{N^+}$	Pd^0	$Pd^{2+}-Cl$	$Pd^{2+}-N$
PANI-Pd Non-conditioned	BE (eV)	399.5	400.7	402.5	2.7	335.8	337.5	338.8
	atomic %	72.6	18.8	8.5		21.5	67.5	11.0
PANI-Pd conditioned	BE (eV)	399.5	401.1	403.0	4.4	335.6	337.5	338.7
	atomic %	81.5	14.1	4.4		8.4	70.2	21.4

7.4.2 Effects of the number of Pd insertion cycles

7.4.2.1 Resonance Raman analysis of Pd_{1-5}

The lack of fully reduced Pd(0) can also be seen in the Resonance Raman spectra using an incident source at 785 nm, Figure 7.3. Samples were created by inserting $PdCl_3(H_2O)^-$ into the PANI matrix using the described cycles, with each being run for a different number of cycles. The notation, Pd_n, denotes each PANI-Pd created with *n* number of insertion cycles. The common features among the spectra of all the samples point to the Pd locking the quinoid structures of the PANI in place, even after the sample is electrochemically reduced.[11] In particular, the $C{\sim}N^{\cdot+}$ vibrations show a greater intensity at 1375 cm^{-1} corresponding to the localized polaron (bipolaron) than the 1332 cm^{-1} assigned to the delocalized polaron. This is consistent with a more conjugated PANI. Also, the C-N stretches at 1225 cm^{-1} for the quinoid units show greater intensity than the 1265cm^{-1} for the benzenoid units.

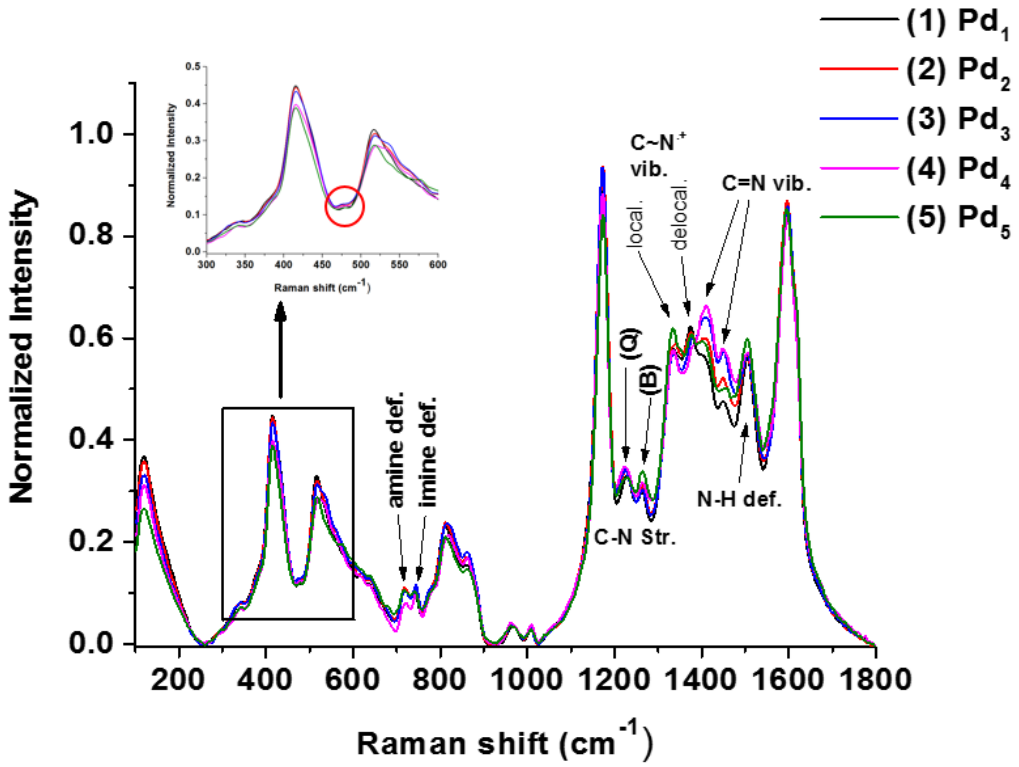

Figure 7.3: Resonance Raman spectra of conditioned PANI-Pd samples. The number of palladium(II) complex insertion cycles was increased with each sample and the spectra taken following each. The greatest change in intensity is seen with bands at 1410 cm^{-1} and 1450 cm^{-1}. Inset is an enlarged section of the spectra between 300 cm^{-1} and 600 cm^{-1} for clarity of the weak band at 476 cm^{-1}.

Some key bands in the spectra change as the number of insertion cycles changes. At 720 cm^{-1} the amine deformation is decreases in intensity and the imine deformation at 745 cm^{-1} increases as the number of insertion cycles increases.[10] The bipolaron $C{\sim}N^{\cdot+}$ vibration intensity remains relatively equal as the number of insertion cycles increases, however, the band shifts to higher wavenumbers as more Pd is introduced. As seen in Figure 7.4, the N-H deformation vibration near 1506 cm^{-1} follows a pattern similar to the percentage of Pd-N calculated from the deconvolution of the XPS Pd3d core scan. This confirms that the Pd is interacting with the N atoms in the PANI and causing a change in the N-H length due to partial charges formed.

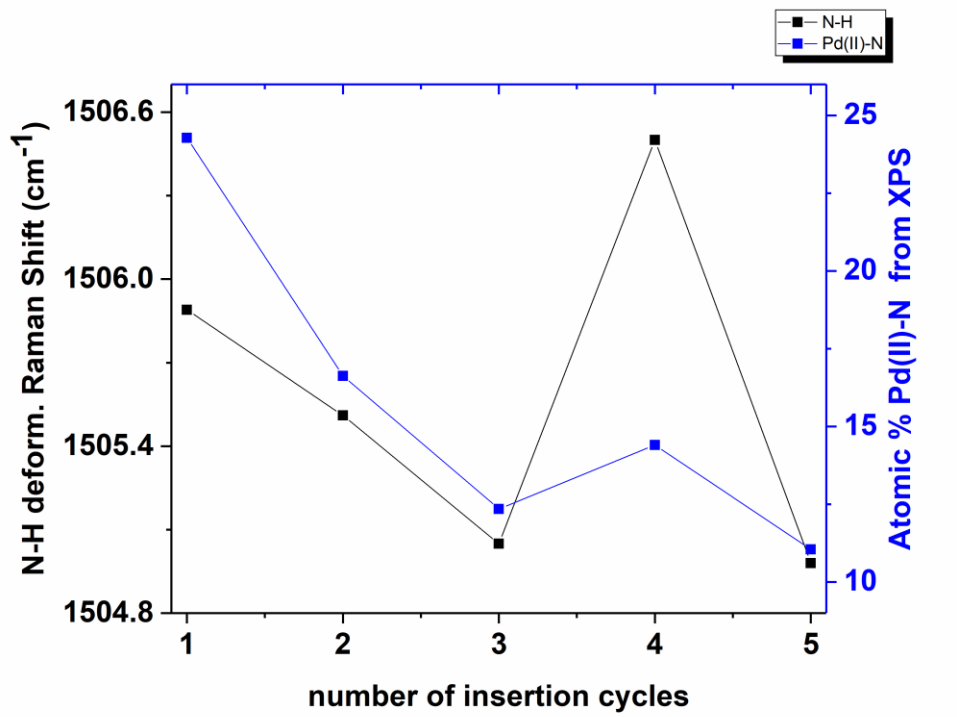

Figure 7.4: Correlation between the Raman shift of the N-H deformation vibration and the atomic % of the Pd-N peak in the XPS Pd3d scan. As the percentage of the Pd-N interaction decreases, the Raman shift also decreases to lower wavenumbers.

As seen previously, peaks present in the 1400 cm^{-1} to 1500 cm^{-1} region are tentatively attributed to the C=N stretch and are present only when palladium is present in the sample. [9,12,13] In particular, the presence of Pd is thought to change the conjugation length of the C=N and therefore changes the vibration, shifting the Raman bands. The peaks at 1410 cm^{-1} and 1450 cm^{-1} are thought to be indicative of this and the intensity of these peaks increases with each palladium insertion cycle. This continual increase provides evidence of greater amounts of Pd entering into the matrix with every cycle, but not necessarily being electrochemically reduced. Reduction of the Pd(II) to Pd(0) would ideally result in little change to the C=N length as the charge-induced interaction between

palladium and nitrogen would change to a weaker induced-dipole, and therefore the Raman bands would not shift and be visible at 1410 cm^{-1} and 1450 cm^{-1}.

7.4.2.2 XPS analysis of Pd_{1-5}

Attempts were made to understand the lack of reduction in palladium (II) chlorocomplex that was inserted into the PANI matrix. In a previous study by Li, Josowicz, and Janata, it was found that poly(phenylenesulfide phenyleneamine) (PPSA) polymer chain underwent a conformational change due to the formation of a ClO_4^- hydrogen/columbic bonded complex. This led to a "bridge" formed by ClO_4^- ions and resulted in the perchlorate ions not being able to be expelled from the polymer matrix.[14] Since PPSA has a similar structure to PANI, it is possible that this could also be true here. It is hypothesized that the perchlorate ions could be causing the conformational change in the polymer that also creates an environment where it is more favored for the palladium (II) chlorocomplex to also form a "bridge" between two nitrogen-containing groups on neighboring polyaniline fibrils.

The XPS data of the palladium samples, Pd_{1-5} was analyzed for the ClO_4^- content and is correlated to the % Pd(II) ion interacting with nitrogen. The results are presented in . This shows that with the exception of Pd_3, the relationship of increased ClO_4^- present in the doped PANI is inversely related to the Pd(II) and N interaction. This relationship shows that the anionic Pd complex is displacing the perchlorate during the insertion process. The XPS data between Figure 7.1 and Figure 7.2 also indicate that after Pd insertion, the PANI is less protonated, this could also account for less ClO_4^- counter ions in the matrix. It remains a possibility that the perchlorate plays a role in bridging the polyaniline fibrils,

possibly allowing the Pd(II) chlorocomplex to bridge or "cross-link" the fibrils as well, but further studies are needed to confirm this relationship.

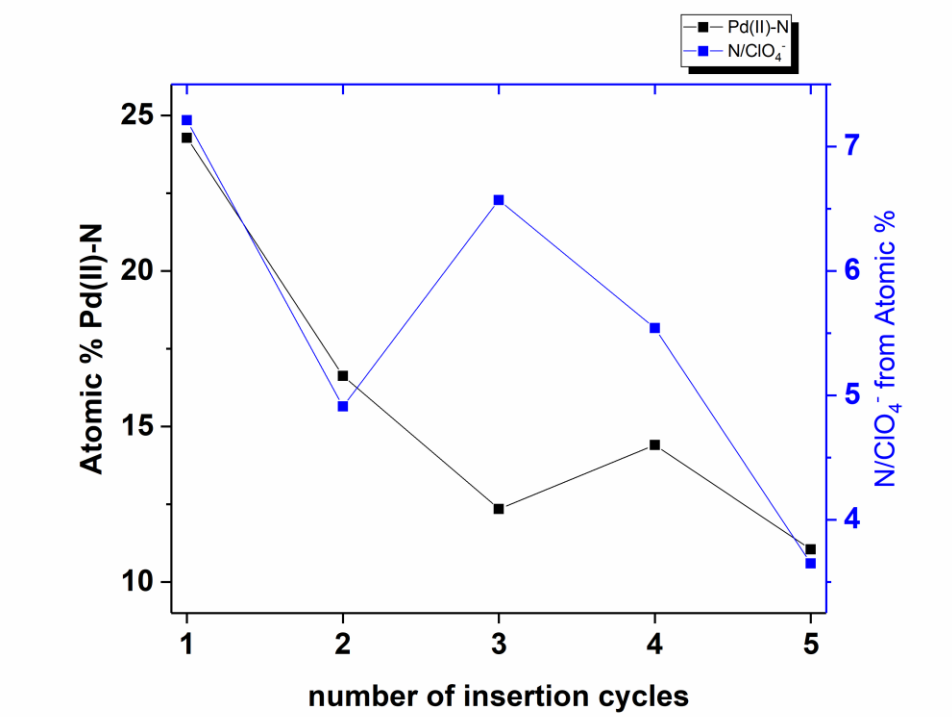

Figure 7.5: Perchlorate doping of PANI correlated to the Pd^{2+}—N interaction from XPS Cl2p and Pd3d core-level scans. Perchlorate doping expressed as ratio of N/ClO_4^- and Pd^{2+}-N interaction expressed as atomic % from Pd3d deconvolution.

7.4.3 Correlation of XPS and Raman bands

Evidence for these strong Pd-N interactions is seen in the Raman band shifts of the C=N vibration, as previously stated, again in the atomic percentage of Pd(II) for the deconvoluted Pd3d XPS scans, and finally in the lack of reduction of Pd(II) to Pd(0) shown in the XPS scans. In the Raman spectra, a unique weak band is seen at 476 cm^{-1} that can has been linked to the asymmetric stretch of the complex, cis-$[Pd(NH_3)_2Cl_2]$.[15] This band is only present after Pd insertion into the PANI and could be indicative of possible cross-

linking of PANI fibers by the Pd(II) complex. The XPS scans of Pd3d also show a strong Pd^{+2} — Cl component which falls in a binding energy range consistent with $PdCl_2$.[16,17] PANI has been known to form cross-linked structures with nickel and tin complexes[1,18] and the hypothesis is made that this is the case with this particular Pd(II) chlorocomplex. This formation of the cross-linked structure could explain why it is difficult to reduce the palladium ion to metal. Attempts have been made to disrupt this strong Pd-N interaction through the changing of various experimental parameters with the idea that the Pd(II) complex would reduce. Sweeping to more negative potentials during the reduction segment of the insertion cycles and the use of chemical reducing agents, such as $NaBH_4$, have also shown to be ineffective at complete reduction of Pd(II).

7.4.4 Correlation between CV, XPS, and Raman with respect to redox state of PANI

The ability to correlate characterization techniques can provide a useful tool when trying to understand the redox state of PANI. The deconvoluted XPS N1s core-level spectra provides information regarding the relative quantification of imine, amine, protonated imine and protonated amine groups. Raman spectra can also provide similar information regarding the quinoid and benzenoid character of the PANI films as well as the polaron forms present. The separation of redox potentials found in the CV can also provide information about the proton and anion exchange in the PANI film as well as the conformation of the polymer. Table 7.3 correlates the data of CV to XPS and the data of XPS to Raman.

Table 7.3: Correlation of CV, XPS and Raman data for redox state of PANI

	CV (V)	XPS (Atomic %)	XPS (Atomic %)	Raman (Norm. Intensity)
	Separation of hydrogen and anion peaks	*-N=/-NH- ratio*	*N/N^+ ratio*	*N/N^+ ratio*
PANI	0.42	0.32	1.83	0.97
PANI-conditioned	0.30	0.21	3.07	1.09
PANI-Pd	0.17	0.11	6.45	1.16

For the nitrogen-to-protonated nitrogen ratio, both XPS and Raman spectra data show that the PANI is the most protonated, followed by the conditioned PANI and the PANI-Pd. Also, the XPS imine/amine ratio decrease follows the decrease in separation of the hydrogen and anion redox peaks in the CV, showing a direct relationship. If the pKa values of the imines and amines are considered, the imines should protonate first with a value of 2.5, and the amines second, with a value of 5.5.[19] As the amine character increases, the protonation level may drop due to the higher pKa value. Likewise, as the protonation decreases, the hydrogen insertion peak in the CV will become less prominent and the potential will shift to reflect conformational changes in the PANI.

7.5 Conclusion

Palladium has been successfully inserted into a polyaniline matrix using the $PdCl_3(H_2O)^-$ complex through controlled insertion cycles and confirmed through XPS. The XPS Pd3d core scans indicate through deconvolution that only a small percentage of the Pd(II) is reduced to Pd(0). The deconvolution of these scans also reveal that there two components to the Pd(II), one for Pd^{2+}—Cl and one for Pd^{2+} — N and the higher the Pd^{2+}—

N percentage, the less Pd(0) is present. These XPS results, along with Resonance Raman spectra show that with successive insertion cycles, there is an increase of Pd entering into the matrix, but little increase in the percentage of Pd(II) being reduced. These results lead us to believe that a strong complex is being formed between the Pd (II) chlorocomplex and the nitrogen-containing groups of the PANI, with possible cross-linking of the polymer fibers.

7.6 References

(1) Dimitriev, O. P. Doping of Polyaniline by Transition-Metal Salts. *Macromolecules* **2004**, *37* (9), 3388–3395.

(2) Hatchett, D. W.; Quy, T.; Goodwin, N.; Millick, N. M. In-Situ Reduction of Au, Pd, and Pt Metal Precursors in Polyaniline: Electrochemistry of Variable Metal Content Polymer/Metal Composites in Alkaline Solution. *Electrochim. Acta* **2017**.

(3) Safenaz, M.; Sheikha, M. Synthesis and Electrical Properties of Polyaniline Composite with Silver Nanoparticles. *Adv. Mater. Phys. Chem.* **2012**, *2*, 75–81.

(4) Tao, S.; Hong, B.; Kerong, Z. An Infrared and Raman Spectroscopic Study of Polyanilines Co-Doped with Metal Ions and H+. *Spectrochim. Acta - Part A Mol. Biomol. Spectrosc.* **2007**, *66* (4–5), 1364–1368.

(5) Hu, C. C.; Chen, E.; Lin, J. Y. Capacitive and Textural Characteristics of Polyaniline-Platinum Composite Films. *Electrochim. Acta* **2002**, *47* (17), 2741–2749.

(6) Izumi, C. M. S.; Ferreira, A. M. D. C.; Constantino, V. R. L.; Temperini, M. L. A. Studies on the Interaction of Emeraldine Base Polyaniline with Cu (II), Fe (III), and Zn (II) Ions in Solutions and Films. *Macromolecules* **2007**, *40*, 3204.

(7) Wang, H.; Li, W.; Jia, Q. X.; Akhadov, E. Tailoring Conducting Polymer Chemistry for the Chemical Deposition of Metal Particles and Clusters. *Synth. Met.* **2007**, *41* (3), 520–525.

(8) Pahovnik, D.; Žagar, E.; Vohlídal, J.; Žigon, M. Effect of Cations on Polyaniline Morphology. *Chem. Pap.* **2013**, *67* (8), 946–951.

(9) Gawron, E. L.; Hira, S. M.; Josowicz, M.; Janata, J. Effects of Palladium (II) Chlorocomplex Speciation on the Controlled Interaction with Polyaniline Film in Acid. *Langmuir* **2017**, *Accepted*.

(10) Trchová, M.; Morávková, Z.; Bláha, M.; Stejskal, J. Raman Spectroscopy of Polyaniline and Oligoaniline Thin Films. *Electrochim. Acta* **2014**, *122*, 28–38.

(11) Hasik, M.; Paluszkiewicz, C.; Bielańska, E. Reactions of Polyaniline with Transition Metal Ions in Nonaqueous Solutions. In *Journal of Molecular Structure*; 2005; Vol. 744–747, pp 677–683.

(12) Louarn, G.; Lapkowski, M.; Quillard, S.; Pron, A.; Buisson, J. P.; Lefrant, S. Vibrational Properties of Polyaniline - Isotope Effects. *J. Phys. Chem.* **1996**, *100* (17), 6998–7006.

(13) Nascimento, G. M. Do. Spectroscopy of Polyaniline Nanofibers. *Nanofibers* **2010**, No. February, 351–366.

(14) Li, G.; Josowicz, M.; Janata, J.; Müllen, K. Structural, Electronic, and Morphological Changes in Poly(phenylenesulfide Phenyleneamine) upon Electrochemical Doping. *J. Phys. Chem. B* **2001**, *105* (11), 2191–2196.

(15) Hartley, F. . *The Chemistry of Platinum and Palladium*; Robinson, P. L., Ed.; Applied Science: London, 1973.

(16) NIST X-ray Photoelectron Spectroscopy Database Version 4.1. NIST X-Ray Photoelectron Spectroscopy Database, Version 4.1. National Institute of Standards and Technology: Gaithersburg 2012.

(17) Hasik, M.; Bernasik, A.; Drelinkiewicz, A.; Kowalski, K.; Wenda, E.; Camra, J. XPS Studies of Nitrogen-Containing Conjugated Polymers–palladium Systems. *Surf. Sci.* **2002**, *507*, 916–921.

(18) Bienkowski, K. Polyaniline and Its Derivatives Doped with Lewis Acids - Synthesis and Spectroscopic Properites. *Univ. Joseph-Fourier- Grenoble I; Warsaw Univ. Technol.* **2006**.

(19) Ray, A.; Richter, A. F.; MacDiarmid, A. G.; Epstein, A. J. Polyaniline: Protonation/deprotonation of Amine and Imine Sites. *Synth. Met.* **1989**, *29* (1), 151–156.

CHAPTER 8. FUTURE WORK

The work presented in this thesis outlines the need for understanding how each component in a composite electrode behaves and contributes to the overall composition. Chapters 2 and 3 outline the experimental procedures and optimization for the insertion process of a metal into a polyaniline matrix. Chapters 4 and 5 focus on the carbon electrode material and the effects that the substrate has on the electrochemical properties of the deposited PANI. Chapter 6 and 7 highlight the interaction between the Pd and PANI and the importance of speciation in that interaction. Since there are still aspects of this interaction that need to be elucidated, it follows that there are several studies needed in the future.

8.1 Reduction of Palladium

In the conclusion of Chapter 7, the study was left with the hypothesis that the lack of reduction of Pd(II) was due to possible "bridging" or "cross-linking" of the PANI fibers by the Pd(II) chlorocomplex. More studies are needed to investigate why these complexes are not reducible. Two late investigations set up a future study into increasing the conversion of Pd(II) to Pd(0).

First, the PANI-Pd electrode was introduced to a chemical reducing agent, $NaBH_4$ in KOH solution. The electrode, with a known Pd(0) content of roughly 20% from previous XPS measurements, was dipped in the solution for 30 minutes. XPS measurements were done post $NaBH_4$ exposure and found to have an increase of Pd(0) at just over 60%. This illustrates that there are possibilities to increase reduction.

Secondly, an interesting phenomenon was encountered when the PANI-Pd electrode was cycled in 0.1M $HClO_4$ at a larger window. On the first scan only, an

oxidation peak at E = 1.1V appears, Figure 8.1. This peak is only seen when Pd is present in the PANI and is only seen on the first scan. If the electrode is taken out of solution, dried, and then re-cycled, this peak no longer appears. This indicates an irreversible change to the composite. After investigation at XPS, it shows that 37% conversion to Pd(0), where prior, the conversion was 1.5%.

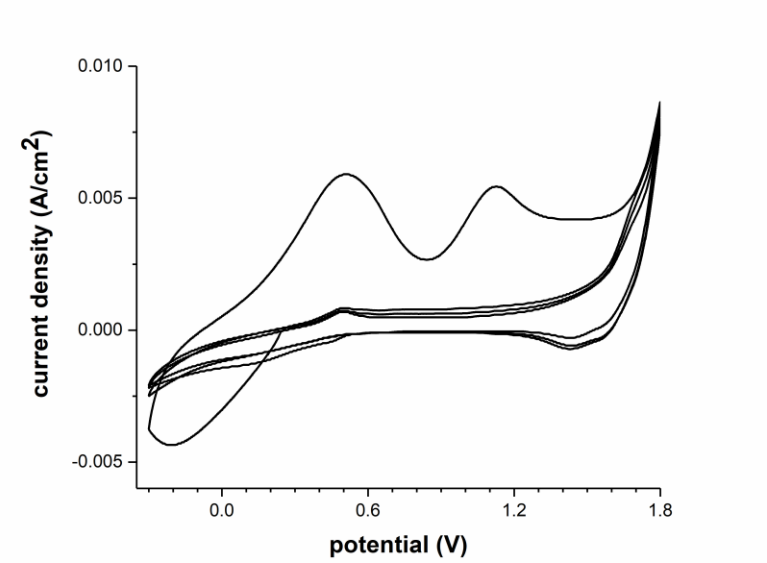

Figure 8.1: PANI-Pd electrode cycled in 0.1M $HClO_4$ at 50 mV/s. The window scanned is -0.3V to 1.8V, as opposed to previous characterizations that scan from -0.3V to 0.95V.

Initially it is thought that the oxidation of the PANI causes a change in conformation that may "unlock" the palladium (II) chlorocomplex, allowing it to reduce on the cathodic scan. More investigation into this is needed to explore how the PANI morphology is changing during the oxidation process here.

8.2 Alloys

From previous work, Jonke et al. were able to create "atomic alloys" of Pd and Au using a similar process on a Pt electrode.[1,2] This previous work also suggested that the catalytic activity was affected by the order of deposition of each metal. This could play an even more important role with this work on the carbon electrode. Due to the difficulty in reducing the Pd, "seeding" the atomic clusters with a different metal, such as Au or Ni, could aid in the reduction of Pd. Combining these metals with Pd to make atomic alloys also aid in increasing the catalytic activity over just Pd.[3]

8.3 Catalytic Activity

Throughout this work, the focus has not been on evaluating the catalytic activity of these C/PANI-Pd composites. Pd inserted into PANI has been shown to be a catalyst for the oxidation of alcohol or glycerol, hydrogenation reactions and Suzuki coupling. [4–7] Once the Pd has significant conversion to Pd(0), the catalytic activity can be investigated. There is much to be explored in this area, from the activity of PANI-Pd only, to using alloys of different metals tuned to catalyze specific reactions. The use of Pd/Ru or Au/Pd would have specific applications in alcohol oxidation.[1,3]

8.4 Different metals or polymers

Another aspect of this work that can be expanded on, is using different metals in the insertion process. After understanding more about the process and the interaction of the metals with the polyaniline allows for the tuning of the process for other metals or applications. Other precious metals that exist in the anionic halide form are platinum,

iridium, or ruthenium. Current research trends in catalysis are moving away from using precious metals. This process could also be adapted for use with nickel, iron, titanium, or other metals. Using different metals can also allow for catalysis in biological processes. Not only can metals be changed, but other conducting polymers could possibly be used, such as polypyrrole. Palladium on polypyrrole has been previously investigated for alcohol oxidation.[8–10]

8.5 Different insertion conditions

Preliminary studies were done using a pH=7 phosphate buffer for insertion conditions instead of pH=1 perchloric acid conditions. The complexation of the $PdCl_4^-$ species with the nitrogen-containing groups of the PANI is a Lewis acid-base interaction. However, the protonation and uptake of anions as charge-balance are Brønsted interactions. By removing the Brønsted interaction in a buffer solution, this reduces the competition for the metal anion to be able to interact with the nitrogen-containing groups. A preliminary Pd insertion into PANI was completed in the phosphate buffer and the resulting composite was analyzed with XPS. It was found that nearly 40% of Pd was converted to Pd(0), compared to the average conversion to Pd(0) of about 10% in our current insertion process. Further studies here could also find a solution to the issue of lack of Pd reduction.

8.6 References

(1) Schwartz, I. T.; Jonke, A. P.; Josowicz, M.; Janata, J. Polyaniline Electrodes with Atomic Au (N) Pd-1 Alloys: Oxidation of Methanol and Ethanol. *Catal. Letters* **2013**, *143* (7), 636–641.

(2) Jonke, A. P.; Steeb, J. L.; Josowicz, M.; Janata, J. Atomic Clusters of Pd and AuNPdM in Polyaniline. *Catal. Letters* **2013**, *143* (6), 531–538.

(3) Lima, A; Hahn, F.; Léger, J. Oxidation of Methanol on Pt , Pt – Ru , and Pt – Ru – Mo Electrocatalysts Dispersed in Polyaniline : An in Situ Infrared Reflectance Spectroscopy Study *. **2004**, *40* (3), 369–379.

(4) Dimitriev, O. P. Doping of Polyaniline by Transition-Metal Salts. *Macromolecules* **2004**, *37* (9), 3388–3395.

(5) Drelinkiewicza, A.; Waksmundzka, A.; Makowski, W.; Sobczak, J. W.; Król, A.; Zięba, A. Acetophenone Hydrogenation on Polymer-Palladium Catalysts. The Effect of Polymer Matrix. *Catal. Letters* **2004**, *94* (3–4), 143–156.

(6) Simões, M.; Baranton, S.; Coutanceau, C. Electro-Oxidation of Glycerol at Pd Based Nano-Catalysts for an Application in Alkaline Fuel Cells for Chemicals and Energy Cogeneration. *Appl. Catal. B Environ.* **2010**, *93* (3), 354–362.

(7) Chen, A.; Ostrom, C. Palladium-Based Nanomaterials : Synthesis and Electrochemical Applications. **2015**.

(8) Hasik, M.; Bernasik, A.; Drelinkiewicz, A.; Kowalski, K.; Wenda, E.; Camra, J. XPS Studies of Nitrogen-Containing Conjugated Polymers–palladium Systems. *Surf. Sci.* **2002**, *507*, 916–921.

(9) Drelinkiewicz, A.; Hasik, M.; Quillard, S.; Paluszkiewicz, C. Infrared and Raman Studies of Palladium—nitrogen-Containing Polymers Interactions. *J. Mol. Struct.* **1999**, *511–512*, 205–215.

(10) Kang, E. T.; Neoh, K. G.; Tan, K. L. The Intrinsic Redox States in Polypyrrole and Polyaniline: A Comparative Study by XPS. *Surf. Interface Anal.* **1992**, *19* (1–12), 33–37.

VITA

Ms. Gawron is originally from Holland, Michigan and has lived in the Chattanooga, TN area, Indianapolis, IN area and the Atlanta, GA area. She obtained her B.S. degree from Rose-Hulman Institute of Technology in Terre Haute, IN in Chemistry and Mathematics in 1999. She was also one of the first women to attend Rose-Hulman. She received her M.S. in science education from Purdue University in West Lafayette, IN in 2002. Erin taught A.P. and gifted chemistry and environmental science at Heritage High School in Conyers, GA from 2002-2012 before choosing to pursue her Ph.D. at Georgia Tech.

Publications

Gawron, E.L.; Krizek, T.; Kowalik, M.A.; Josowicz, M,; Janata, J., Preparation of a Carbon-Platinum-Polyaniline Support for Atomic Metal Deposition. *J. Electrochem Soc*. **2015,** 162(7), H423-H427

Gawron, E.L.; Hira, S.M.; Josowicz, M.; Janata, J., Effects of palladium (II) chlorocomplex speciation on the controlled interaction with polyaniline film in acid. *Langmuir* **2017** (Accepted).

Gawron, E.L.; Josowicz, M.; Janata, J., Effect of carbon structures and surfaces on the electrochemical properties of supported polyaniline in composite materials. *Manuscript submitted. Journal of the Electrochemical Society.*

Gawron, E.L.; Hira, S.M.; Josowicz, M.; Janata, J., Probing palladium – polyaniline interactions in electrochemically prepared palladium clusters. *Manuscript in preparation.*